1976

Measured surface charge and current distributions on scattering rectangular plates.

Wiedemann, Hans-Joachim

Monterey, California. Naval Postgraduate School

Report Number -- NPS-52ZN76051

NAVAL POSTGRADUATE SCHOOL
Monterey, California

THESIS

MEASURED SURFACE CHARGE
AND CURRENT DISTRIBUTIONS ON
SCATTERING RECTANGULAR PLATES

by

Hans-Joachim Wiedemann

June 1976

Thesis Advisor: R. W. Burton

Prepared for: Air Force Weapons Laboratory/PRP
Kirtland AFB
New Mexico 87117

Report Number -- NPS-52ZN76051

NAVAL POSTGRADUATE SCHOOL
Monterey, California

THESIS

MEASURED SURFACE CHARGE
AND CURRENT DISTRIBUTIONS ON
SCATTERING RECTANGULAR PLATES

by

Hans-Joachim Wiedemann

June 1976

Thesis Advisor: R. W. Burton

Prepared for: Air Force Weapons Laboratory/PRP
Kirtland AFB
New Mexico 87117

UNCLASSIFIED

SECURITY CLASSIFICATION OF THIS PAGE (When Data Entered)

REPORT DOCUMENTATION PAGE		READ INSTRUCTIONS BEFORE COMPLETING FORM
1. REPORT NUMBER NPS-52Zn76501	2. GOVT ACCESSION NO.	3. RECIPIENT'S CATALOG NUMBER
4. TITLE (and Subtitle) Measured Surface Charge and Current Distributions on Scattering Rectangular Plates		5. TYPE OF REPORT & PERIOD COVERED 6. PERFORMING ORG. REPORT NUMBER
7. AUTHOR(s) Hans-Joachim Wiedemann in conjunction with Robert W. Burton		8. CONTRACT OR GRANT NUMBER(s)
9. PERFORMING ORGANIZATION NAME AND ADDRESS Naval Postgraduate School Monterey, California 93940		10. PROGRAM ELEMENT, PROJECT, TASK AREA & WORK UNIT NUMBERS
11. CONTROLLING OFFICE NAME AND ADDRESS Air Force Weapons Laboratory/PRP Kirtland AFB New Mexico 87117		12. REPORT DATE June 1976 13. NUMBER OF PAGES
14. MONITORING AGENCY NAME & ADDRESS(if different from Controlling Office)		15. SECURITY CLASS. (of this report) UNCLASSIFIED 15a. DECLASSIFICATION/DOWNGRADING SCHEDULE

16. DISTRIBUTION STATEMENT (of this Report)

Approved for public release; distribution unlimited.

17. DISTRIBUTION STATEMENT (of the abstract entered in Block 20, if different from Report)

18. SUPPLEMENTARY NOTES

19. KEY WORDS (Continue on reverse side if necessary and identify by block number)

Charge and current distributions,
scattering by conducting surfaces,
rectangular metal plates

20. ABSTRACT (Continue on reverse side if necessary and identify by block number)

This work describes the measurement of surface charge and current distributions on rectangular conducting plates under monochromatic, electromagnetic illumination. Different plate widths and angles of incidence are investigated. The results are graphed, analyzed and compared to theoretical computations.

DD FORM 1 JAN 73 1473 EDITION OF 1 NOV 68 IS OBSOLETE
S/N 0102-014-6601 |
(Page 1)

UNCLASSIFIED

SECURITY CLASSIFICATION OF THIS PAGE (When Data Entered)

MEASURED SURFACE CHARGE AND CURRENT DISTRIBUTIONS ON SCATTERING RECTANGULAR PLATES

by

Hans-Joachim Wiedemann

Lieutenant Commander, Federal German Navy

Submitted in partial fulfillment of the
requirements for the degree of

MASTER OF SCIENCE IN ELECTRICAL ENGINEERING

from the

NAVAL POSTGRADUATE SCHOOL

June 1976

ABSTRACT

This work describes the measurement of surface charge and current distributions on rectangular conducting plates under monochromatic, electromagnetic illumination. Different plate widths and angles of incidence are investigated. The results are graphed, analyzed and compared to theoretical computations.

TABLE OF CONTENTS

ACKNOWLEDGEMENT

This thesis is the summary of my research efforts over the past nine months and reflects part of the knowledge and skills that were passed to me during my study in the Electrical Engineering Department of the Naval Postgraduate School. I wish to express my admiration and thanks to the members of the academic staff, who patiently contributed their time and effort to my education, first of them all to Associate Professor R. W. Burton.

I. INTRODUCTION

A. PROBLEM DEFINITION

The research described in this thesis was conducted with two major objectives. First was the experimental measurement of surface charge and current distributions on rectangular metal structures illuminated by a monochromatic source. Second was the development of suitable techniques to engineer the metal structures and the sensors and integrate them with the necessary instrumentation to form the experimental apparatus.

B. MOTIVATION FOR THE EXPERIMENT

The distribution of charge and current on metal surfaces of certain configurations and illuminated by an external electromagnetic source has been investigated with varying degree of intensity over the past decades. Particular interest was given to those structures, which have direct technical application, such as antennas and surfaces of vehicles. This interest has been enhanced by the threat of the electromagnetic pulse (EMP) associated with a nuclear detonation. The EMP will induce charge and current on unprotected metal surfaces and thus has the potential to severely interfere with the performance of communication and computer systems on airplanes, missiles or ships. A complete knowledge and understanding of the distribution of the induced charge and currents is essential to understanding how to accomplish suitable protection against EMP. Because of the nature of the problem, it seems to be logical to begin the research with simpler structures and later on move to higher complexity. Whereas solutions using numerical techniques to the distribution problem associated with rectangular conducting plates already exist [Refs. 1, 2,

3], no experimental data have been published to this date to validate the numerical theory. The results of the experimental work conducted by the author are therefore an opportunity to compare computer aided and experimentally obtained data.

II. EXPERIMENTAL APPARATUS

A. IMAGE PLANE

Experimental measurements reported herein were taken with metal plates resting on an aluminum surface, which was ten wavelengths square (10 Meters x 10 Meters). This surface served as an image plane for the transmitting and receiving system (Fig. 1). Below was a room which contained the driving source, the measuring instruments and the mechanism to move the pick-up probes (described later).

B. DRIVING SYSTEM

The driving source was a power signal generator (Airborne Instruments Laboratory, Type 124C), which delivered a CW-signal of 300 MHz to the antenna system consisting of a 1/4 wavelength monopole and a 90° corner reflector having a physical aperture D equal to 1.73 Meters and height .31 Meters. The theory of corner reflectors is explained in Ref. 4. The advantage of using a corner reflector was, that by simple adjustment of monopole-to-corner spacing the input impedance could be matched very closely to the feeding transmission line impedance. A fine adjustment was made by a double-stub-tuner in front of the antenna input.

The following values were calculated for the antenna system:

1. Gain of corner reflector = 10.2 dB.

2. Minimum range from where on far field approximation holds by formula $R = \frac{2\,d^2}{\lambda}$, i.e., R = 1.28 Meters. Since R was less than 3 wavelengths, the more customary value of 3 wavelengths was taken to approximate the far field boundary. (Note: Because a 90° corner reflector

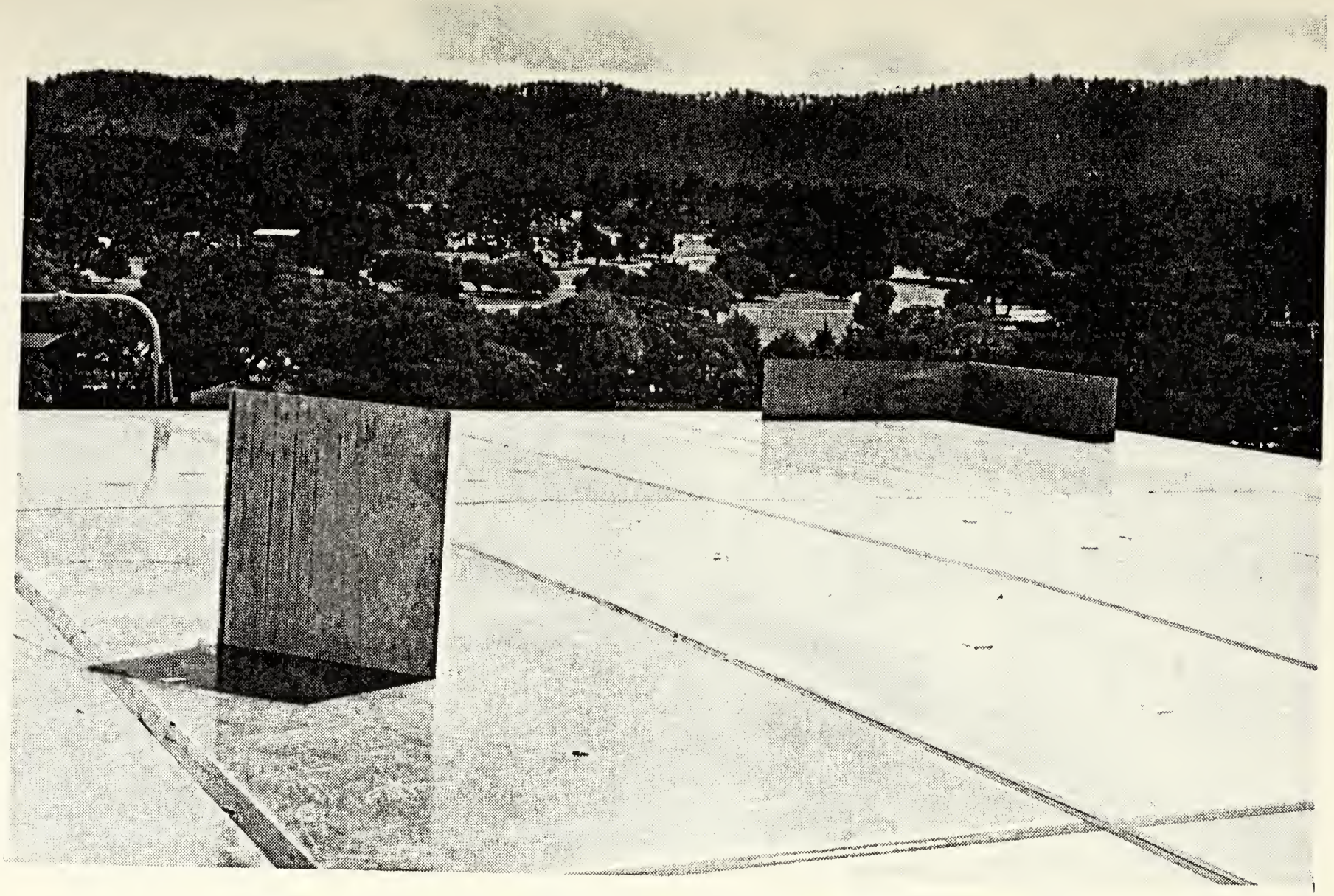

Figure 1. Ground Plane with Plate C, Corner Reflector and Monopole

with monopole can be represented by four monopoles in the vertices of a square with a half-diagonal equal to the monopole-to-corner spacing d, the effective aperture is only 2d, which was .90 Meters in the experiment [Ref. 5]).

3. Beamwidth estimation by formula $BW \approx \frac{\lambda}{d} \cdot \frac{360}{2\pi}$ yielded 71.62°. BW at the receiving plate, 7 Meters from antenna, was close to 10 Meters.

4. Power into antenna feed was 14 W.

5. Voltage standing wave ratio was .30 .

The oscillator power and frequency were constantly monitored during the experiment and held within less than 1% deviation from the nominal values 14 W and 300 MHz.

C. RECEIVING SYSTEM

1. Metal Plates

The transmitted wave was received by a metal plate at 7.07λ (1λ = 1 Meter) from the transmitting antenna. This distance was sufficient to assume a uniform plane wave, as was shown in section II B.

Four different sized plates were used, one at a time. The dimensions are shown in Fig. 2. The plates carried numerous T-slots, which made the insertion of the probe-bar (discussed later) possible. The number of slots in the different plates are listed in Fig. 2. The slot nearest to the edge had a centerline 0.0125λ from the edge. Spacing between centerlines of two adjacent slots was 0.0250λ. The slot dimensions were designed to be 0.05 Millimeters bigger than for the probe-bar. The slots not occupied by the probe-bar were filled by bars with

matching dimensions (Fig. 3, Fig. 4). The slot, where the measurements were taken, was filled above the probe-bar by 0.01 Meter long filler pieces that were slanted at the bottom. When pushing up by the probe-bar, the slanting caused the fillers to fall one by one behind the plate and to be scattered over a certain region on the ground plane. Measurement results did not change, whether the filler pieces were or were not lying on the ground plane.

The plates B, C, D did not carry longitudinal slots over the whole width. Instead only one half of the total width was slotted, plus one slot beyond the half width line (Fig. 3). When measurements over the whole width were conducted, the plate was simply turned over. The reason for this one slot beyond the half width line was as follows: The phase behavior about the middle of the plate's width was of particular interest and could be observed without turning the plate. When the plate had to be turned, it was possible to make measurements (using this slot in reverse direction) on the same relative position on the plate as done before turning. This was very helpful and allowed to compare corresponding values, which could have changed because of the mechanical changes related to the turning.

The plates were supported by a thin bent rectangular plate, which was screwed to the ground plane and to the side of the plate opposing the slotted one.

2. Probe System

In order to measure relative magnitude and phase of surface charge and current distributions on the plates, it was necessary to

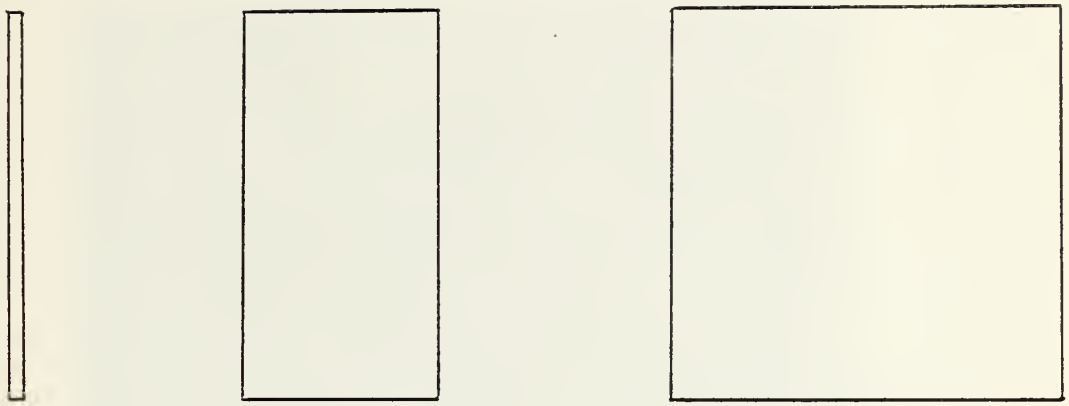

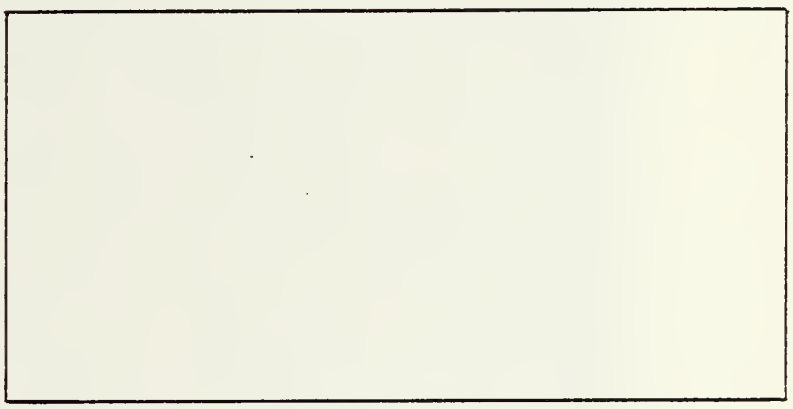

Plate	Height/λ	Width/λ	Thickness/λ	Number of Slots
A	.5	.024	.02	1
B	.5	.25	.02	6
C	.5	.5	.02	11
D	.5	1.0	.02	21

Figure 2. Plates A, B, C, D and Their Dimensions

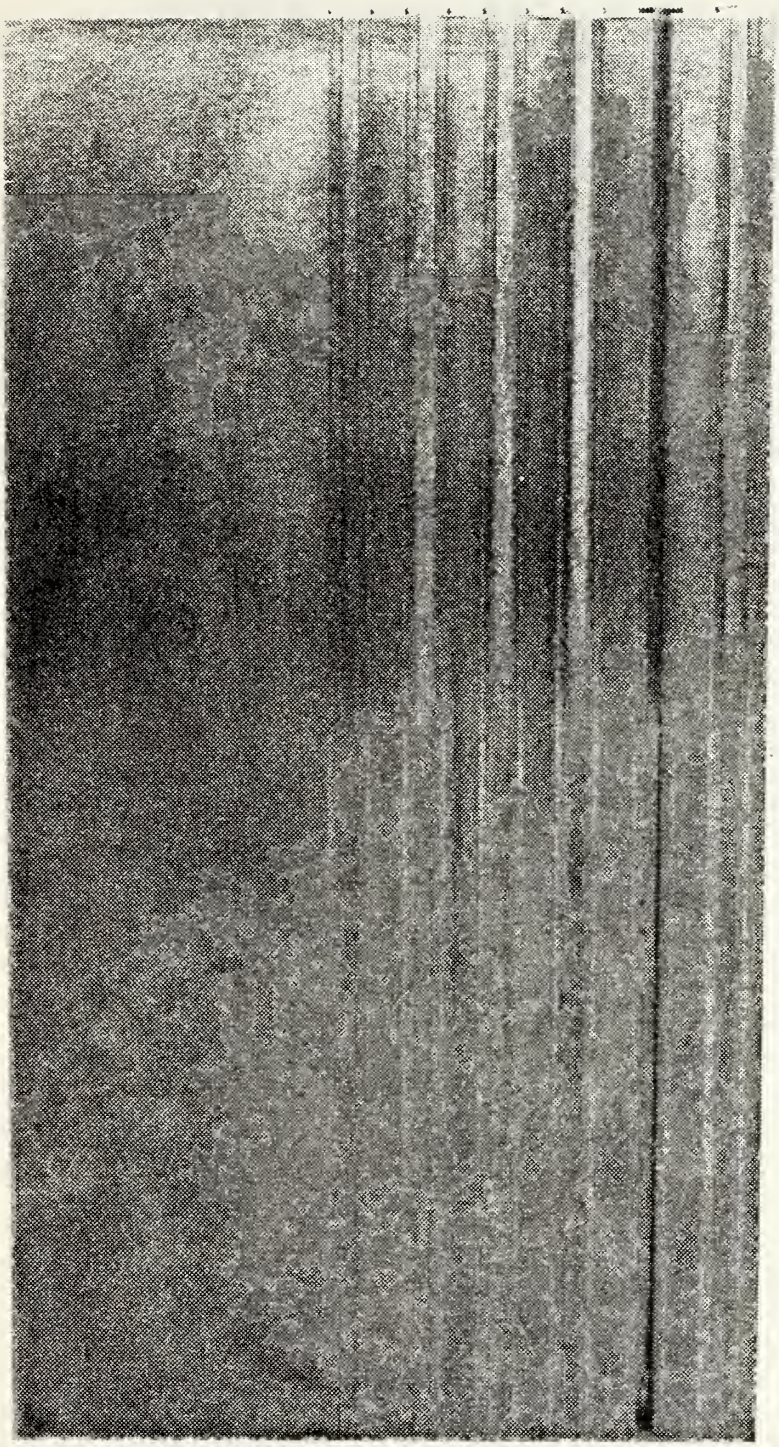

Figure 3. Plate B with One Open and Five Filled Slots

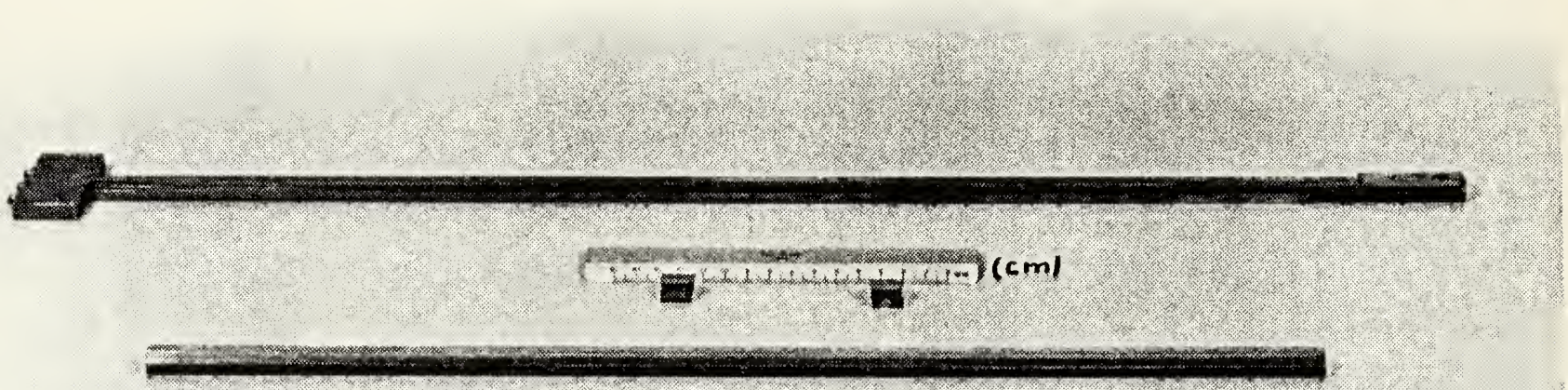

Figure 4. Probe-Bar, Filler and Two Filler Pieces

loosely couple small antenna-like structures to the surface distributions. The underlying theory is explained in Ref. 6, II.26. A charge probe and a current probe are shown in Fig. 5. Two orthogonal current probes were used. The integration of the probes into the probe-bar can be seen in Fig. 7a.

The probe-bar had cross-sectional dimensions a little less than the T-slots of the plates (Fig. 6) to allow for clearance. A small spring-loaded copper-beryllium plate was mounted to the top of the bar to make steady contact to the aluminum plate in the immediate vicinity of the probes. The bar had a narrow slot in its back to accomodate three small coaxial lines from the probes to three connectors at its bottom.

3. Sub-Structure

The probe-bar subtended through a hole in a lid-like disk below the level of the ground plane. The disc filled a circular hole in the plane. Screwed to the disc was a rack and pinion mechanism to which the probe-bar could be fixed, allowing it to be moved up and down by turning a small hand-wheel. A circular tube with a removable bottom section shielded the region through which the probe-bar could move below the ground plane (Fig. 7b).

4. Instruments

A rigid coaxial line was connected to the terminals of the probe-bar (one at a time) and terminated by a matched load. The "B" probe of a Vector Voltmeter (HP-8405A) was inserted into the line. The "A" probe (reference) of the Vector Voltmeter was inserted into a coaxial line which was matched terminated at that side and connected to the signal source via an attenuator and a directional coupler. This enabled the

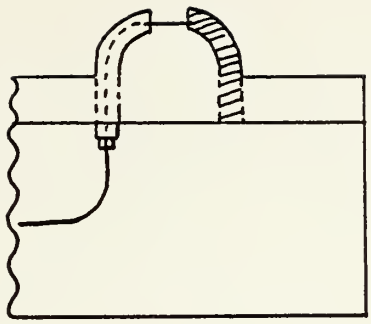

Shielded Loop
Current Probe

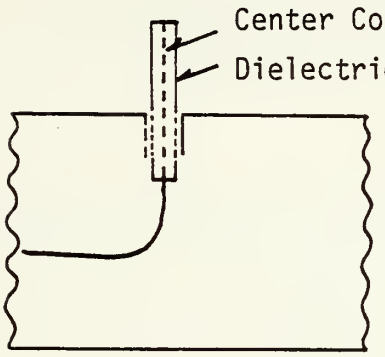

Charge Probe

Figure 5.

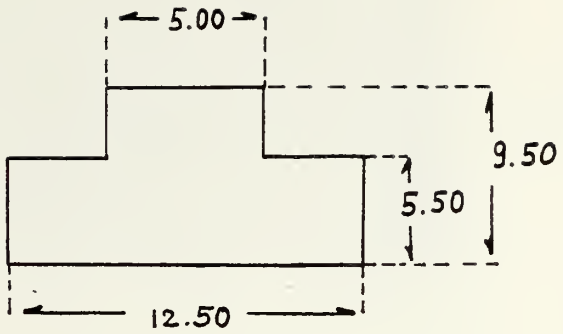

Cross-Section of the Probe-Bar
(Dimensions in mm)

Figure 6.

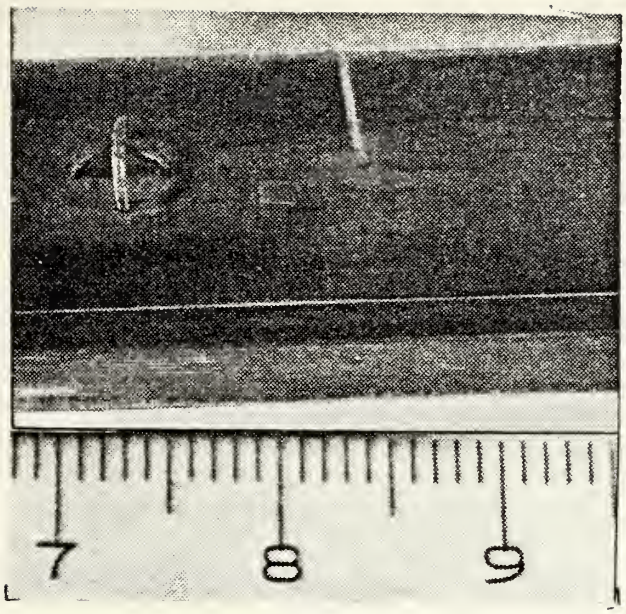

Figure 7a.
Pick-Up Probes

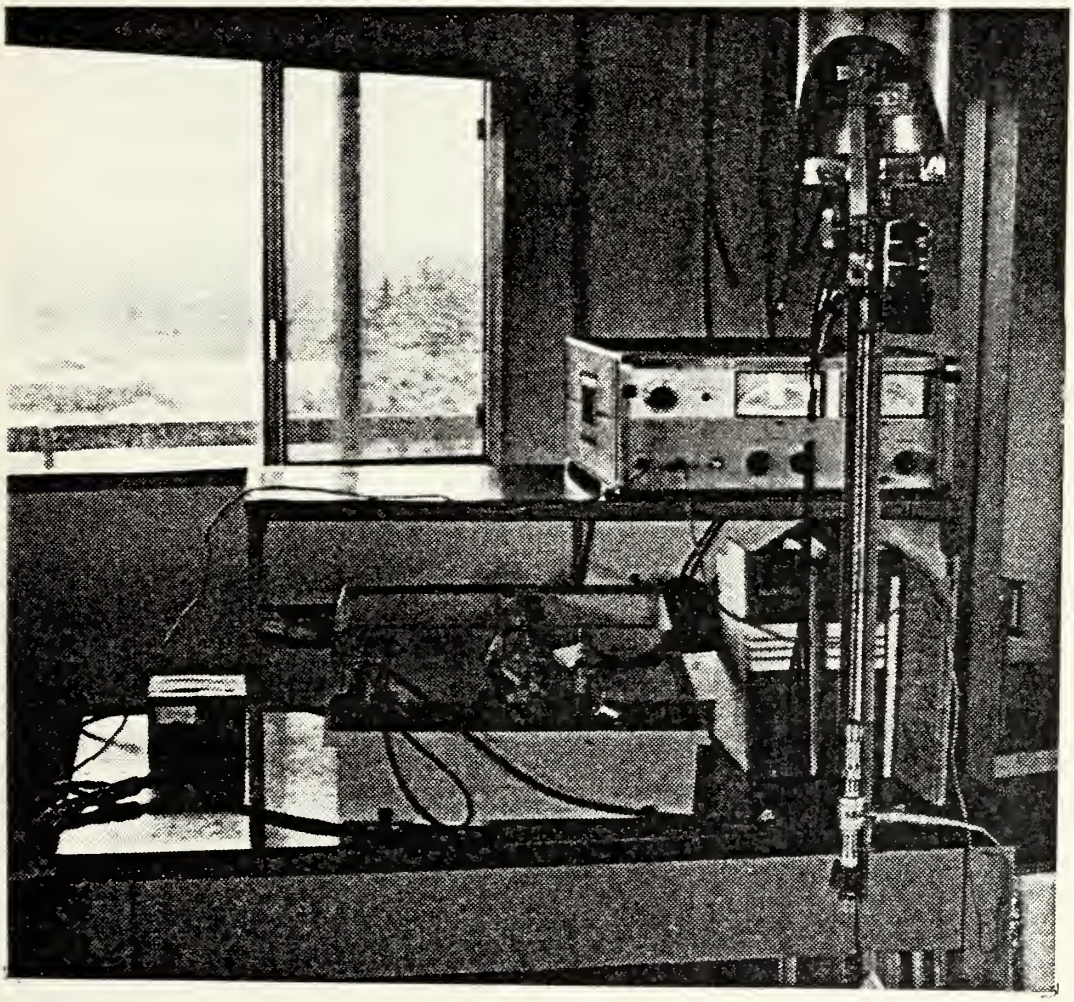

Figure 7b. Part of the Substructure

Vector Voltmeter to measure the relative magnitude and phase of the signal which was received by the surface probes.

Relative magnitude and phase values were fed into an X-Y Recorder (HP 7046), which could monitor two Y values at the same time. The X-axis, taken as the position axis, was controlled by the relative position of the surface probes in the slot. This was done by means of a bridge-circuit with a multi-turn precision potentiometer, which had a tooth-wheel on its axle and was turned by the movement of the rack, that positioned the probe bar in the slot. The potentiometer was spring-mounted to eliminate backlash.

D. PERFORMANCE LIMITATIONS

1. Distortions

The working frequency for the set-up was 300 MHz. Because of other users, the environment was not always free of signals in proximity to this frequency. Antennas of high power transmitters were located very close to the site and, when radiating, caused a considerable threat to meaningful measurements because of harmonic generation and intermodulation in the nonlinear processor of the Vector Voltmeter. It was possible to partly eliminate this kind of interference by avoiding the time of frequency congestion (normal working days).

The power signal source used in the experiment was placed within the shelter under the ground plane, where the measuring instruments were also located. During the initial testing it was observed that the signal source contaminated the shelter with a 300 MHz continuous wave, which was dwelling on the outer conductors of the coaxial lines leading

to the instruments and was processed together with the signal that was received by the surface probes. To counter this effect, a shielding box was placed around the signal source. Its 60 Hz power lead was shielded, too, by a grounded braid. Double shielded and rigid coaxial lines were used. These measures reduced the contamination to an average of one-twentieth the value of the signal delivered by the probes.

When moving the probe-bar along the slot, two distinct positions about $1/4\lambda$ apart caused considerable problems. In these confined locations a signal of far greater strength than reasonable and of uncertain phase was recorded. It was believed, that the lower part of the probe-bar together with other portions of the mechanical system provided resonant conditions for those vagabound currents which were not completely eliminated by the source shielding. This erroneous peaking effect was countered by placing two additional, sliding ground connections next to the probe-bar end and the location where the Vector Voltmeter probe was inserted into the rigid line carrying the received signal. Also a cylin- shield was placed around the sub-structure accommodating rack and pinion.

Another kind of distortion was caused by the fact that no gap-free connection between the plates under test and the ground plane could be made. As mentioned before, the plane had a circular hole necessary to hold different structures for testing, controlling the probe-bar, and to feed signals, either from above or below the plane, through it. The hole was put nearly in the center of the ground plane when this was constructed. The ground plane was slightly slanted to both sides from one of its middle lines for rain drain off. This caused the plates C and D to remain off the ground plane with a portion of the lower edge during

part of the experiment. To increase contact, a special copper tape was used between plate and plane. Vibration caused by moving the probe-bar, wind or heavy traffic from the nearby freeway rapidly changed the air-gap and considerably distorted the readings of the instruments.

Other distortions were caused by sliding electrical contacts which unintentionally and randomly changed their impedance with position. This was true for the contact between the plate and the probe-bar and also for the sliding ground connections mentioned before. This problem was also experienced by researchers at Harvard, who were using very similar T-slots [Ref. 7]. Whereas they improved the contact by silver-plating slots and probe-bar, this author obtained good results by thorough cleaning slots and bar with steel wool and applying a spray-on contact cleaner before each run of the bar through a slot.

The above discussed distortions interfered with the reproducibility of measurements in a way that successive measurements deviated about 5 to 10% in magnitude.

2. Geometric Physical Limitations

a. Only an infinite ground plane can constitute an ideal image plane. The plane used in the experiment measured 10 x 10 Meters^2 and therefore was not ideal.

b. The edge effects of the plates were not evenly distributed as can be observed in Fig. 8. In the direction of arrow "1" the effective aperture had two edges. In the direction of arrow "2" it had four edges; two more because the gap between plate and plane could not be made zero. This, for example, caused plate D to appear not perfectly square in the electromagnetic sense.

c. The current probes were very accurately built, but they deviated very slightly from mutual orthogonality and the Y and Z directions (defined later).

d. The incident wave was only approximately plane and uniform. In reality it had a finite bend resulting from the spherical wave front originating at the monopole. Also a small misalignment between the direction of the E-field and the Z direction was very probable. This could occur because of a small tilt of the monopole and the distortion of the E-field near the feed point.

E. CALIBRATION

Because the current was investigated in two mutual orthogonal directions, it was desirable to calibrate one current probe relative to the other. This was done in the following way (Fig. 9): The probes were placed in the center of a square plate ($.5\lambda \times .5\lambda$), which was lying flat in the center of the ground plane. A 14 Meter (14λ) long very thin wire was threaded through the semi-loops of the current probes and held tight. The wire positioned at an angle of exactly 45° to both probes. A signal of 300 MHz was fed into one end of the wire and adjusted to the level that produced the same magnitude of response in the probe system as experienced when the plate was illuminated by the monopole and corner reflector. Because the angular conditions for both probes relative to the wire were equal, the measured magnitudes and phase relation immediately delivered the desired calibration "factors". The experiment was repeated after the wire was rethreaded to form a 90° angle with its previous direction. This time the phase relation increased by almost 180° between the probes which is understandable considering the relative directions of the induced currents (Fig. 9).

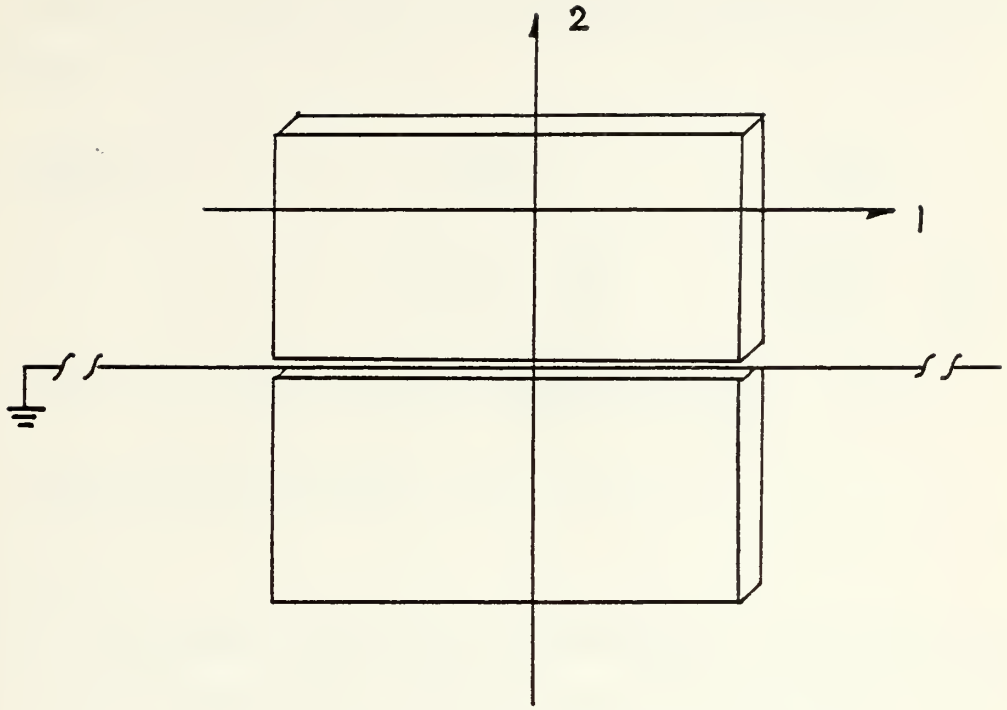

Figure 8. Plate and Image

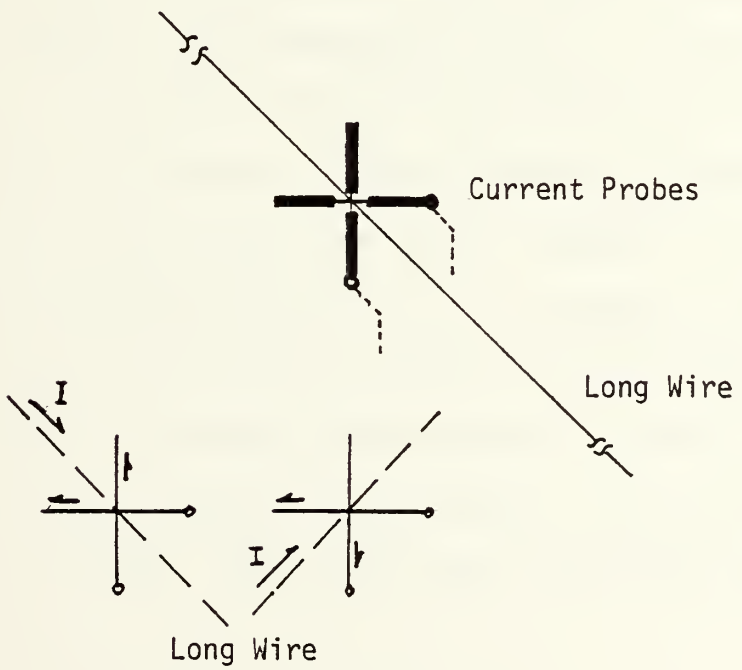

Figure 9. Calibration Procedure

The results of the calibration were as follows (Y and Z corresponds to the direction of normal use in the coordinate system that will be defined later):

Wire Direction	Z - Probe		Y - Probe	
1	.151 mV	26°	.165 mV	21°
2	.177 mV	135°	.191 mV	-44°

average calibration factor (magnitude): $\frac{|Tz|}{|Ty|} = .92$

average phase correction: $\theta_z = \theta_y + 2°$

F. DATA DISPLAY

As described before, the surface distributions of charge and current excited the probes which fed a portion of the received energy into the Vector Voltmeter where it was detected, measured and referenced to the output signal of the driving source. The result was immediately displayed on the X-Y Recorder by electromechanical means. Thus, the way of the sensed signal to the final display on the recorder was direct and instantaneous. Moving the probe-bar caused distortions, as discussed before, which eventually died out when the bar was stopped. This made it necessary to stop recording while the bar was in movement. Instead a stepwise advance was chosen with recordings between the steps (stepsize = .01 Meter, tracklength = .50 Meter), which appeared as points. A total of 15 thousand points were recorded in this fashion. Later the obtained graphs were stacked in groups. This is the form in which they appear in the following chapter.

Magnitude and phase of all presented curves are relative to a common value. This allows immediate cross-referencing not only between the curves of one particular plate, but also between different plates.

III. THEORY AND MEASUREMENTS

A. GENERAL CONSIDERATIONS

1. Geometry of the Problem

The configurations under study were four metal plates, all equal in height and thickness but different in width. They rested on an image plane and were illuminated by a monochromatic electromagnetic uniform plane wave, which had an electric field vector E_{inc} parallel to the vertical edge of the plate, i.e., perpendicular to the surface of the plane. Fig. 10 shows how plate, plane and antenna were placed into the X-Y-Z coordinate system.

2. Non-Experimental Solutions

Other than the thin wire problem, the scattering by a plate is at least two dimensional. It is two dimensional if the (infinite) thin plate is considered, and three dimensional, if the plate is of finite thickness. The three dimensionality makes the problem far more difficult because it involves coupled axial and transverse current components.

The two dimensional case has been studied by several authors, using different approaches:

a. Physical optics or geometrical diffraction theory approach by Mentzer, 1955, Ross, 1966 [Refs. 8, 9].

b. Using a grid mesh as model by Richmond, 1966 [Ref. 10].

c. Using an integral equation by Mittra, Ramat-Samii, Jamnejad, Davis, 1973; Tsai, Dudley, Wilton, 1974 [Refs. 1, 2].

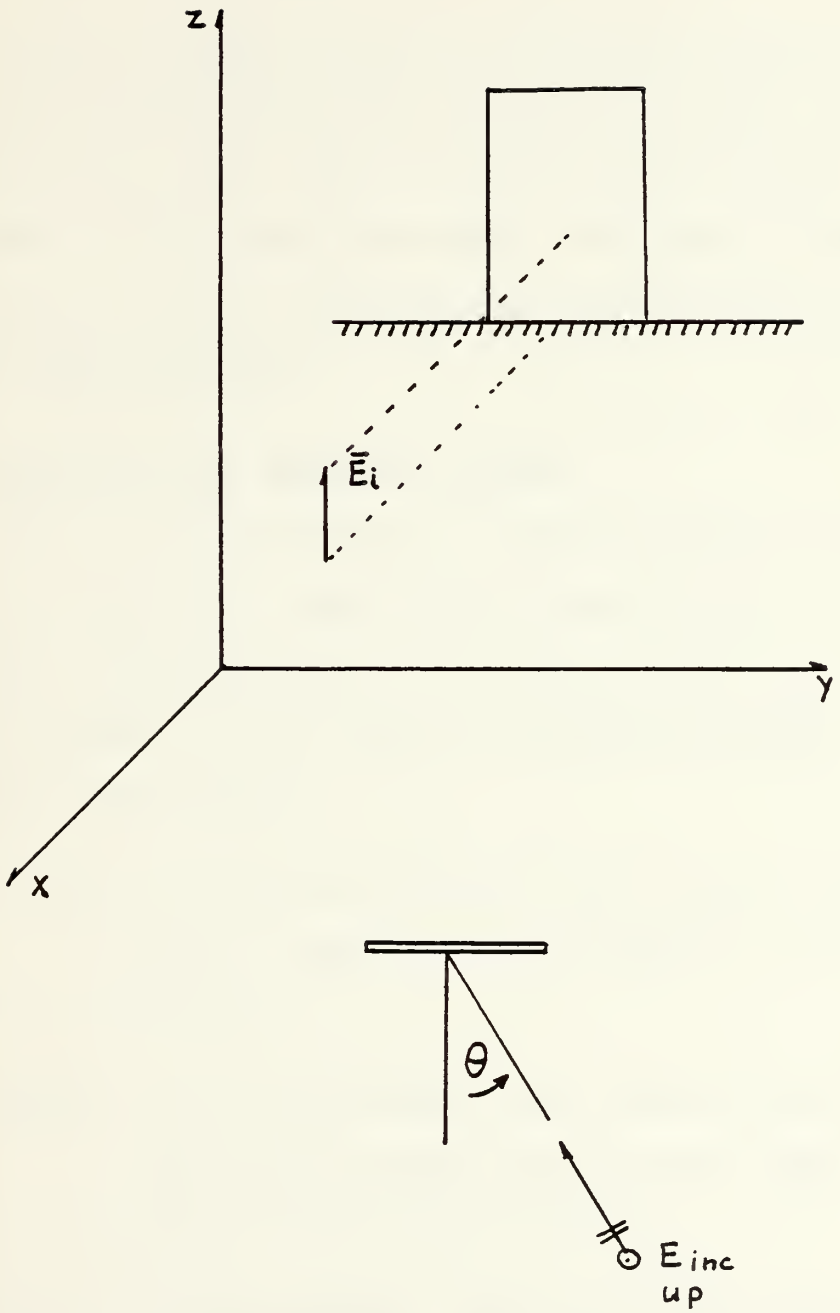

Figure 10. Geometry of the Problem

d. Approach by current patch model, i.e., subdivide the plate into numerous small rectangular areas and use of the piecewise sinusoidal reaction matching technique by Richmond, Wang, 1974 [Ref. 11].

So far no complete solution to the surface charge and current distributions has been published in the sense that either only one current direction was under study, or the charge distribution or the phase calculation (or both) were not presented. This made an experimental research approach meaningful that obtained both, magnitude and phase of surface current and charge.

3. The Role of the Continuity Equation

Since, as mentioned above, no complete theoretical analysis was available to immediately support the experimental results presented in this thesis, it was thought to be useful to try to extract a kind of "data-self-support" directly from the obtained measurements. This was attempted by three methods:

First: By crossexamining data in the Y-direction, that was obtained by sampling in the Z-direction, and test for consistency.

Second: By examining dominant curve shapes (such as those near the edges) and comparison to similar shapes found on different but known structures.

Third: By testing whether charge and current magnitudes satisfy the continuity equation.

Whereas the first and second method are strongly subject to interpretations, the third one is far more objective and therefore the

most powerful tool used herein. Because of the great significance, the continuity equation will be reviewed briefly. More detailed versions are found in most every major text on electromagnetic theory, such as Ref. 12.

The continuity equation follows from the principle, that charges can be neither created or destroyed, although equal amounts of positive and negative charges may be simultaneously created by separation or lost by recombination. If a closed surface is considered, the current through it is $\vec{I} = \oint \vec{J} \cdot d\vec{S}$. (A list of used symbols is given in the appendix). The current flow through the surface must be balanced by a change of charge Q_i within the volume enclosed by the surface.

$$\vec{I} = \oint_S \vec{J} \cdot d\vec{S} = \pm \frac{d\, Q_i}{dt}$$

where the minus sign applies to the outward flow and the plus sign to the inward flow. The above equation is the integral form of the continuity equation, which can be transformed into the point form (or differential form) by using the divergence theorem

$$\oint_S \vec{J} \cdot d\vec{S} = \int_V (\vec{\nabla} \cdot \vec{J})\, dv \ .$$

Applying the relation $Q_i = \int_V \rho\, dv$ yields

$$\int_V (\vec{\nabla} \cdot \vec{J})\, dv = - \frac{d}{dt} \int_V \rho\, dv$$

If the surface is not varied with time, the right hand side of above equation can be written as $\int_V - \frac{\partial \rho}{\partial t}\, dv$

For an incremental volume ∇v the equation

$$(\vec{\nabla} \cdot \vec{J}) \nabla v = - \frac{\partial \rho}{\partial t} \nabla v$$

is obtained, from which follows

$$\vec{\nabla} \cdot \vec{J} = - \frac{\partial \rho}{\partial t} \quad .$$

This indicates that the current, or charge per second, diverging from a small volume per unit volume is equal to the time rate of decrease of charge per unit volume at every point. If this result is related to the surface charge and current on the studied plates, it becomes obvious that the absolute value of the measured charge should increase where the absolute value of the slope of the corresponding current increases. This was examined independently for each plate in the following analysis of the obtained measurements.

4. Policy

Clearly, the three methods described in section III-3 could be applied in different ways because it is possible to look at the presented data in a large scale or in a kind of microscale, where in its extreme, each point is compared with its neighbor. The policy of this analysis was to look sufficiently close at the data but also preserve the overall picture.

Although there was a great temptation to perform smoothing on some of the presented curves, especially where the need was obvious, this was not done because of the aforementioned lack of a complete theory and the risk to unintentionally destroy relevant information.

B. ANALYSIS OF PLATE A

1. Introduction

The geometry of plate A and the corresponding titles and obtained data curves are shown in Fig. 11a, b, c. The length of plate A was

.5λ, the width .024λ, and the thickness .02λ. It had one slot. This plate had the dimensions of a fat rectangular monopole. They were chosen to obtain a kind of intermediate configuration between a fat cylinder (as described by King and Burton in Ref. 13) and the plates of larger width. It also served as a means to compare the magnitudes of current and charge and their phases of an isolated slot to those of a slot imbedded in a wider plate.

2. Surface Charge and Current

Looking at the Z-component of the induced current along the centerline of plate A (Fig. 12), it is noticed that the magnitude curve of the zero aspect angle has a higher value at Z = 0 and falls down with increasing distance from the origin, and the phase advances by approximately 65°. This is exactly the behavior of the axial current of a parasitic (i.e., unloaded and receiving) thin wire antenna, which was theoretically described by King in Ref. 6. A graph is shown in Fig. 15 for comparison.

Since plate A constituted a fat (rectangular) cylinder, suitable means were sought, to make a comparison possible between this plate and the fat (circular) cylinder studied by King, Burton et al in Ref. 13. The two cylinders were not equal in height, and the significance of this difference had to be investigated.

King showed by theory and Burton by experiment [Refs. 6, 14, 15] that the difficult and complex equations for charge and current on a thin parasitic antenna can be approximated by[1] $\vec{I}_z \approx \vec{I}_o \frac{\cos \beta z - \cos \beta h}{1 - \cos \beta h}$ and $\vec{Q}_z \approx \vec{Q}_o \frac{\sin \beta h}{1 - \cos \beta h}$ where $\vec{I}_o$ and $\vec{Q}_o$ are complex functions depending

[1] List of used symbols is given in the appendix.

on h, the incident E-field and the radius of the antenna. Above equations state that a variation of h shifts $\vec{I}_z$ along the coordinate axis, that $\vec{Q}_z$ is not shifted and that both amplitudes are changed. In Fig. 16 charge and current distributions are drawn for six antennas of different heights. The currents are zero at the ends. It can easily be seen, how the distributions are related to each other, if h is changed. For example, if the distributions on an antenna of $h = \lambda/2$ shall be obtained from an antenna of $h = 3/4\ \lambda$, a simple procedure can be applied: The distributions on the longer antenna are truncated at the ends (in this case each end is shortened by $\lambda/4$), the current curve is shifted to yield zero magnitude at the new ends, and the charge curve remains unshifted.

Clearly, this procedure cannot produce exact quantitative results; but, it is sufficient if only curve shapes, rather than their particular values are to be compared.

Applying this concept to the aforementioned cylinders means that the charge and current curves of the longer circular cylinder have to be truncated beyond $z/\lambda = 1/2$ to be comparable to plate A (Fig. 17). (Since the following comparisons address the shape of the curves and their relative positions only, it is not necessary to decide, by what amount the current distribution(s) should be shifted along the coordinate axis after truncation is performed.)

If the measured current and charge distributions on plate A in Fig. 12 and 14 are compared to the theoretical distributions on the fat circular cylinder in Fig. 17, it is observed, that the corresponding curves are similar in shapes. This does not only apply for the magnitude curves but also for the phase curves.

On plate A the maximum magnitude of the current in the Z-direction was higher for the 0° aspect angel than that for the 45° aspect, which in turn was higher than that for the 180° aspect. The charge density magnitude for 0° aspect was lower than that for 180°, whereas the magnitude for the 45° case (and $.25 < Z/\lambda < .40$) was even lower than for the 0° aspect. These observations were reasonably consistent with the theoretical curves in the above mentioned Ref. 13.

Furthermore it can be seen that the experimental current curves for the Z-component considerably differ in shape between the three chosen aspect angles. At 0° aspect the curve minimum lies at $Z/\lambda \approx 1/2$, at 180° aspect the minimum is shifted to $Z/\lambda \approx 3/8$ and is also lower in magnitude. The curve for the 45° aspect locates itself in between the two above extremes. This significant fact is explained by the shadow-illumination difference: The standing wave ratio on the shadowed side (180° aspect) was higher than on the illuminated side (0° aspect), which is expressed by the greater flatness of the curve on the illuminated side. Therefore, compared to the shadowed side, the behavior of the current on the illuminated side resembled more that of a forced current. This occurred because the scattered H-field and the incident H-field were measured together on the illuminated side, whereas on the shadow side only the scattered H-field was measured. The 45° case constituted a transition between the 0° case and the 180° case because here, the scattered H-field was measured together with $\sqrt{2}/2$ the value of the incident H-field of the 0° case. (Clearly, this effect could not be observed with the charge probe, since it was always perpendicular to the incident field.) The magnitude of the Y-component of the current was very small in all three aspects (Fig. 13).

By comparing the charge density curves along the Z-direction with the current in the Z-direction it becomes immediately obvious, that the continuity equation was qualitatively satisfied. Since the current in the Y-direction was so small compared to that in the Z-direction, it did not contribute substantially to the total (surface) current. Thus, the divergence of the total current occurred almost exclusively in the Z-direction, and the continuity equation simplifies to $\frac{\partial J}{\partial z} = \frac{\partial \rho}{\partial t}$. This means on plate A for example the maximum absolute value of the charge density had to be coincident with the steepest slope of the current in the Z-direction. Consider Fig. 12 and 14. The current curves for the three aspect angels have their steepest slope at $Y/\lambda = .25$, where the three corresponding charge density curves have their maxima.

C. ANALYSIS OF PLATE B

1. Introduction

Plate B had a height of $.5\lambda$, a width of $.25\lambda$ and was $.02\lambda$ thick. The distribution of the slots, the titles and the labels of the obtained graphs are shown in Fig. 18 a, b, c. Measurements were taken for 0° and 180° aspect angles. The geometry of the plate naturally divides along the Z axis into two symmetric parts of width $.125\lambda$ each. Because of the symmetry argument, measurements were taken only slightly beyond half-width of the plate.

2. Plate B at 0° Aspect Angle

a. For this angle the magnitude curves of the current in the Z-directional experience a gradual change from the outer Z-edge going inward to the middle of the plate (Fig. 19, 20). The current curve nearest to the edge is very similar to that obtained with plate A, but consider-

ably lower in magnitude. Towards the middle of the plate, the curves flatten out but preserve their parasitic nature. The form of the corresponding phase curves is similar to that found on plate A. Sampled in the Y-direction, their position remains essentially constant for all slots. To visualize the overall picture, a generalized three dimensional (3-D) current plot is shown in Fig. 29.

b. The magnitude of the current component in the Y-direction was only about one tenth of that in the Z-direction (Fig. 21). Its contribution to the total surface current was therefore very small. The obtained magnitude curves are very smooth whereas the corresponding phase curves (Fig. 22) make greater excursions between $Z/\lambda = 1/8$ and $Z/\lambda = 3/8$, which are not meaningful when compared to the corresponding curve with plate A. It is therefore doubtful whether these excursions really occurred on the plate. More probable is that they were caused by instrumental limitations; i.e., the signal was too weak for reliable phase measurements.

c. The magnitudes of the two current components were sampled parallel to the Y-axis at different distances from $Z = 0$ (Fig. 26). The curve belonging to the Z-component shows a great increase in magnitude towards the Z-edge of the plate, but is flat in the remaining portion. The other curves in the same graph behave similar, but have consecutively decreasing peaks at the Z-edge. The Y-component decreases near the Z-edge and remains essentially constant over the middle portion of the plate.

d. Regarding the surface charge density (Fig. 23, 25), it is noted that the magnitude and phase curves are very similar to the corresponding curves obtained with plate A. To show the overall surface

charge density a contour plot was drawn (Fig. 28), which indicates that the measured charge density behaved like a warped or curved sheet with a pronounced maximum near the Z-edge, between Z/λ = .25 and .30, and a sub-maximum at the upper Y-Z corner. The minima are denoted by the lower "1" -line and the upper "2"-line. To visualize the overall picture, a generalized 3-D plot is shown in Fig. 30. Regarding the Z-component of the current and the charge density together, it is obvious that the continuity equation is qualitatively satisfied because the highest current and the highest charge density variation occurred together near the center of the Z-edge. Furthermore, the current was low towards the geometric center of the plate where the charge density underwent no variation.

3. Plate B at 180° Aspect Angle

a. For this angle, the magnitude curves of the current in the Z-direction (Fig. 31) flatten towards Y/λ = 0, similar to those in the 0° aspect case, (except curve no. 4, which has to be mentally smoothed to fit into the picture). Consistently it is observed that (after a little smoothing) the curve nearest to the Z-edge resembles the corresponding one obtained with plate A. The explanation for the noticeable trough near Z/λ = 3/8 is similar to that given for plate A and stems from the illumination vs. shadow argument given there.

The phase curves of the current in the Z-direction (Fig. 32) comply in shape with the corresponding one measured with plate A, except for the middle portion, where they show a broad peak. Sampled in the Y-direction, their positions shift slightly, about totally 15°.

b. For the current in the Y-direction (Fig. 33, 34) the same arguments apply as given for the 0° aspect angle.

c. The current profile (sampled in the Y-direction) (Fig. 27) shows great similarity to the 0° aspect case, but the maxima are lower. No immediate explanation can be given for the trough occurring with curves no. 8 and 9 near $Y/\lambda = 0$ and it is believed that this was an erroneous measurement which should be smoothed.

d. The charge density contour plot (Fig. 36) is similar to that of the 0° aspect, but the magnitudes are considerably higher especially near the Z-edge. This is consistent with the behavior of the charge density described with plate A. By the same argument given for the 0° aspect case, it can be shown that the continuity equation is satisfied for the shadow region also.

D. ANALYSIS OF PLATE C

1. Introduction

The geometry of plate C together with the slot distribution, the titles and the labels of the graphs are shown in Fig. 37 a, b, c. Height and width of this plate were both equal to $\lambda/2$, the thickness was $.02\lambda$. Measurements were taken for three aspect angles: 0°, 45°, 180°.

2. Plate C at 0° Aspect Angle

a. The current in the Z-direction showed strongly parasitic behavior, consistent with plates A and B. The magnitude curve belonging to the slot nearest to the Z-edge has a far greater excursion than the curves obtained from inside slots, which gradually flatten towards $Y = 0$ (Fig. 38). This and the stability of the phase (Fig. 39) was also observed on plate B (cf. Fig. 29).

b. The current in the Y-direction was higher in magnitude than observed on plate B (Fig. 40). Sampling parallel and very close to the

upper Y-edge it is noticed that this current component increased near the Z-edge and decreased towards the middle portion. This tendency is far more pronounced than with plate B, where it was barely noticeable at 180° aspect angle. The phase of the current in the Y-direction (plate C) was very stable. The curves (Fig. 41) show a slight phase advance for higher Z-values which is consistent with plates A and B.

c. The current profile (sampled in the Y-direction) is shown in Fig. 42. The behavior of the Z-component is readily identified to be consistent with plate B. The profile of the Y-component shows higher magnitude and variation than observed with plate B. This is related to the greater width of plate C and the argument, that in general a current can only have a noticeable "profile" if the structure has a sufficient length compared to the wavelength.

d. The charge density curves (Fig. 44, 45) are consistent with those on plate A and B and show a very smooth and gradual development which is also reflected in the contour plot (Fig. 46). The overall magnitude of the charge density was higher than for plate B. Again two maxima are noticed, one slightly above the middle of the Z-edge, the other at the upper Y-Z corner. Very smooth continuous lines were obtained towards the middle of the plate. A broader submaximum is observed in the middle of the upper Y-edge. (Compare to Fig. 30.) The continuity equation is satisfied by the same argument given with plate B.

3. Plate C at 180° Aspect Angle

a. For the current in the Z-direction a striking correspondence to plate A (and thereby to the fat circular cylinder) and also to plate B is noticed. This is especially expressed in the location of the minimum

of the magnitude curve nearest to the Z-edge and the pronounced phase change at the same location (Fig. 47, 48).

If slots 1 to 11 are considered together, it is observed that the minima of the current curves (magnitude, Z-direction) shift towards $Z/\lambda = 0$, whereas the corresponding phase changes decrease in steepness. For reference purposes, some theoretical results for the fat circular cylinder, which has been cited earlier in this thesis, are redrawn in Fig. 54 a, b. If the behavior of the curves of the cylinder and the plate are compared, (starting at $\Theta = 180°$ with the cylinder and slot 1 with the plate), a very distinct similarity between both structures is observed. If the particular transitions of the curve shapes are considered, the plate appears as an unrolled cylinder.

b. The current in the Y-direction qualitatively agreed in phase with the results found on plates A and B (Fig. 49, 50). However, the magnitude curves show a very broad maximum in their middle sections, which is higher than observed with plate B, whereas no such maximum occurred with plate A. This is explained by the phenomenon of coupling between the Z- and Y- components of the current. Experiments with crossed dipoles [Ref. 16] showed, that certain conditions have to be met in order to obtain coupling. One such condition is resonant or near resonant length, which was satisfied by the width of plate C but not plates A and B. (Compare to section III E 2b.)

c. The obtained current profile (sampled in the Y-direction), (Fig. 43) is in intimate agreement with the $0°$ aspect case of the same plate and the described aspect angles of plate B. The maximum current in the Z-direction, too, was lower on the shadowed side than on the illuminated side. (Compare Fig. 29.)

d. The charge density curves (Fig. 51, 52) and the contour plot (Fig. 53) are similar to the illuminated side. Again smooth continuous contours were obtained. (Compare Fig. 30.) The continuity equation is satisfied by equal arguments as given for the illuminated side before.

4. Plate C at 45° Aspect Angle

It was necessary for this case, that the distributions were measured over the whole width of the plate, because it was expected that the symmetry argument would not hold.

a. The current in the Z-direction was measured to be highest at the Z-edges and decreased in magnitude towards the middle of the plate (Fig. 55). This and the parasitic shape is strongly analogous to the results that were found for the other aspects of this plate and plate B. The maxima of this current component at the two edges were measured to be different from each other. The edge nearer to the source carried the higher current.

Since the probe system did not change its position relative to the ground plane and the antenna, but instead the plate was moved stepwise to cover all indicated slots, a phase error was introduced into the measurements. This occurred because the plate was advanced relative to the direction of propagation of the incident field about a total distance equal to $\sqrt{\text{width}/2}$. Therefore the phase of each slot was corrected later by an amount resulting from the corresponding free space advance of the incident field.

The phase curves of the current in the Z-direction (Fig. 56) show a gradual progression in the Y-direction and agree in shape with those obtained at the other aspect angles of this plate and plate A and B

(besides a ripple in most middle sections, which is believed to be caused by instrumental difficulties).

b. The current in the Y-direction (Fig. 57) was found to be essentially higher in magnitude along the upper Y-edge than for the 0° and 180° aspects. This was expected because the Y-edge (for the 45° case) had a projection of $\sqrt{2}/4\ \lambda$ on the line describing the direction of propagation, whereas for the 0° and 180° aspects this projection was zero. The magnitude curves rise towards the upper Y-edge, similar to the corresponding aspect angle with the fat cylinder in Ref. 13. The phase curves undergo the same transitions as was described for the current in the Z-direction of this plate (Fig. 58).

c. The current profile (sampled in the Y-direction) (Fig. 29) shows a higher magnitude of the current in the Z-direction on the Z-edge facing the source (as mentioned before) and is recognized to be very consistent with the profiles that were analyzed before. The curve of the current in the Y-direction shows a broad maximum in the middle section and falls off towards the Z-edges. The value obtained with slot 3 (near $Z/\lambda = 1/4$) seems to be a little too high and should be smoothed to get the right picture.

d. The charge density plot (Fig. 62) shows smooth, continuous contours, very consistent with the previously analyzed charge density plots. A slightly distorted symmetry is noticed. It is observed, that the Z-edge facing the source carried less charge near $Z/\lambda = .25$ than the opposite edge. This is understood, if the corresponding current curves no. 1 and no. 20 in Fig. 55 are compared. The slope of curve no. 1 is greater than the slope of curve no. 20. Since the current in the Y-

direction was very small compared to the current in the Z-direction, the continuity equation simplifiers to $\frac{\partial J_z}{\partial z} = -\frac{\partial \rho}{\partial t}$. This indicates that the steeper slope in the curves of the current in the Z-direction must coincide with greater magnitude of the charge in the same location. This occurred exactly on the Z-edge, which was not facing the source.

E. ANALYSIS OF PLATE D

1. Introduction

The charge and current distributions on plate D were investigated for the three aspect angles 0°, 45° and 180°. The geometry of the plate, slot distribution, titles and labels of the graphs are given in Fig. 63 a, b, c. The thickness of the plate was .02λ, the height .5λ and the width 1λ. Thus, the plate D formed a 1λ square conducting surface when taken together with its image. Contrary to the other plates discussed before, some theoretical results have been available [Refs. 1, 3, and 17] and are taken for comparison. As stated in section II D 2, the width of this plate constituted a kind of upper limit of suitability for the relevant physical system. Therefore although generally very smooth, some of the presented curves show less measurement stability than observed with the smaller plates before. However, this is no handicap because the general character of the curve shapes can readily be recognized in all cases.

2. Plate D at 0° Aspect Angle

a. The current in the Z-direction showed a clear agreement with the parasitic nature described with plate A (Fig. 64, 65). The growing flatness of the curves, sampled from the Z-edge towards the middle of the plate and the behavior of the corresponding phase curves is consistent with plates B and C. (Compare Fig. 29).

b. The magnitude of the current in the Y-direction (Fig. 66) was consistent with the results found on plates A, B and C, if the excursions near $Z/\lambda = 1/4$ were neglected. These excursions were far less pronounced near the Z-edge and changed to greater values toward the middle of the plate. They are interpreted as the manifestation of a certain coupling process between the X- and Y-components of the currents. No theoretical or experimental study of coupling on (square) plates has been published to this date. Ref. 16 gives insight into the coupling process between the members of a crossed dipole, from where can be deduced that resonant (or near resonant) conditions and particular relations between charge and current distributions have to be met simultaneously, in order to get coupling. In a simplified way of looking at it, the Z-component can be regarded as driver of the Y-component. As shown in the above reference, driving can be understood to be initiated by current peaks as well as charge peaks. The same argument suggests itself for the plate, if the peaks of the corresponding distributions are compared with each other.

Consider Fig. 69. The charge density curves have pronounced maxima near $Z/\lambda = .25$. The corresponding curves for the current in the Y-direction have maxima between $Z/\lambda = .25$ and $Z/\lambda = .35$ [Fig. 66], where the charge density curves are still very high in magnitude. Therefore, the charge can be assumed as the driver of the current in the Y-direction.

c. The current profile (sampled in the Y-direction) (Fig. 68) shows a profound similarity to those obtained for plates B and C (Z-component). Curve no. 2 has a high spot between $y/\lambda = 1/4$ and 0. If it were eliminated, this curve would agree better with curves no. 3 and 4 which show a kind of ripple, the significance of which will be explained

later. The Y-component exhibits a magnitude decrease at the Z-edge and the middle of the plate with a broad maximum in between.

d. The charge density contours (Fig. 71) are very smooth and very consistent to plates B and C. Again it is noticed that a submaximum developed near the middle of the upper Y-edge. The continuity equation is satisfied by the same argument given for plates B and C.

e. Figure 72 shows a comparison between the experimental results and those which were theoretically obtained for a square plate of the same length but infinitely thin [Ref. 1]. The agreement between theory and experiment is obvious, if some minor differences are explained. The theoretically predicted singularily of the current in the Z-direction did not happen becuase of the plate's thickness. (Also, it was not possible to measure directly on the Z-edge.) This is in correspondence with calculations performed by Tsai, Dudley, and Wilton for plates of various thicknesses (Fig. 73), [Ref. 2], and can be explained, if the neighborhood of the edge is examined there.

Also shown is the result, which was obtained by the current-patch-model in Ref. 3, which shows ripples in the Y-component of the current similar to those found in the experiment.

3. Plate D at 180° Aspect Angle

a. The magnitude of the current in the Z-direction (Fig. 74) experienced the same dip as was already described for the same aspect of plate C. The corresponding phase curves (Fig. 75) show the similar kind of flattening found there. Therefore the same argument given in section III D 3a applies, that this side of the plate behaved in the described manner like an unrolled fat cylinder. (Compare Fig. 29.)

b. The magnitude of the current in the Y-direction (Fig. 76) was consistent with the results obtained with the plates discussed before and the illuminated side of this plate. However, the phase curves (Fig. 77) experienced a transition from a shape very similar to that observed with plate A to the mirror image of that shape (near the Z-edge).

c. The current profile (sampled in the Y-direction) was similar to the illuminated side and plates B and C (Fig. 78). Curves no. 2 and 4 show slight ripples, similar to the ripples which were observed for the 0° aspect of this plate. Curve no. 3 appears distorted in its middle section. Again, the maximum of the Z-component was noticeably smaller than on the illuminated side, whereas the Y-components of both sides were almost the same in magnitude.

d. The charge density plot (Fig. 81) closely resembles that of the 0° aspect case of plate D and also those obtained with plates B and C. The fact that the "10"-line forms two islands is of no major significance, because the "9"-line, if drawn, would be similar to the "10"-line in the 0° case.

4. Plate D at 45° Aspect Angle

a. The current in the Z-direction (Fig. 82, 83) behaved as was found for plates A, B and particularly C. The parasitic nature and the flattening effect noted before are readily seen in the presented graphs.

b. The current in the Y-direction was considerably higher than found on the other plates (Fig. 84, 85). This indicates how big the role was played by the length of the projection of the Y-edge onto the direction of propagation of the incident field. This length was doubled compared to the 45° aspect case of plate C, and measured $\sqrt{2}\lambda$. A pro-

nounced increase of this current component towards the upper Y-edge was noticed. If the corresponding phase curves were accurately smoothed, they would show the same transition in the Y-direction as was discussed for the 180° aspect angle.

c. The current profile (sampled in the Y-direction) (Fig. 86) is in agreement with the cases discussed before. Again, the maximum of the current in the Z-direction was higher on the Z-edge that was nearer to the source.

Near the upper Y-edge, the current in the Y-direction had two pronounced maxima. The maximum nearer to the source was a little higher. The actual current was antisymmetric as can be seen from the phase shift (Fig. 85). The magnitude curve appears slightly shifted towards the negative Y-side, which also occurred with the corresponding curve and plate C.

d. The charge density plot (Fig. 89), again, is very consistent with the plots discussed previously, especially with plate C. The contours are not symmetric about the Y-axis. The charge density was higher at the Z-edge, which was not facing the source. This is consistent with the continuity equation, from where it was expected that the higher measured charge density coincided with the greater divergence of the current. (Since the current in the Y-direction was far smaller than in the Z-direction, it did not contribute substantially to the total current and was not considered in this argument.) Compare curves no. 1 and 40 in Fig. 82. It is obvious that curve no. 1 has the greater slope (middle section), justifying the greater charge density on this Z-edge.

e. Figure 90 compares the measured current (experiment) and the theoretical current computed by Mittra et al in Refs. 1 and 17. Although the experiment used a moderately thick plate (thickness = 0.023λ) and the theoretical result was obtained for an infinitely thin plate, they show an intimate relationship.

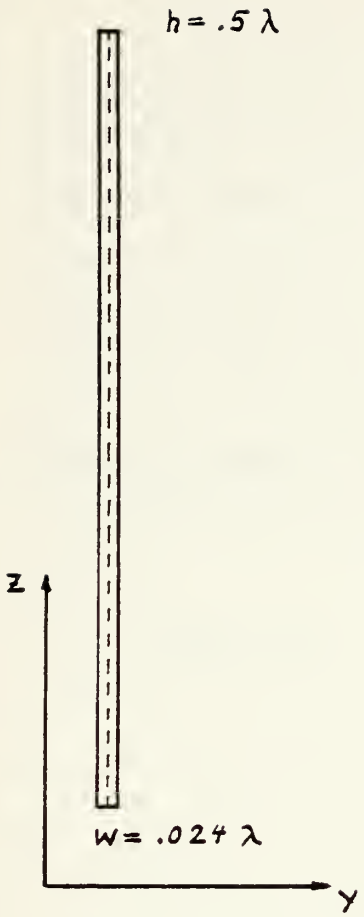

Figure 11a. Plate A

TITLE (PLATE A)	FIGURE
Measured current in Z-direction	12
Measured phase of current in Z-direction	12
Measured current in Y-direction	13
Measured phase of current in Y-direction	13
Measured charge density	14
Measured phase of charge density	14

Figure 11b. Titles of Graphs of Plate A

Current	Charge Density	Component			Sampling Direction		Magn.	Phase	Figure and Aspect		
		Y	Z	Total	Y	Z			0°	180°	45°
X			X			X	X		12	12	12
X			X			X		X	12	12	12
		X				X	X		13	13	13
		X				X		X	13	13	13
	X			X		X	X		14	14	14
	X			X		X		X	14	14	14

Figure 11c. Labels of Graphs (Plate A)

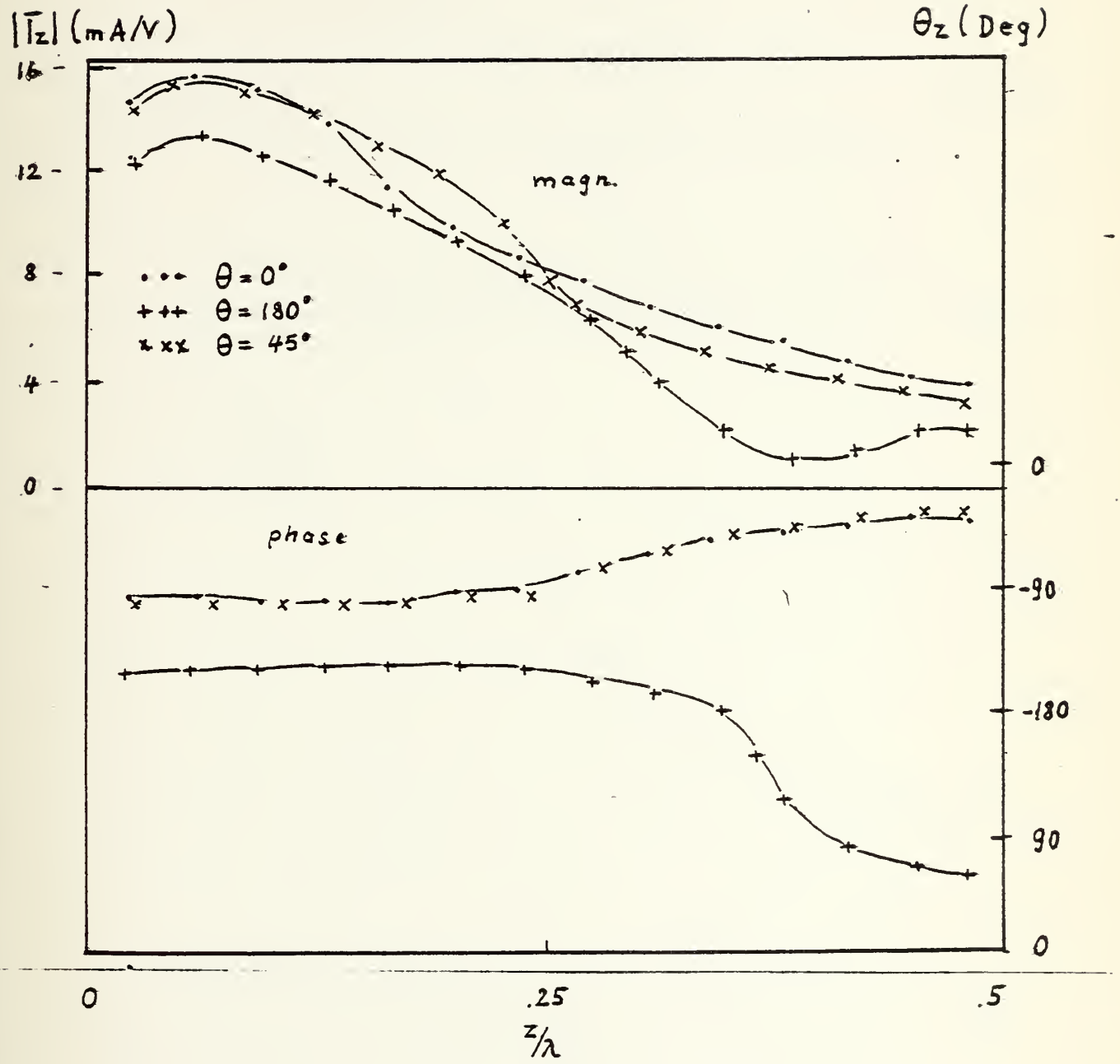
|Iz| (mA/V)
θz (Deg)
16
12
8
4
0
magn.
• •• θ = 0°
+ ++ θ = 180°
x xx θ = 45°
phase
0
-90
-180
90
0
0
.25
.5
z/λ

Figure 12.

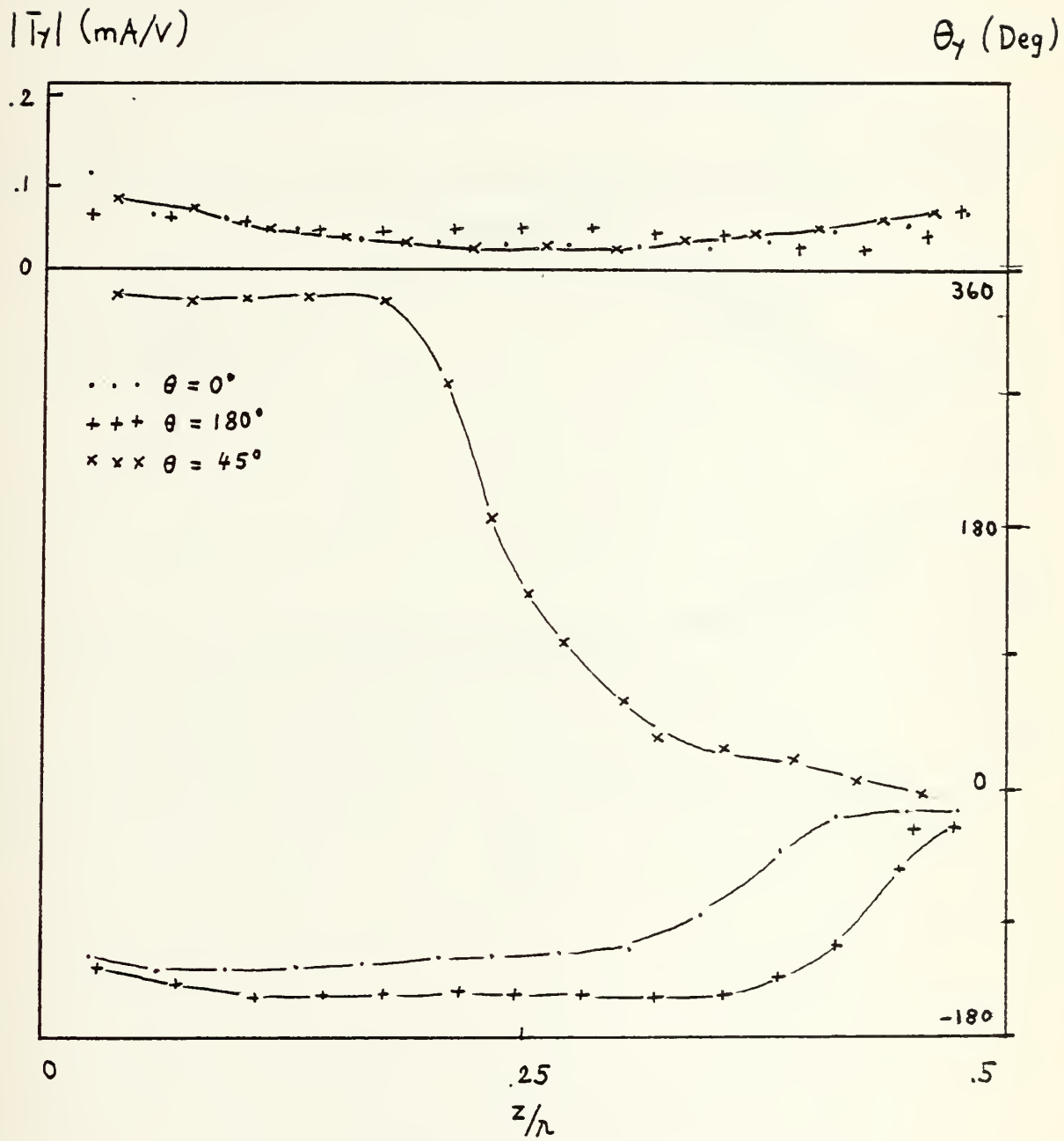

Figure 13.

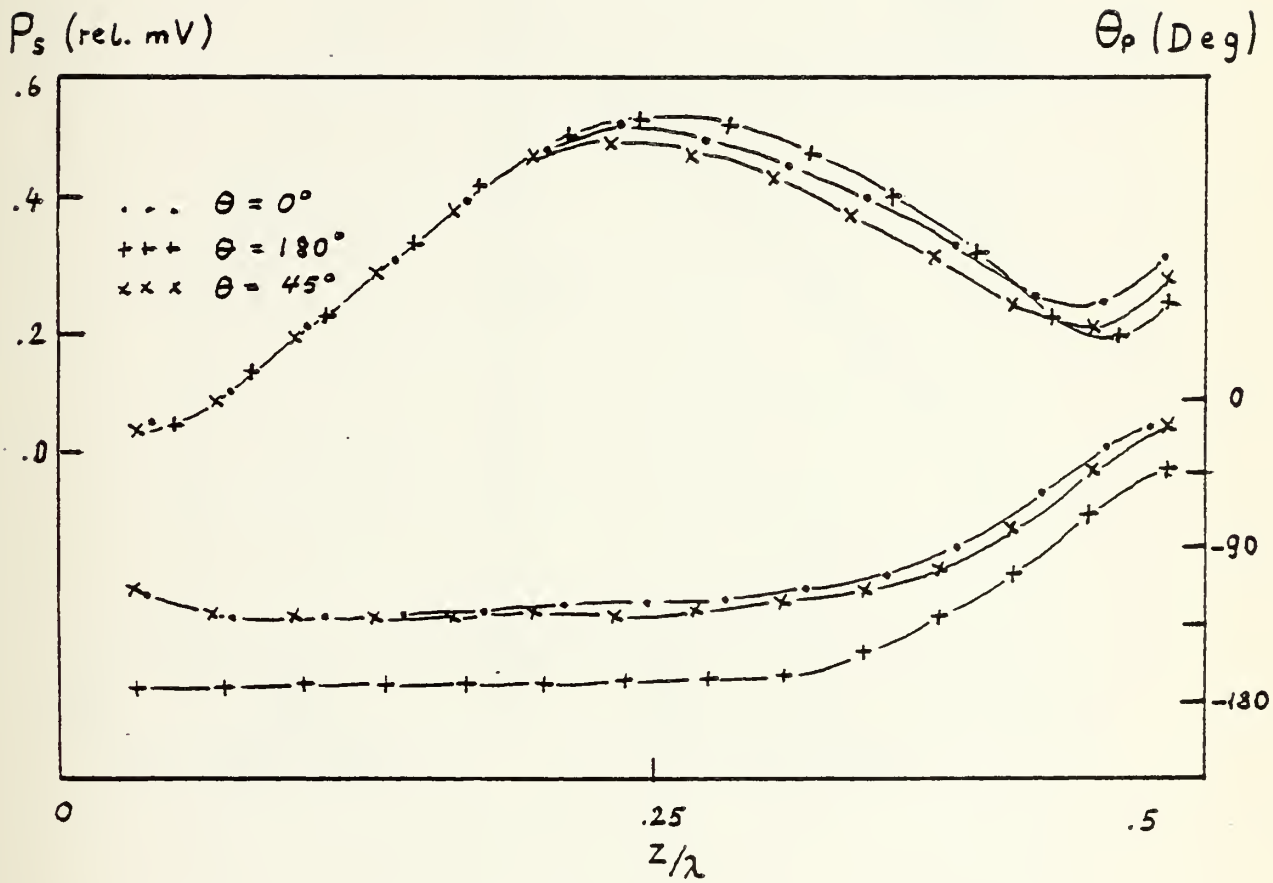

Figure 14.

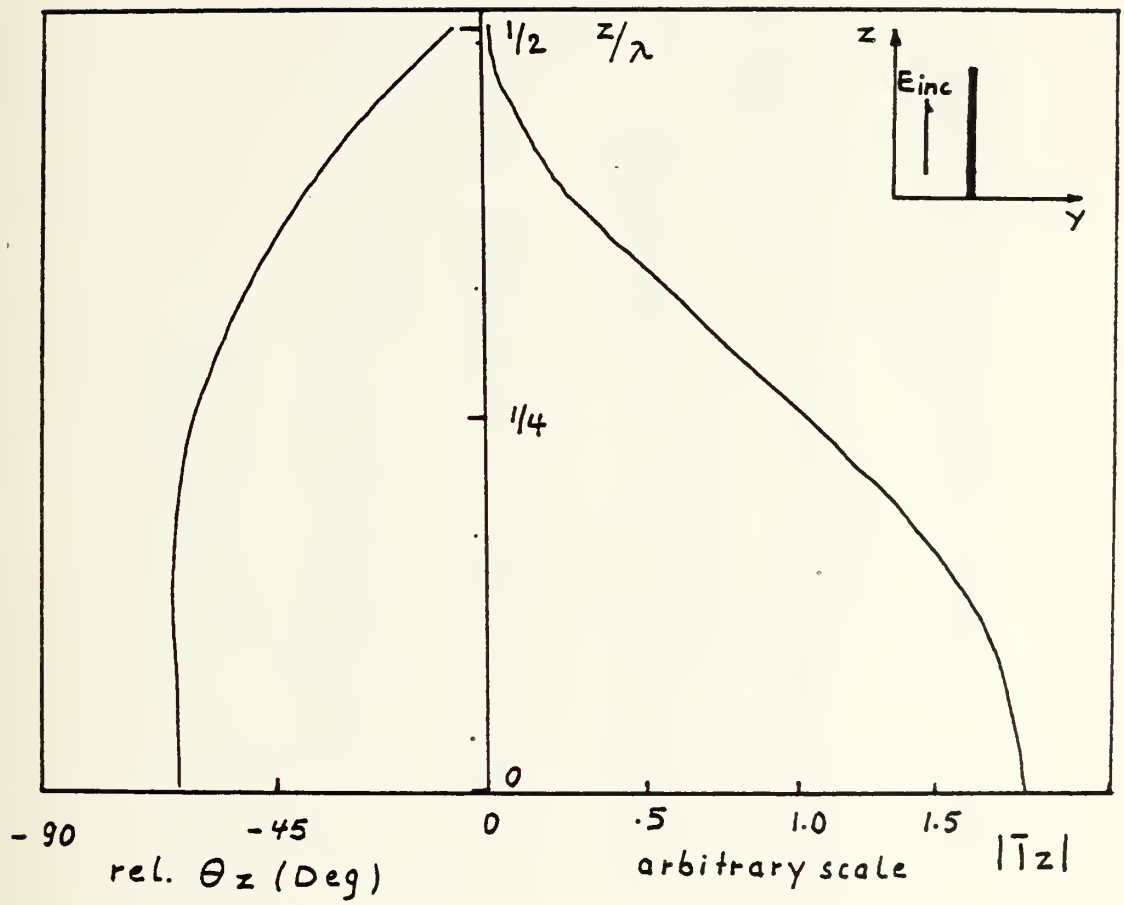

Figure 15. Axial Current on a Thin Parasitic Antenna of Halflength Equal to λ (King)

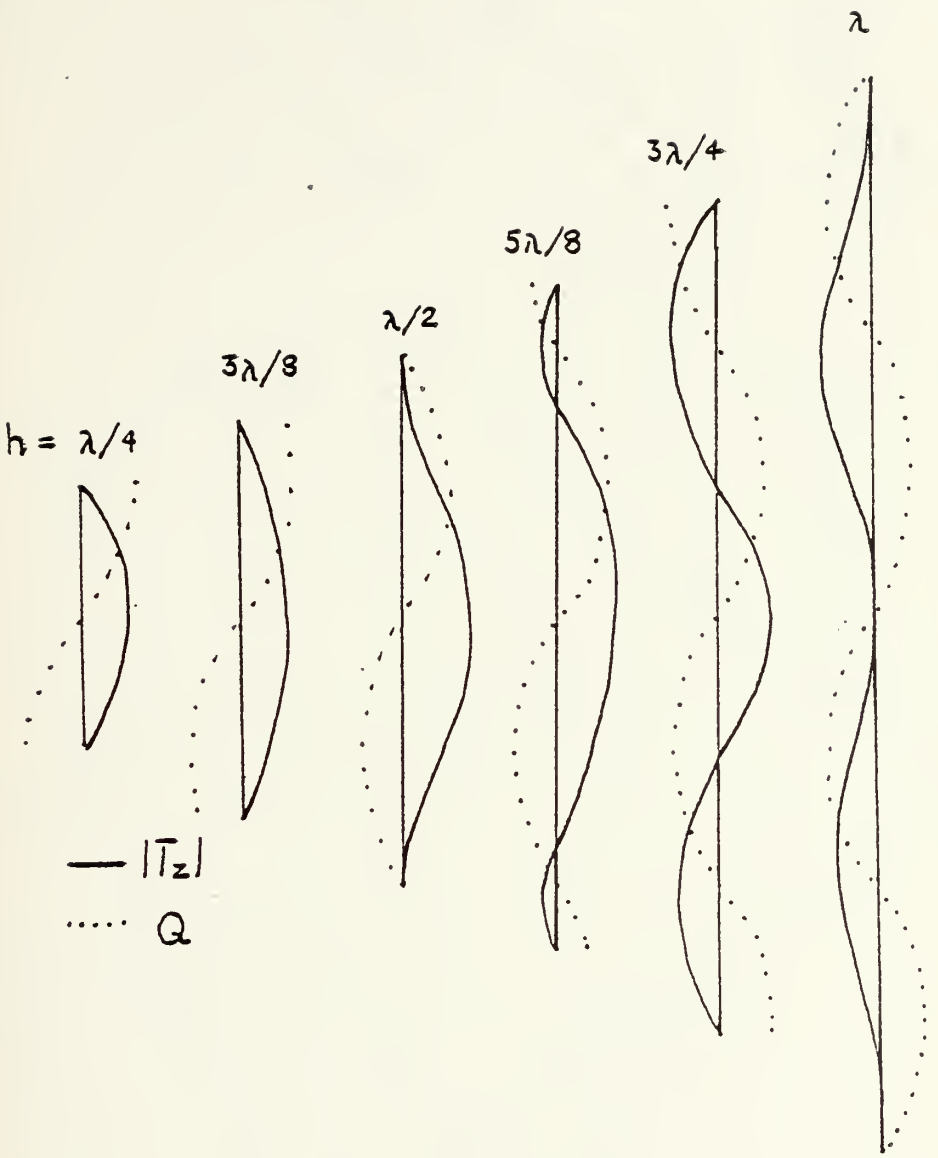

Figure 16. Distribution of Current and Charge Along Parasitic Antennas of Different Half-lengths (h) (Amplitudes of successive antennas not to scale)

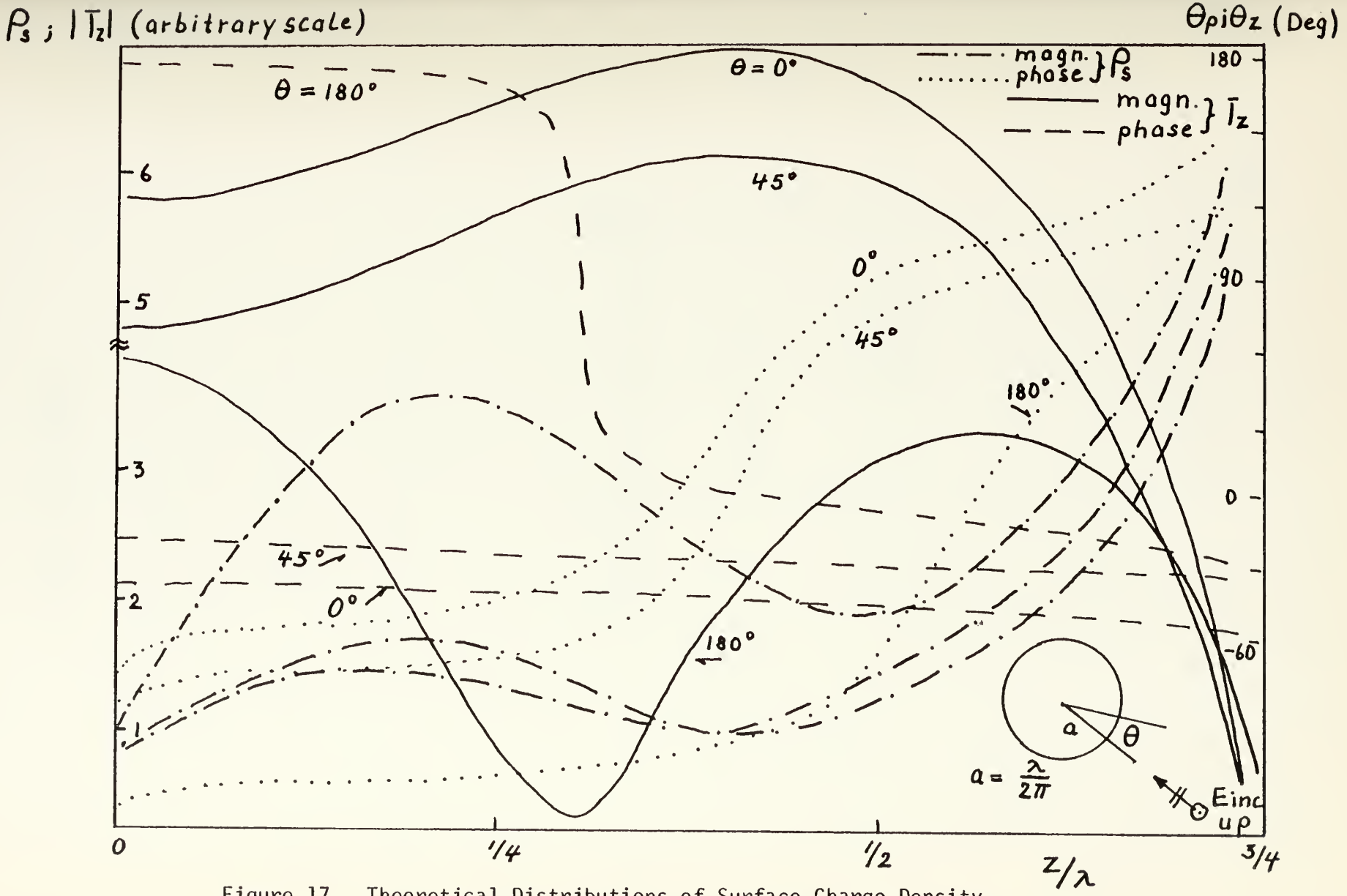

Figure 17. Theoretical Distributions of Surface Charge Density and Current on a Fat Circular Cylinder (King, Burton et al.)

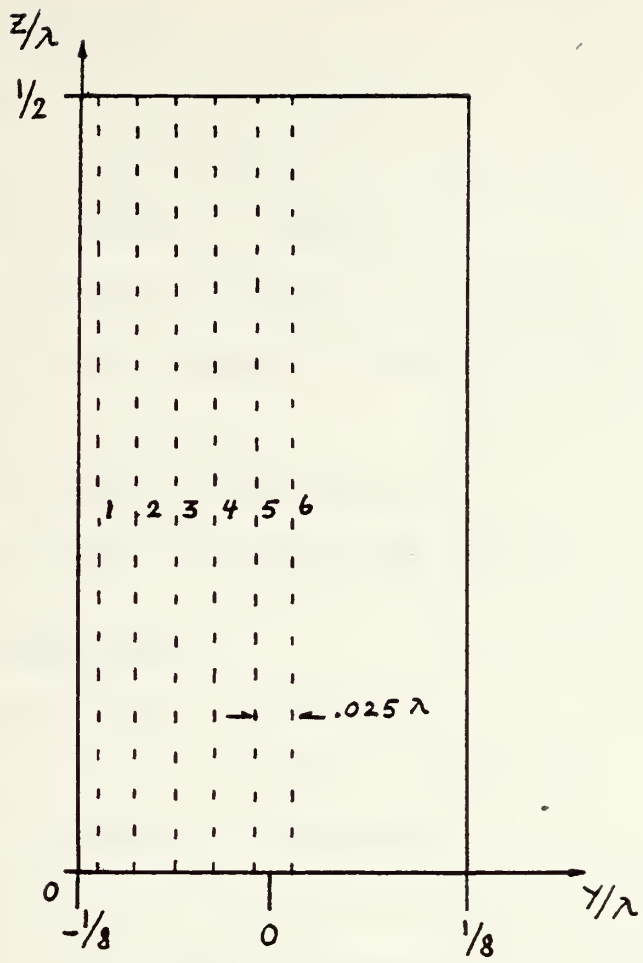

Figure 18a. Plate B

TITLE (PLATE B)	FIGURE
0° Aspect Angle	
Measured current in Z-direction	19
Measured phase of current in Z-direction	20
Measured current in Y-direction	21
Measured phase of current in Y-direction	22
Profile plot of measured currents in Y- and Z-direction	26
Measured charge density	23
Measured phase of charge density	25
Contour plot of measured charge density	28
180° Aspect Angle	
Measured current in Z-direction	31
Measured phase of current in Z-direction	32
Measured current in Y-direction	33
Measured phase of current in Y-direction	34
Profile plot of measured currents in Y- and Z-direction	27
Measured charge density	24
Measured phase of charge density	35
Contour plot of measured charge density	36

Figure 18b. Titles of Graphs of Plate B

Current	Charge Density	Component			Sampling Direction		Magn.	Phase	Figure and Aspect		
		Y	Z	Total	Y	Z			0°	180°	45°
X			X			X	X		19	31	
X			X			X		X	20	32	
X		X				X	X		21	33	
X		X				X		X	22	34	
X		X	X		X		X		26	27	
	X			X		X	X		23	24	
	X			X		X		X	25	35	
	X			X	X	X	X		28	36	

Figure 18c. Labels of Graphs (Plate B)

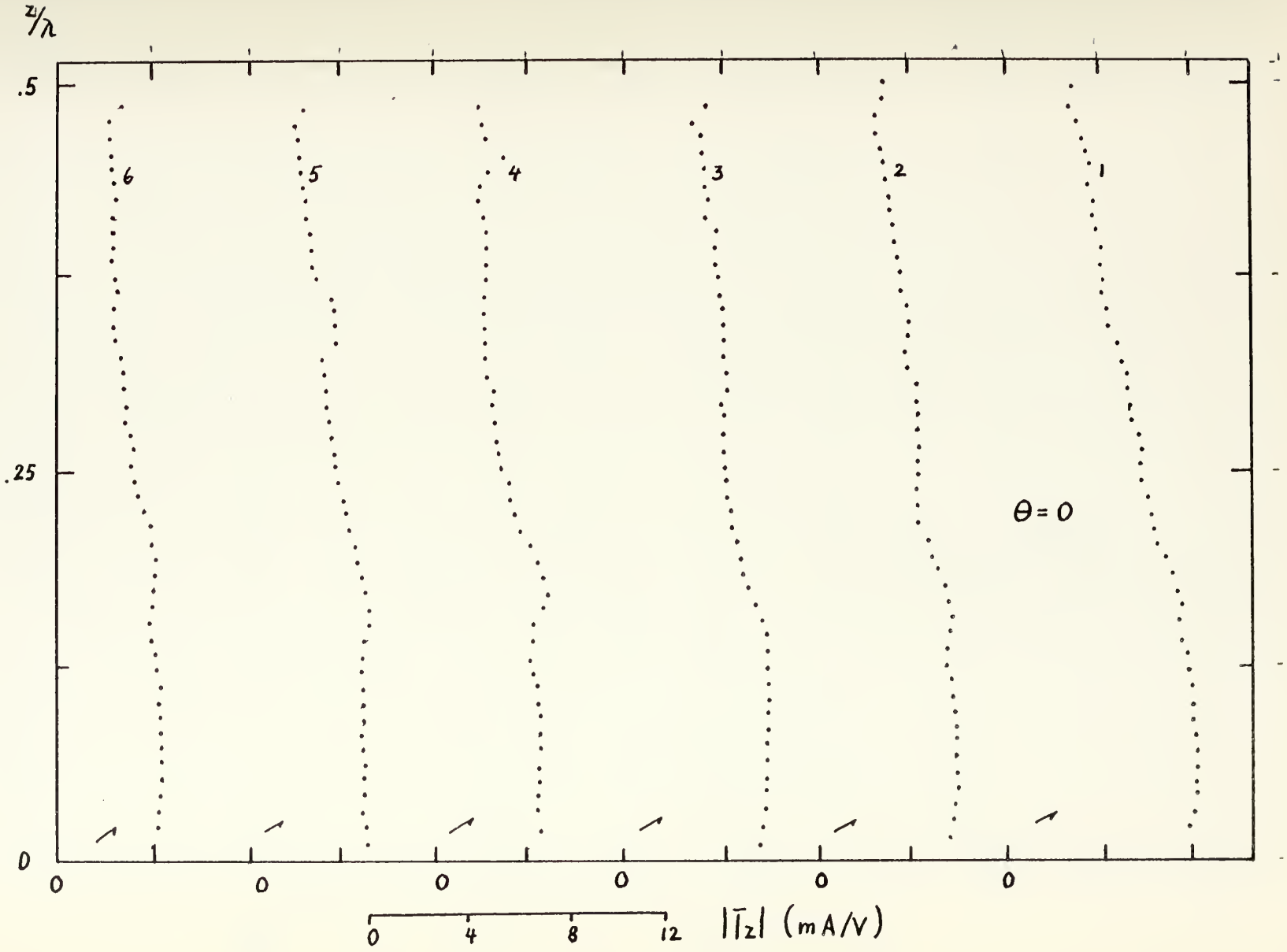

Figure 19.

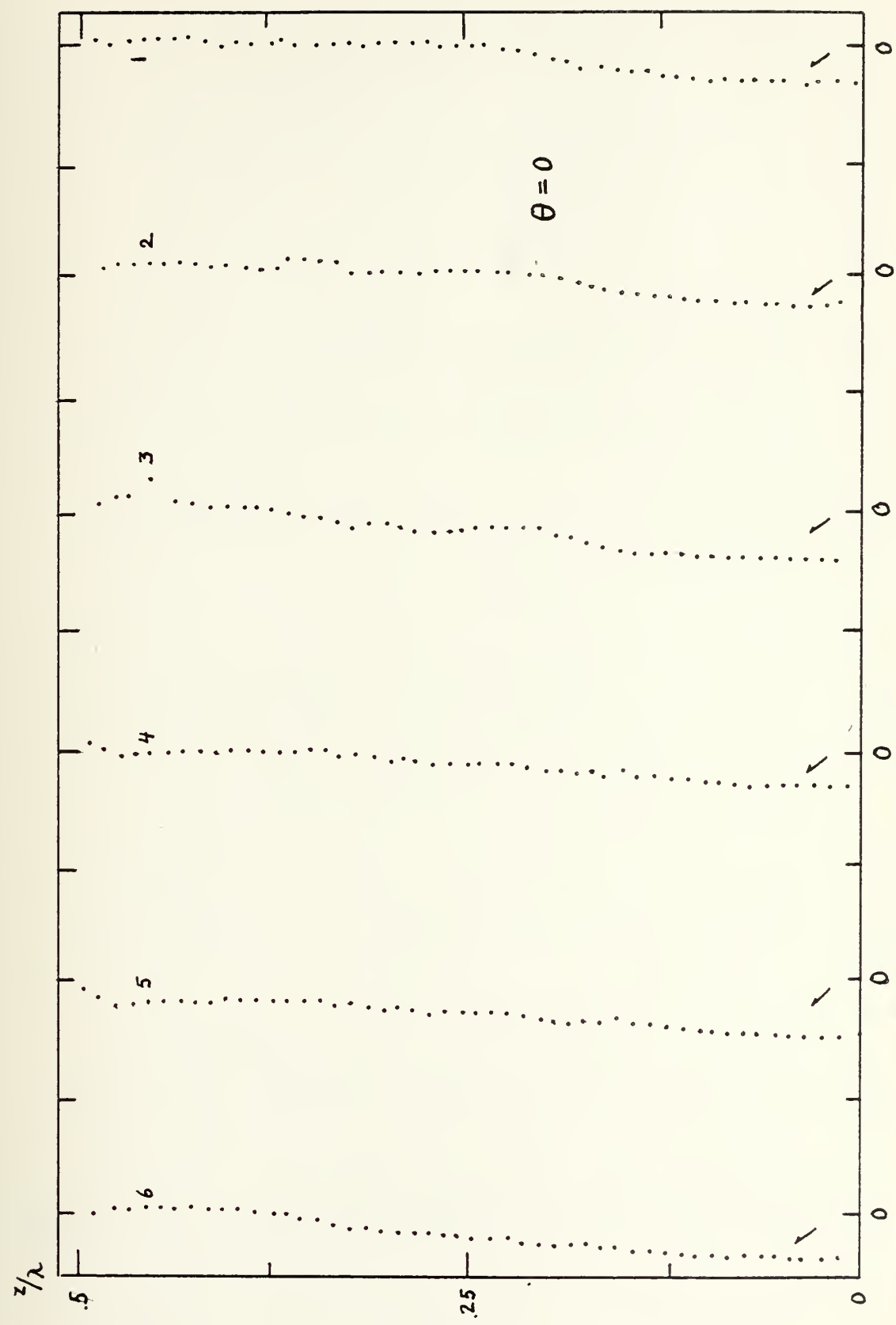

Figure 20.

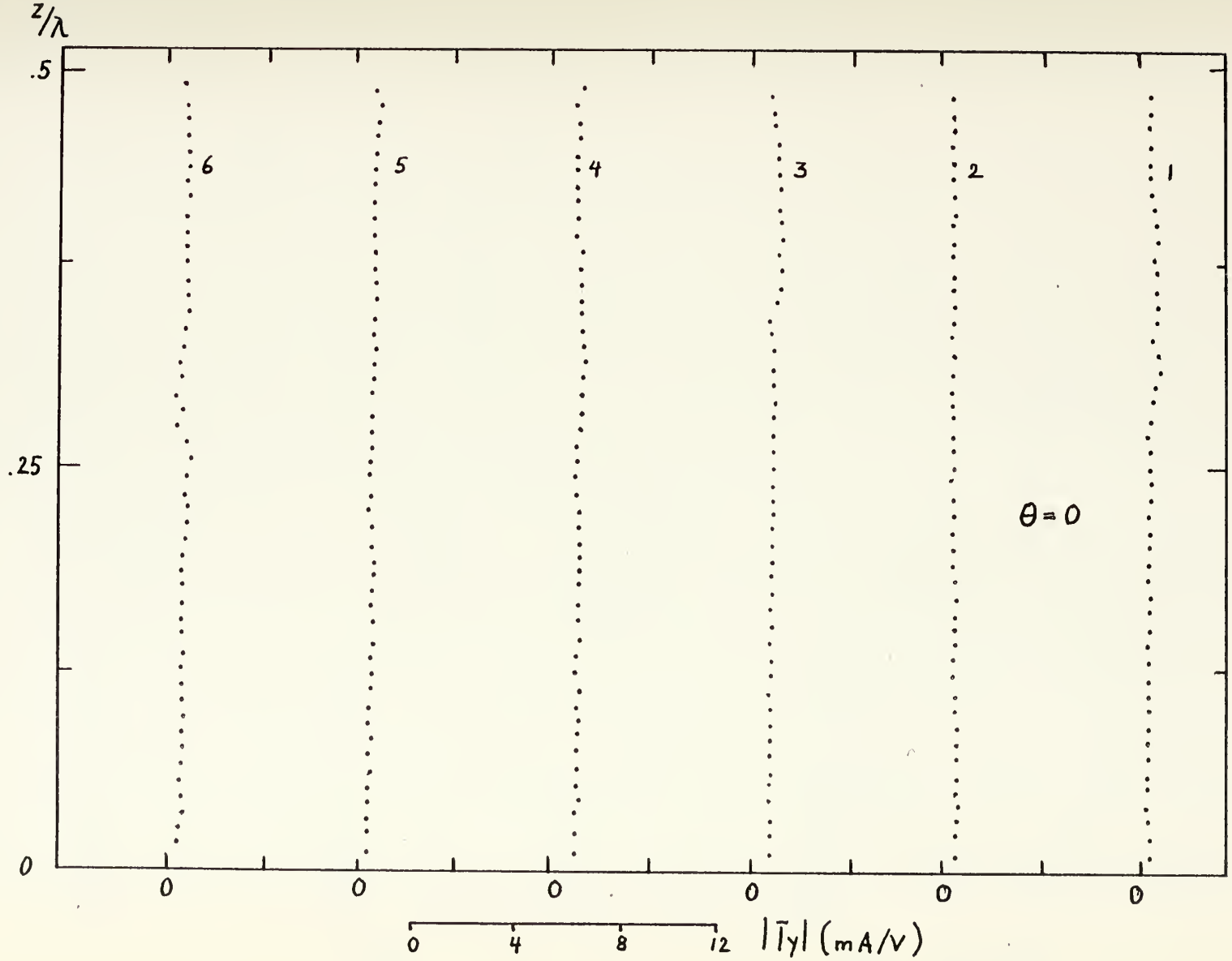

Figure 21.

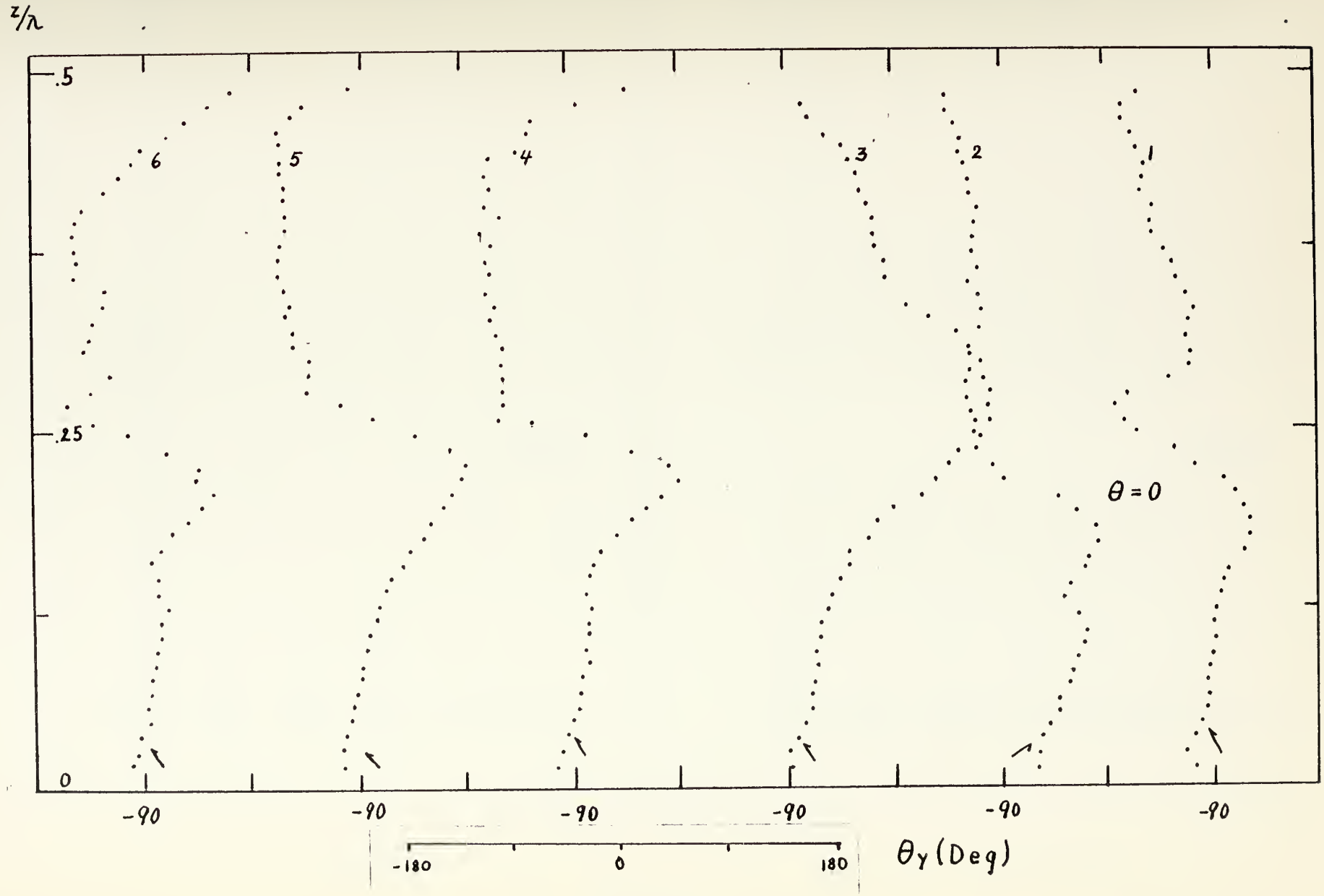

Figure 22.

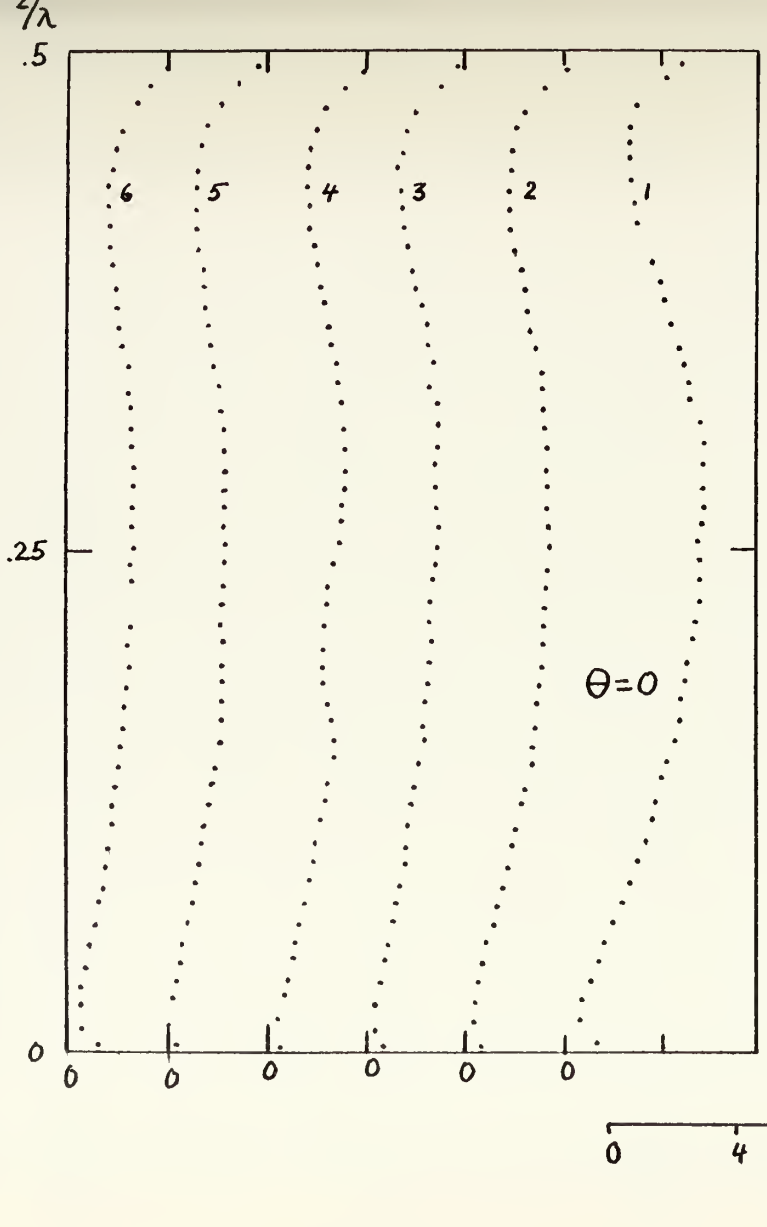

Figure 23.

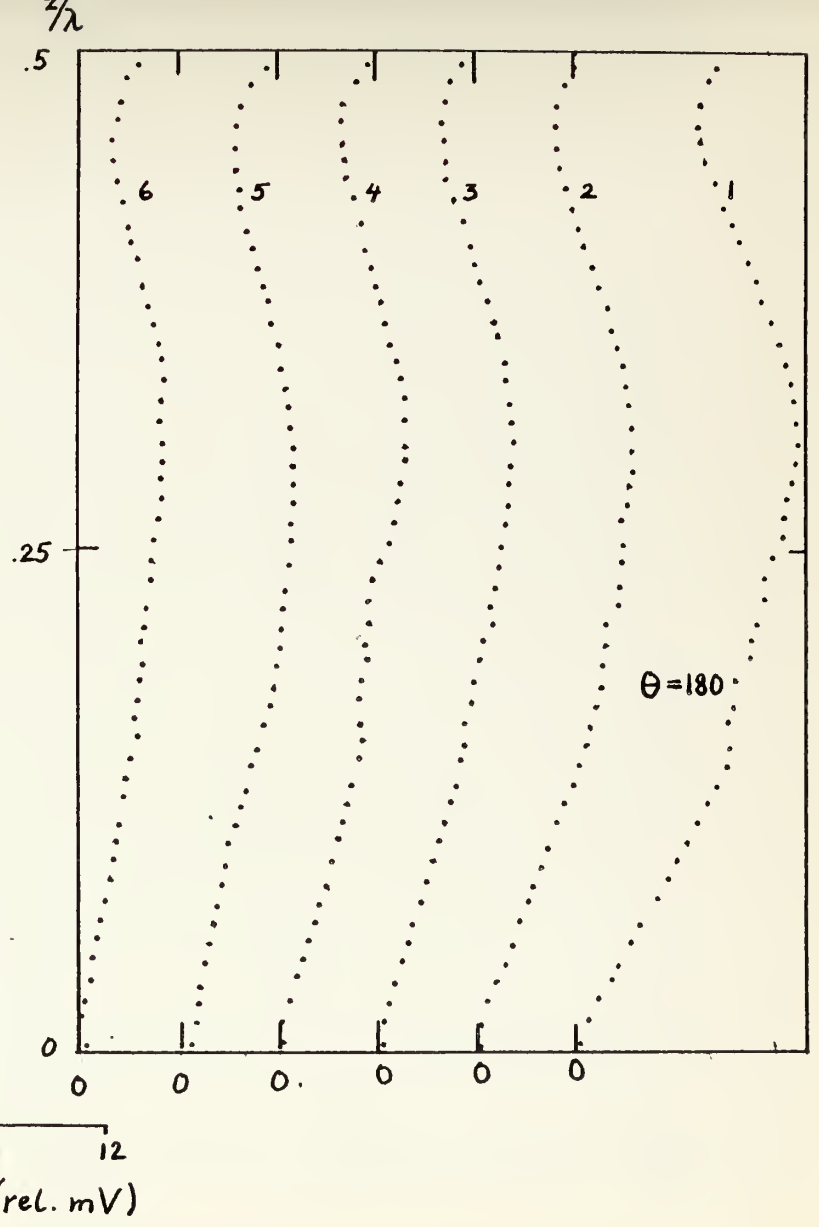

Figure 24.

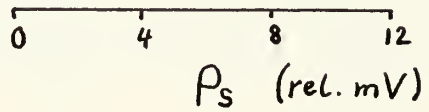

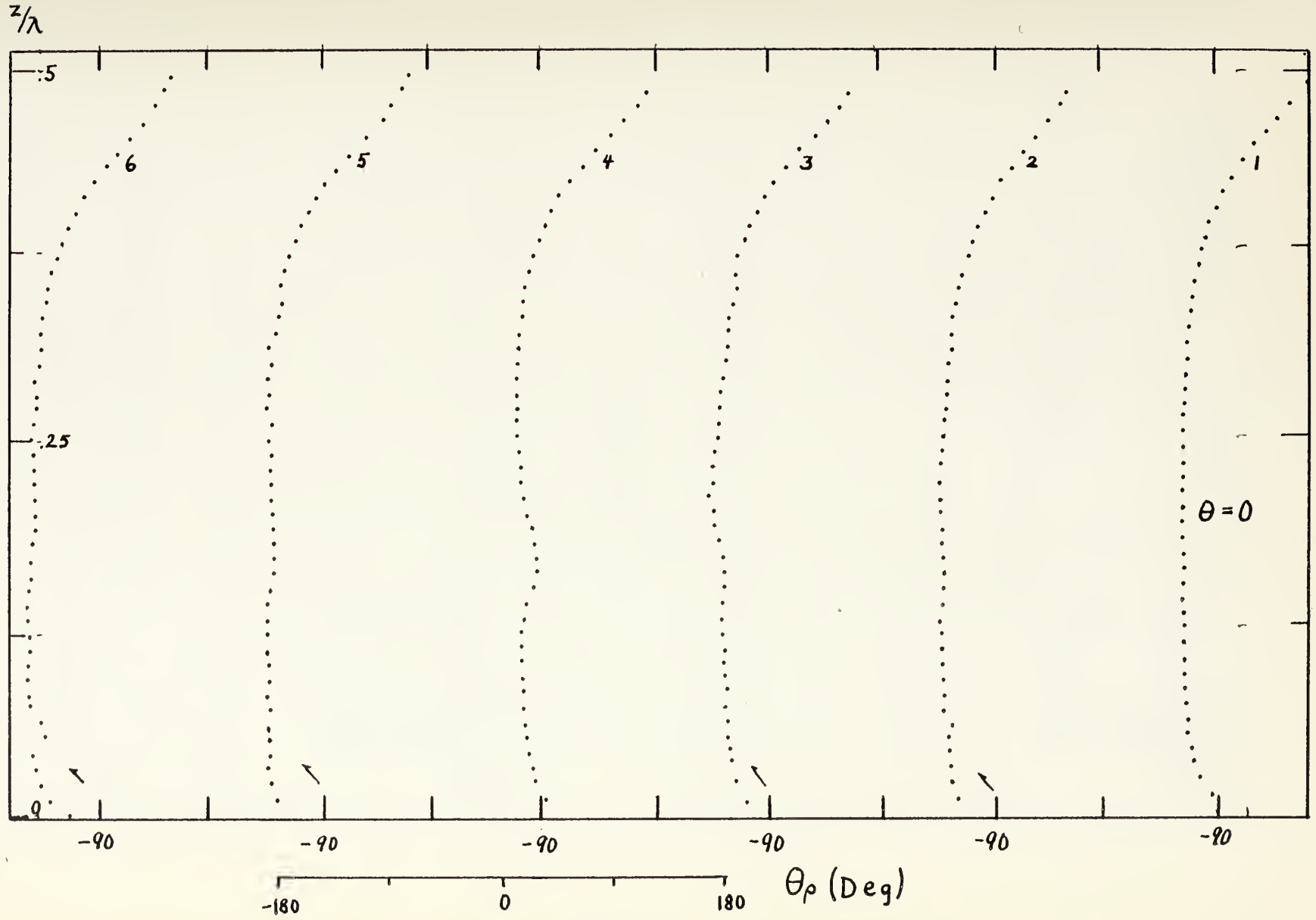

Figure 25.

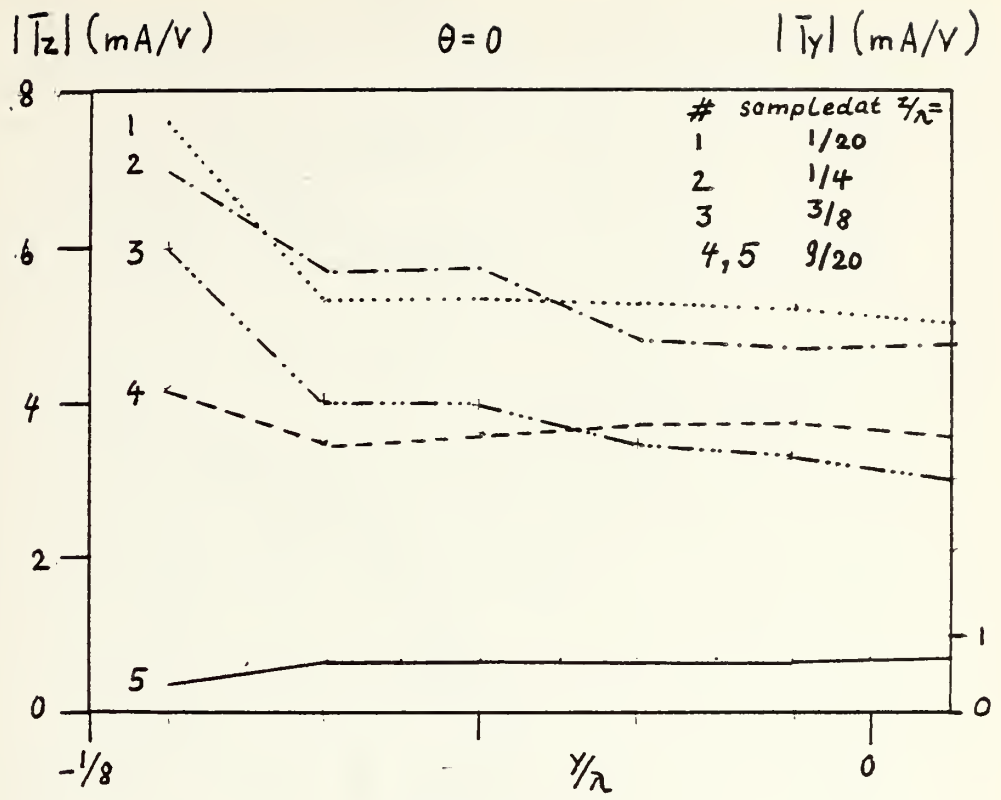

Figure 26.

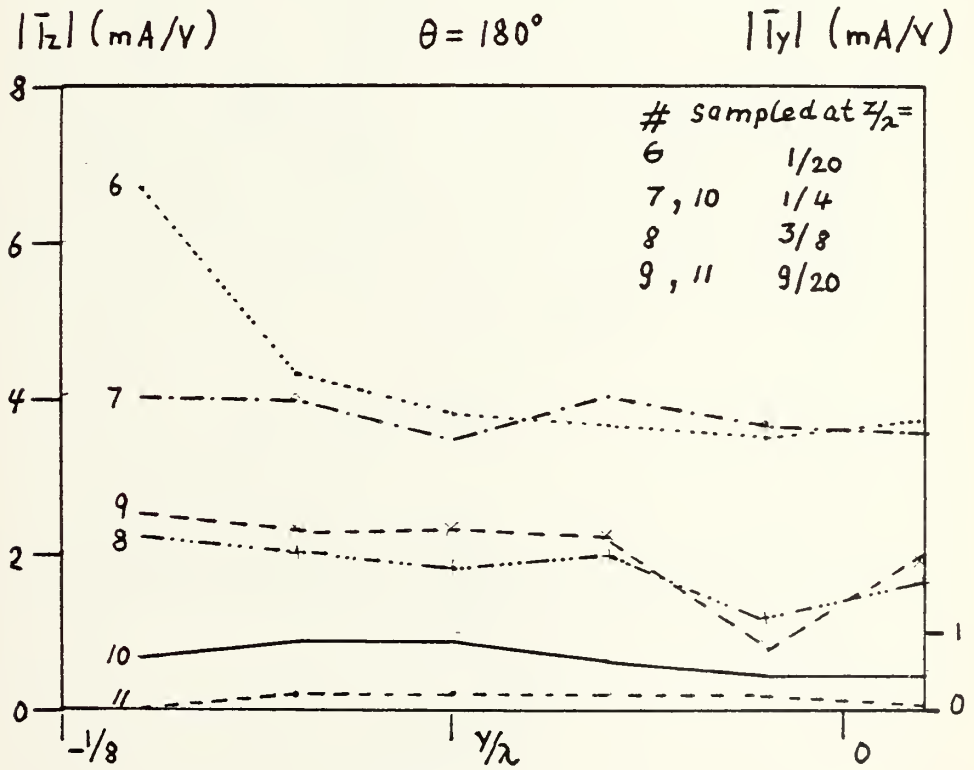

Figure 27.

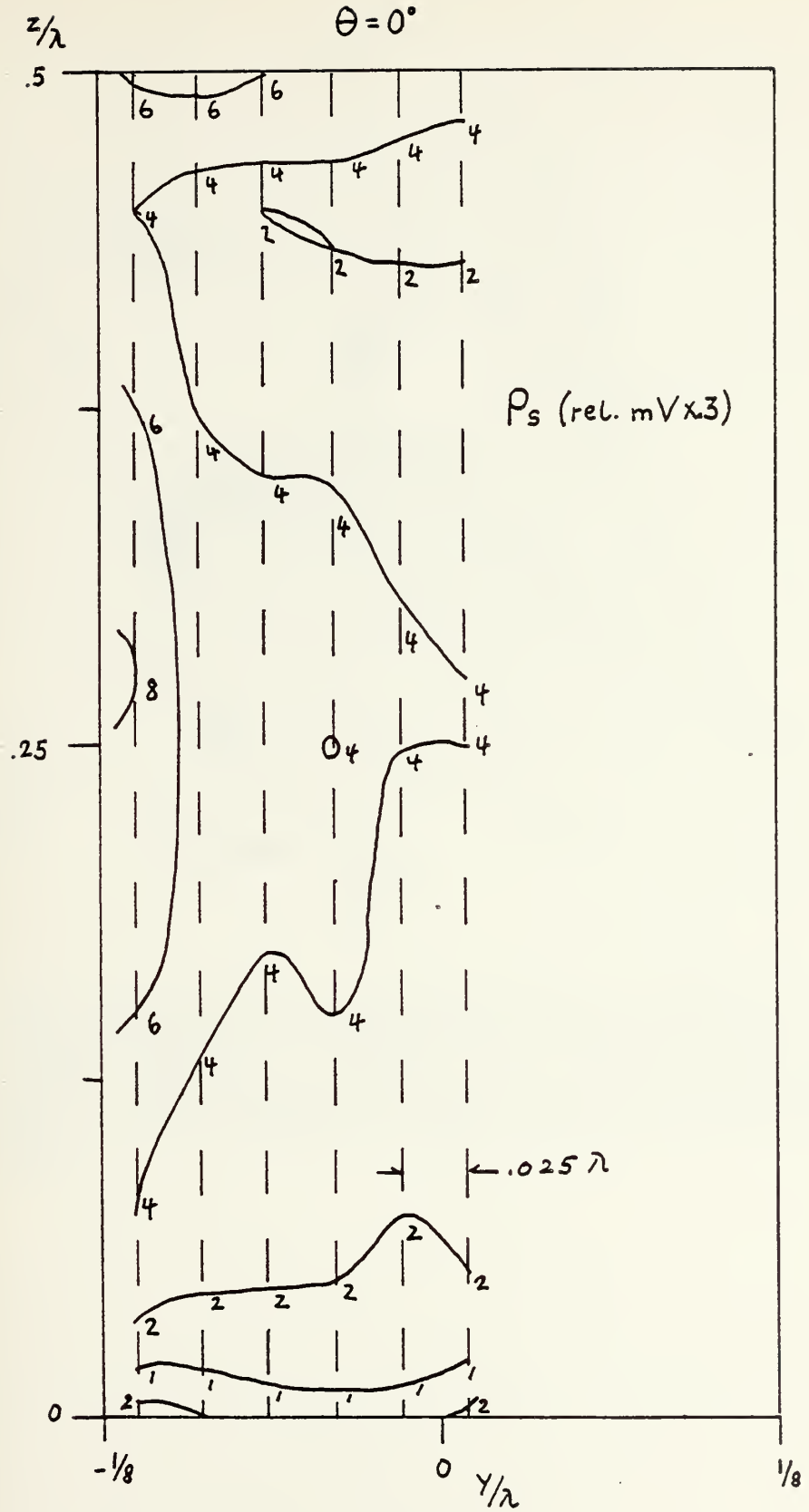

Figure 28.

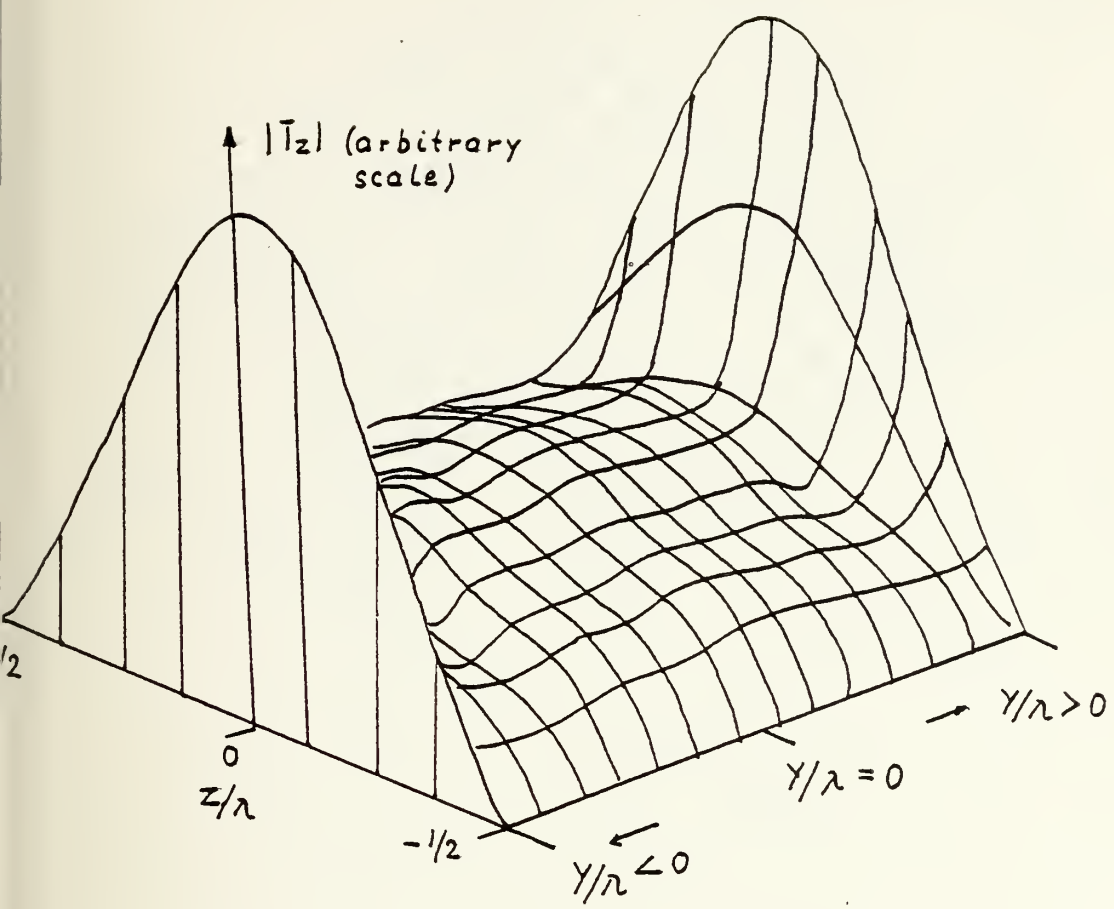

Figure 29. Generalized 3-D Plot of Surface Current in Z-direction. (The plot was obtained from the current curves of plate C in Fig. 38 after smoothing. If the Y/λ axis is scaled accordingly, the plot gives the overall picture for plates B and D also. Therefore, the scale of the magnitude axis was left arbitrary).

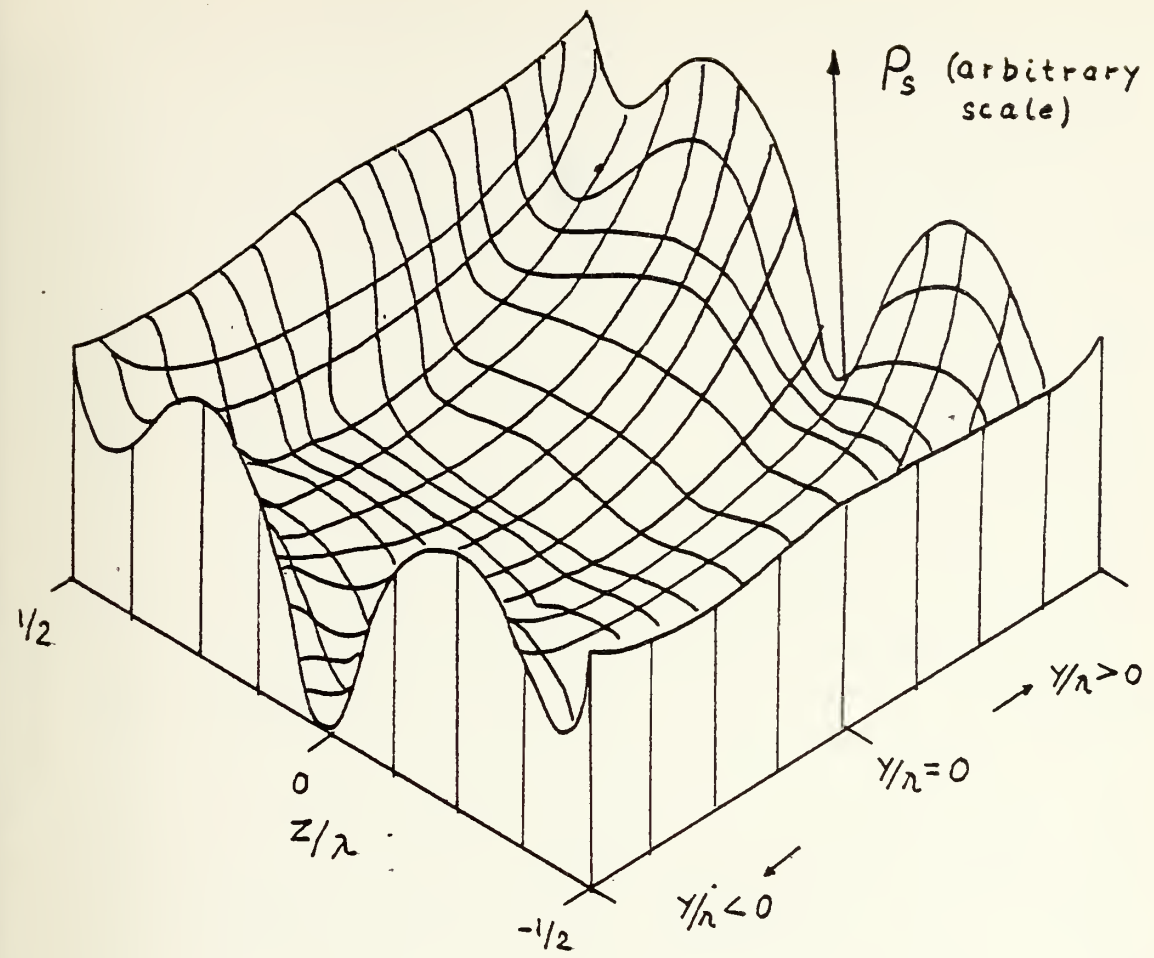

Figure 30. Generalized 3-D Plot of Change Density. (The plot was obtained from the charge density curves of plate D in Fig. 69. If the Y/λ axis is scaled accordingly, the plot gives the overall picture for plates B and C also. Therefore, the scale of the magnitude axis was left arbitrary.)

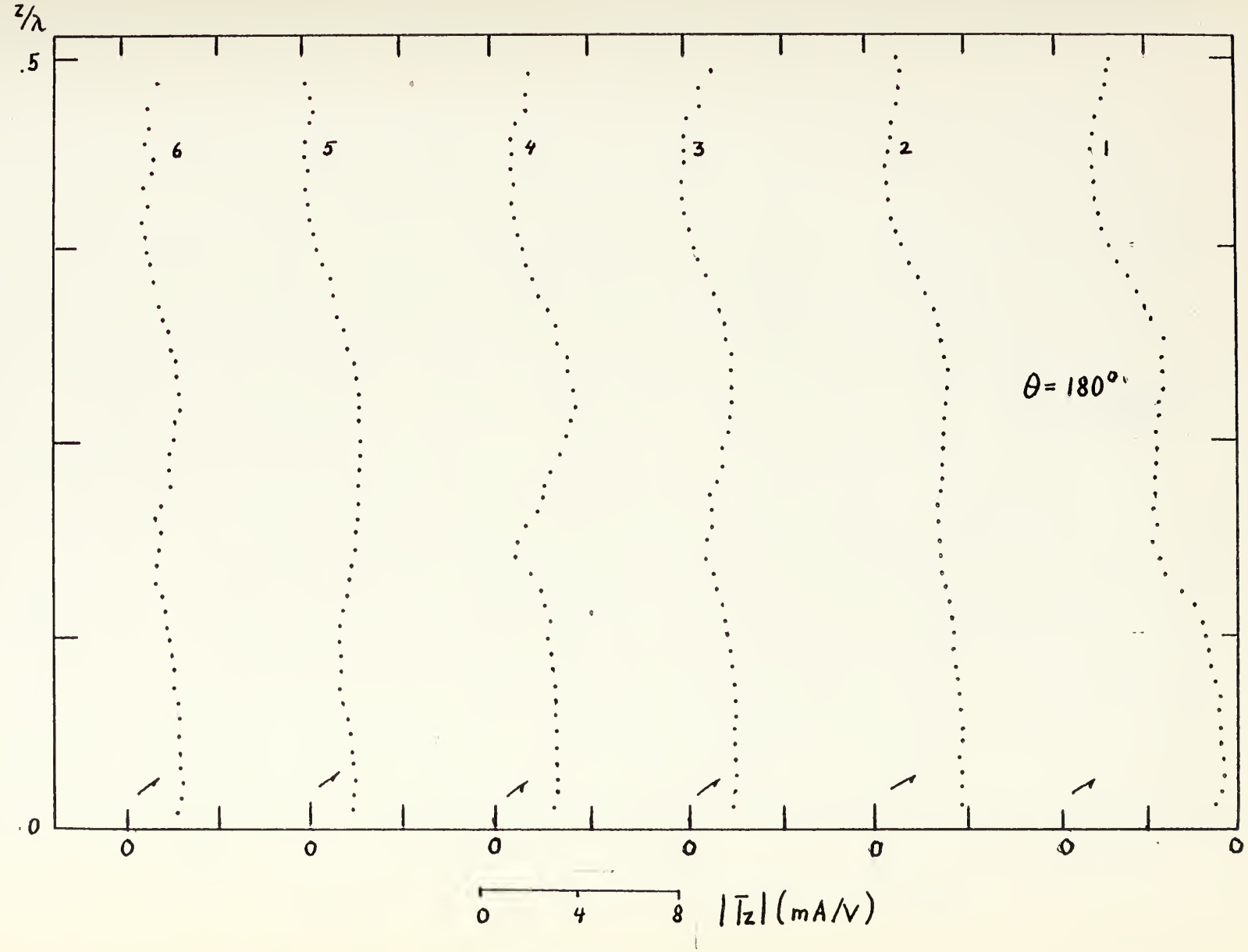

Figure 31.

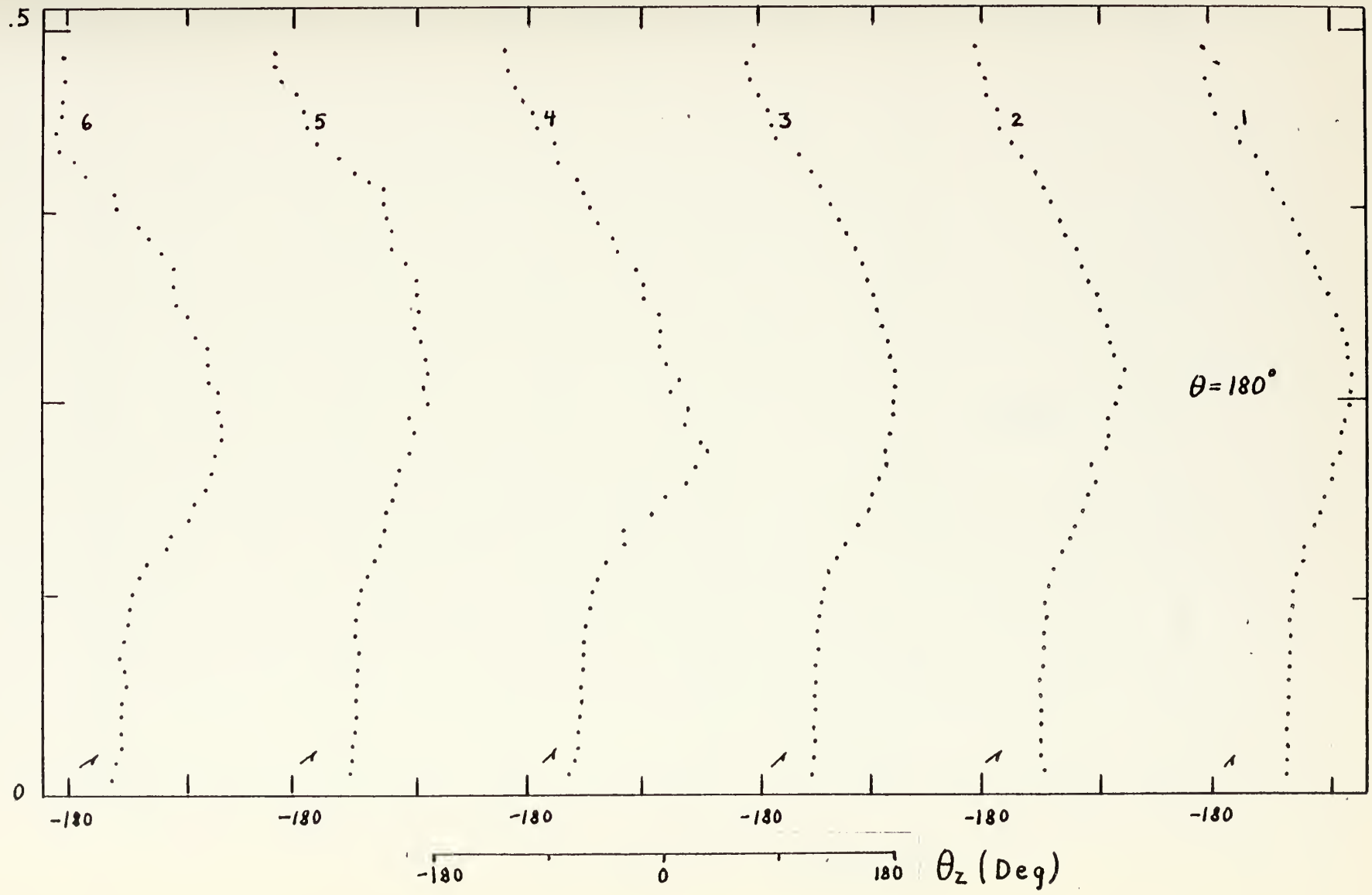

Figure 32.

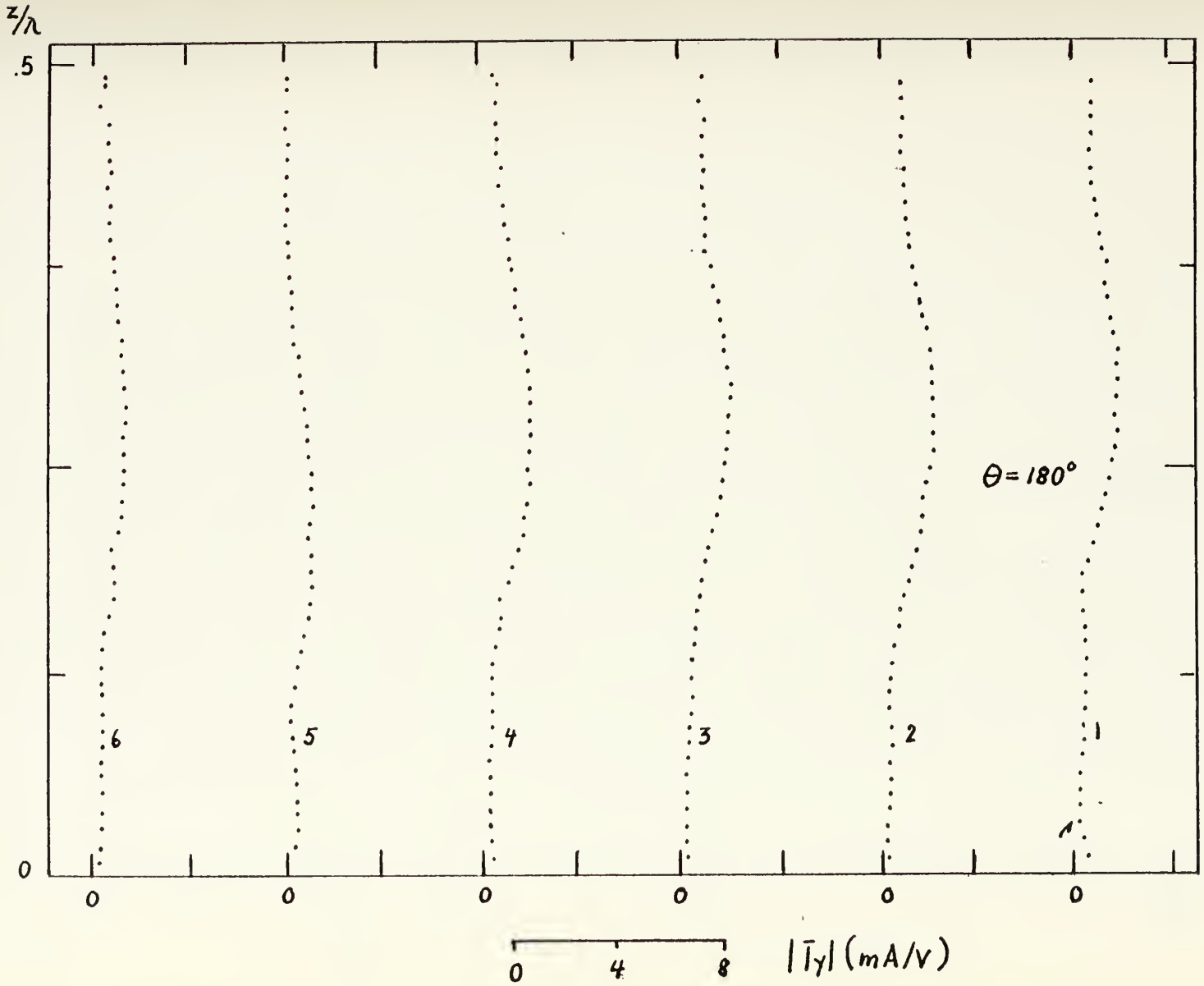

Figure 33.

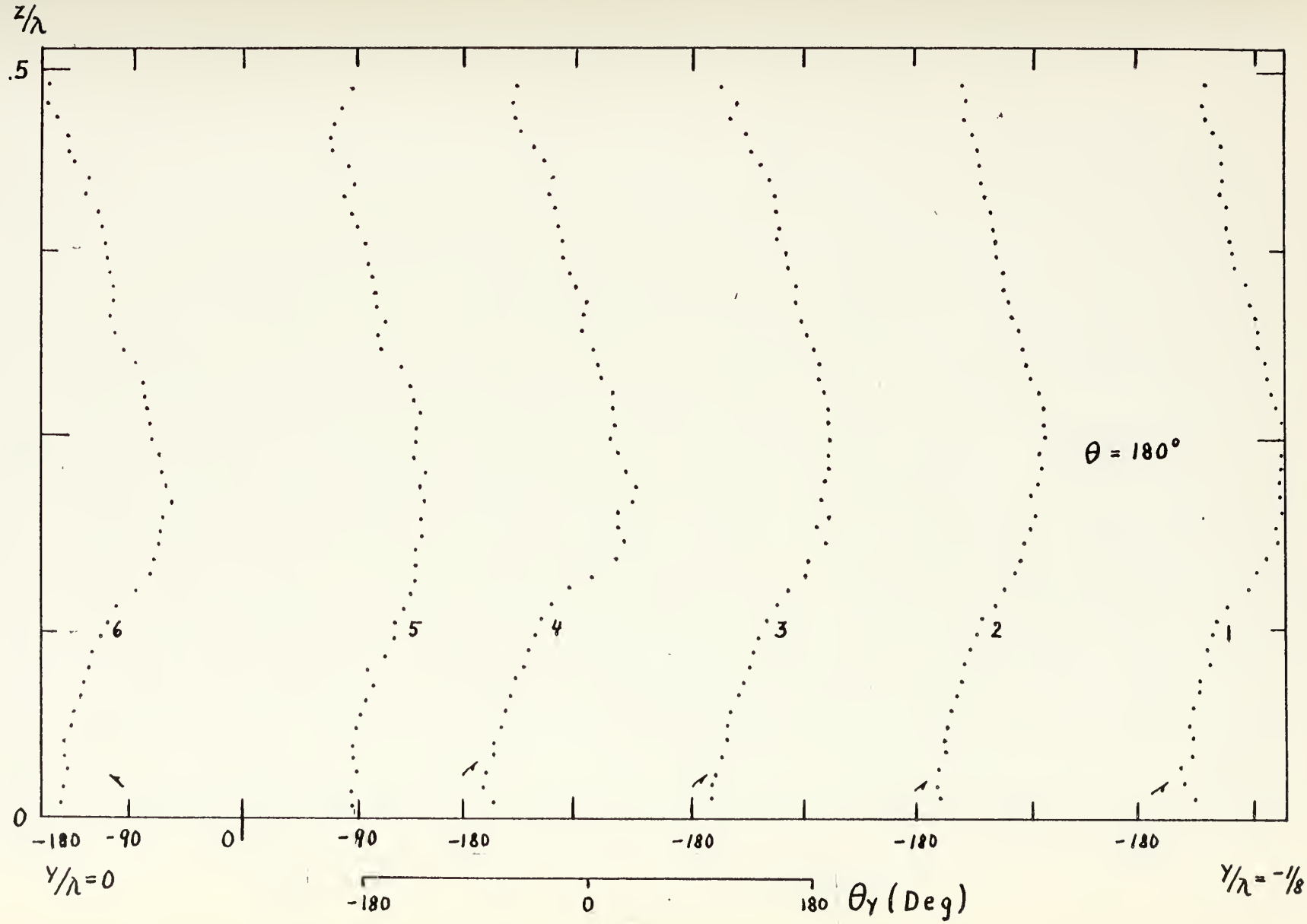
z/λ
.5
0
θ = 180°
6
5
4
3
2
1
-180
-90
0
-90
-180
-180
-180
-180
Y/λ = 0
Y/λ = -1/8
-180
0
180
θγ (Deg)

Figure 34.

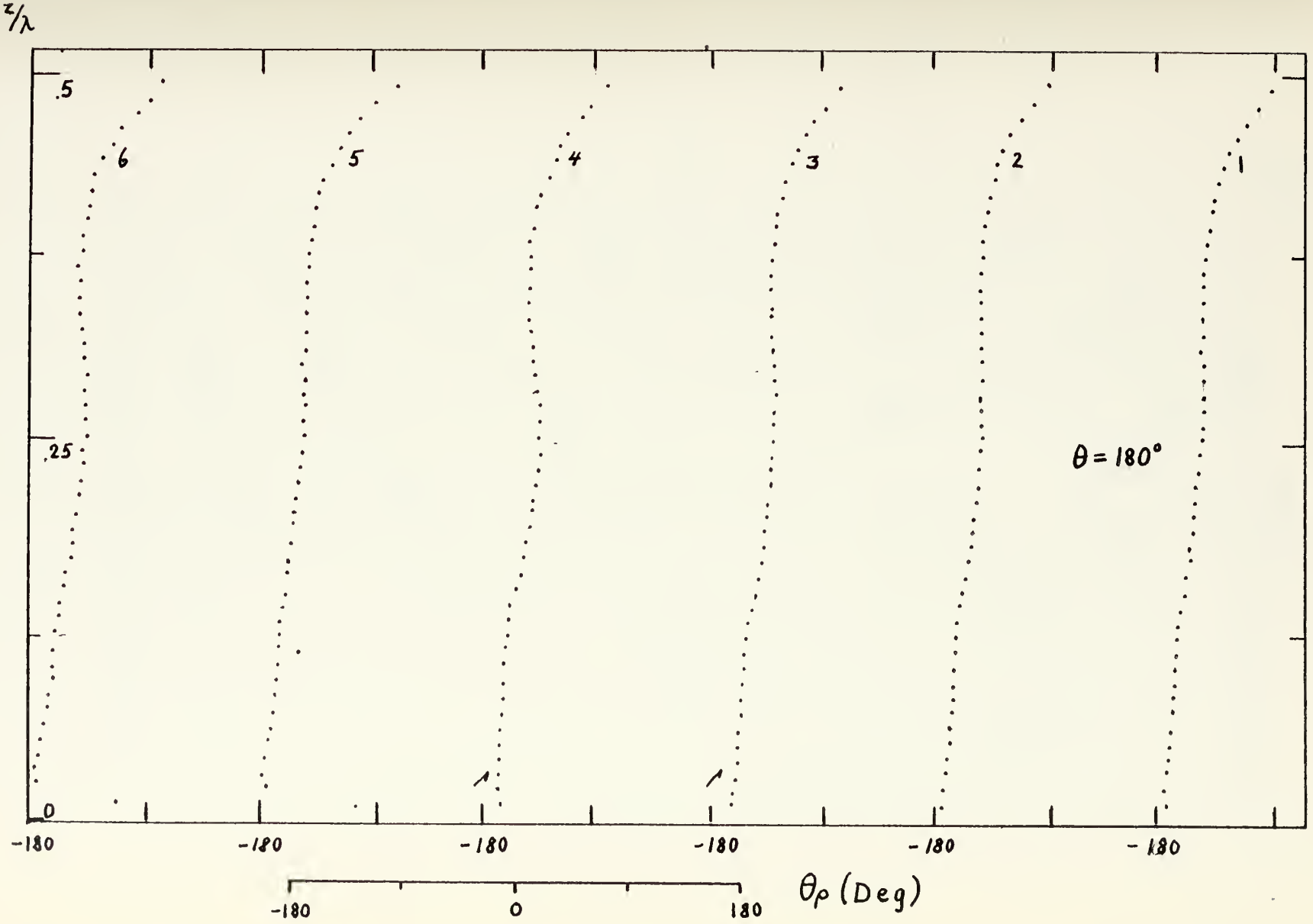

Figure 35.

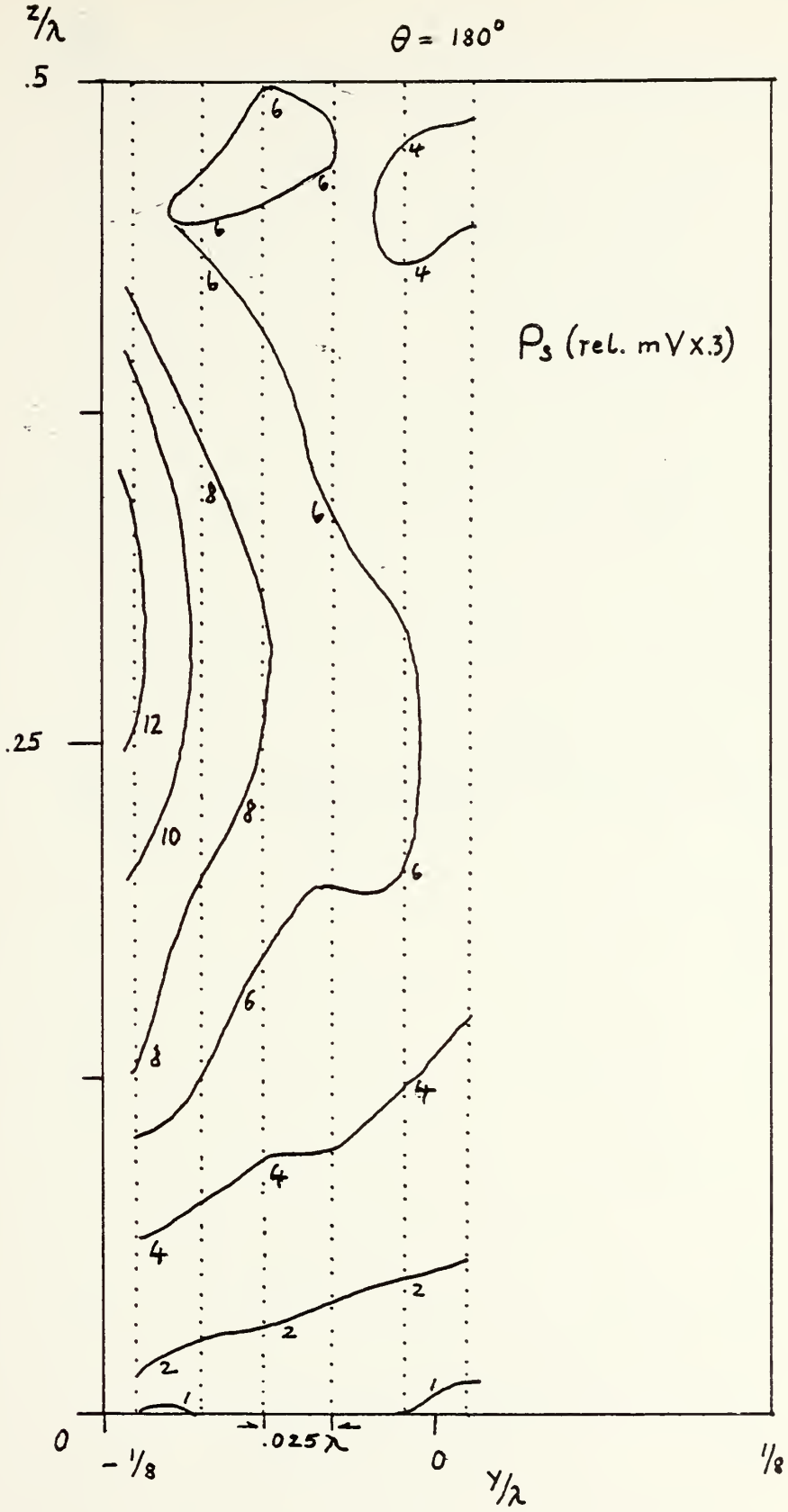

Figure 36.

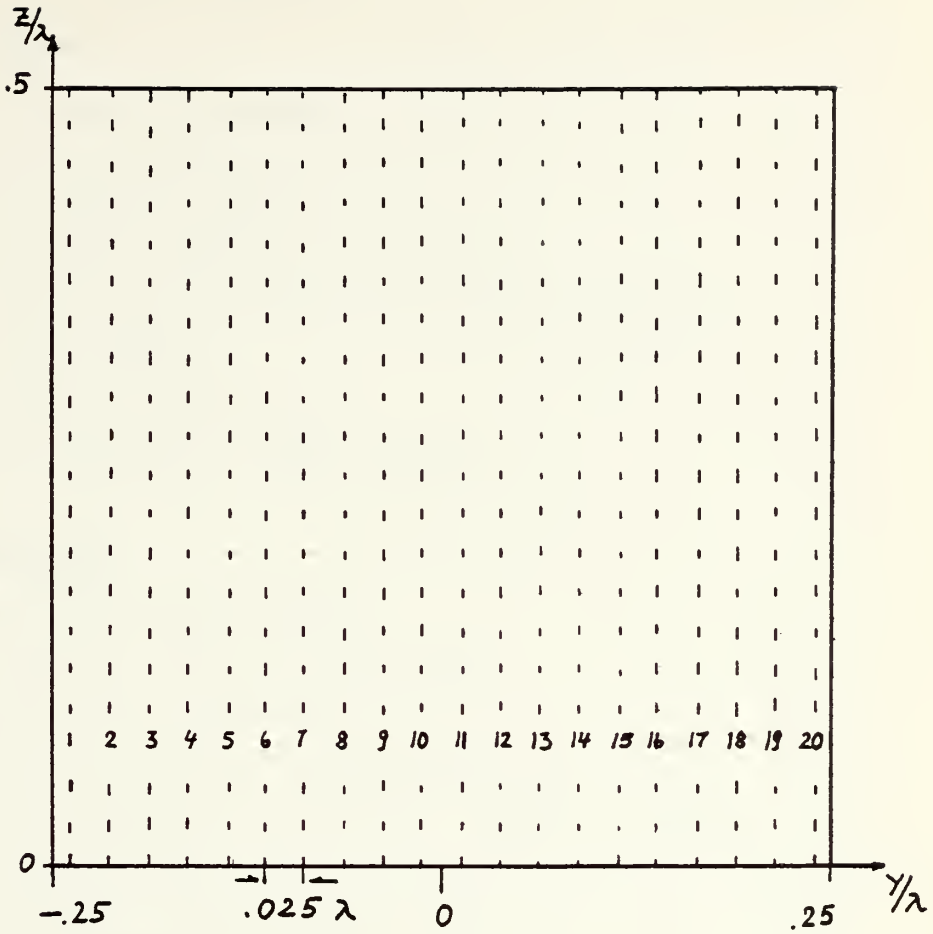

Figure 37a. Plate C

TITLE (PLATE C)	FIGURE
0° Aspect Angle	
Measured current in Z-direction	38
Measured phase of current in Z-direction	39
Measured current in Y-direction	40
Measured phase of current in Y-direction	41
Profile plot of measured currents in Y- and Z-direction	42
Measured change density	44
Measured phase of charge density	45
Contour plot of measured charge density	46
180° Aspect Angle	
Measured current in Z-direction	47
Measured phase of current in Z-direction	48
Measured current in Y-direction	49
Measured phase of current in Y-direction	50
Profile plot of measured currents in Y- and Z-direction	43
Measured charge density	51
Measured phase of charge density	52
Contour plot of measured charge density	53
45° Aspect Angle	
Measured current in Z-direction	55
Measured phase of current in Z-direction	56
Measured current in Y-direction	57
Measured phase of current in Y-direction	58
Profile plot of measured currents in Y- and Z-direction	59
Measured charge density	60
Measured phase of charge density	61
Contour plot of measured charge density	62

Figure 37b. Titles of Graphs of Plate C

Current	Charge Density	Component			Sampling Direction		Magn.	Phase	Figure and Aspect		
		Y	Z	Total	Y	Z			0°	180°	45°
X			X			X	X		38	47	55
X			X			X		X	39	48	56
X		X				X	X		40	49	57
X		X				X		X	41	50	58
X		X	X		X		X		42	43	59
	X			X		X	X		44	51	60
	X			X		X		X	45	52	61
	X			X	X	X	X		46	53	62

Figure 37c. Labels of Graphs (Plate C)

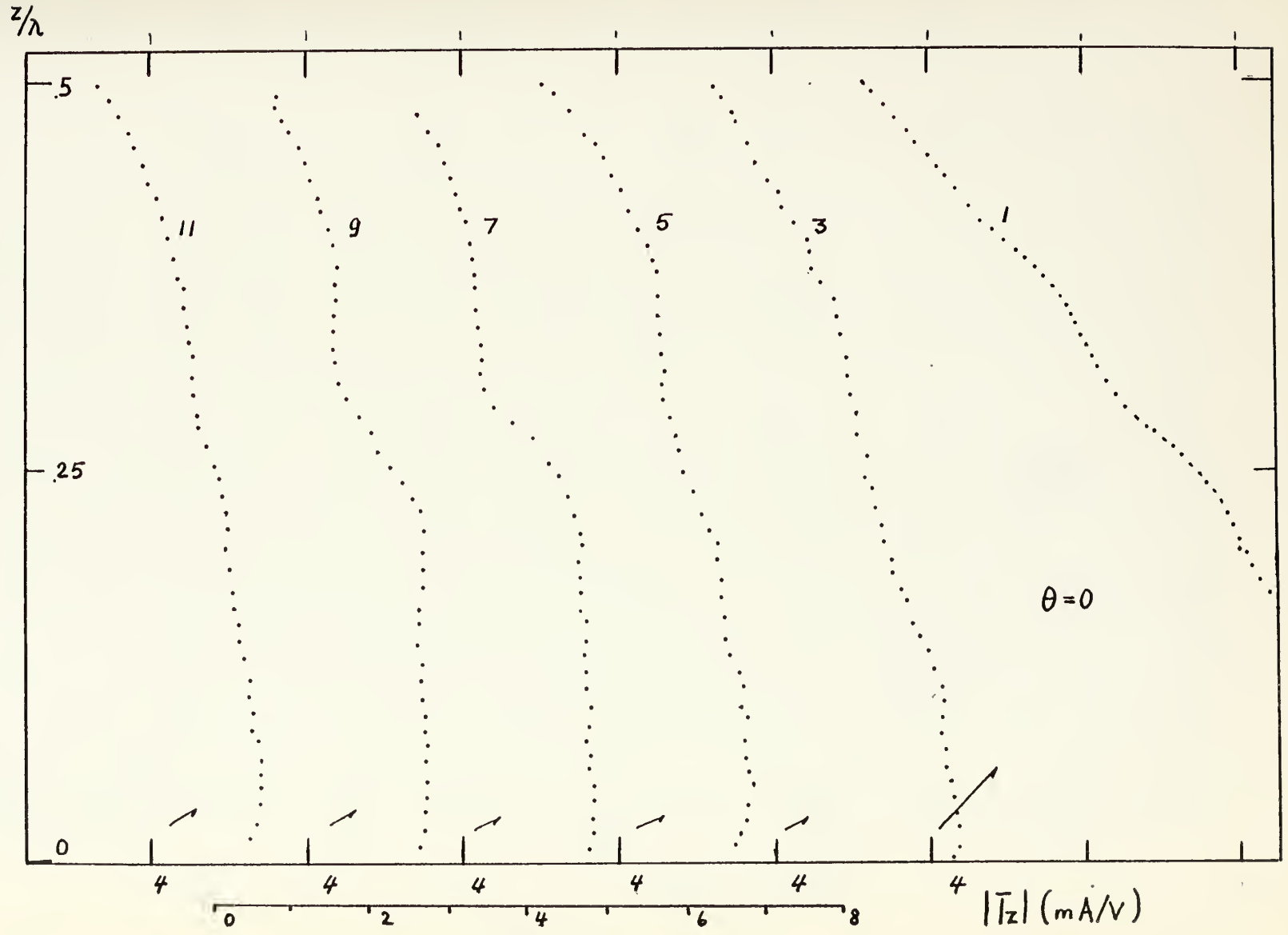

Figure 38.

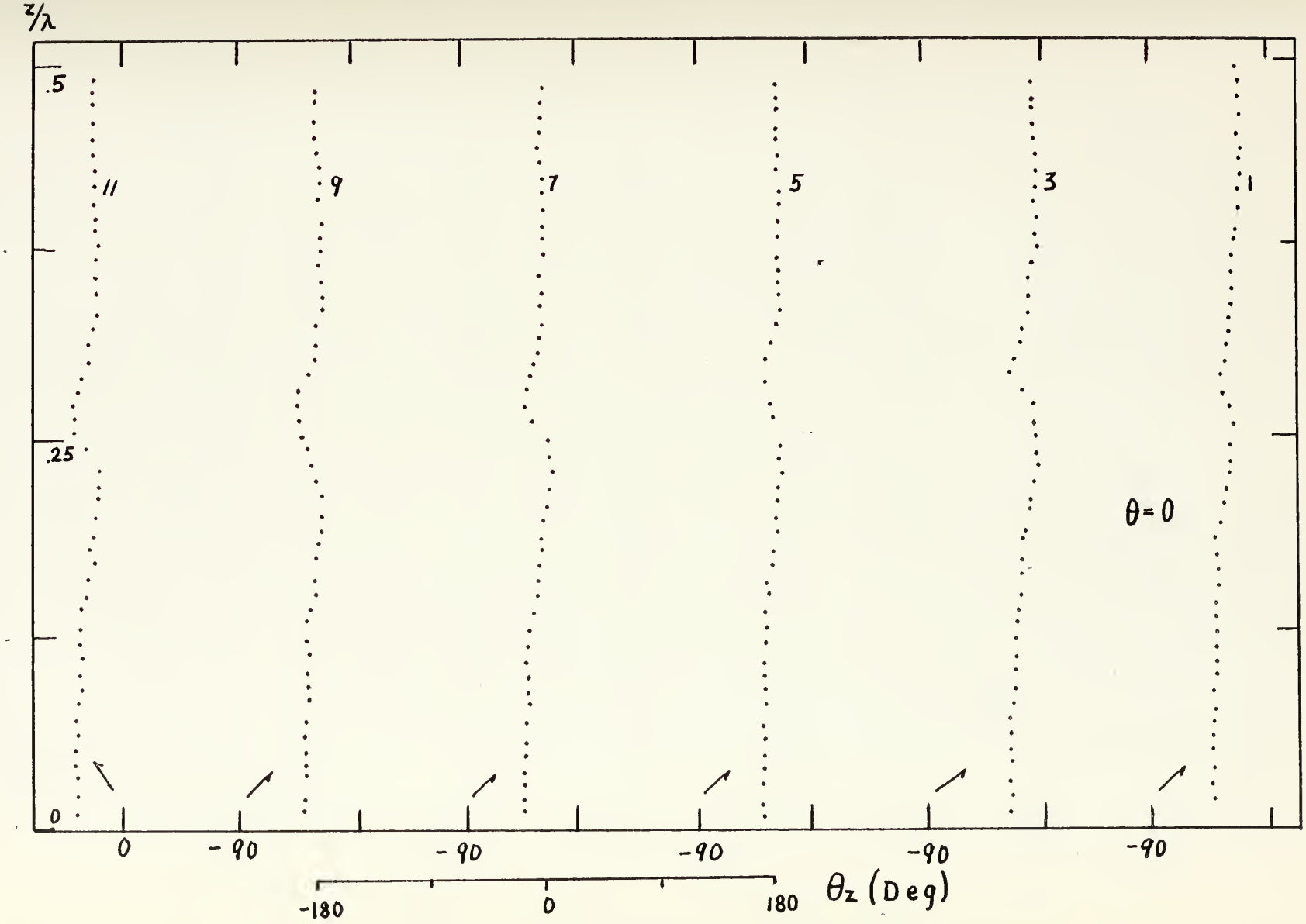

Figure 39.

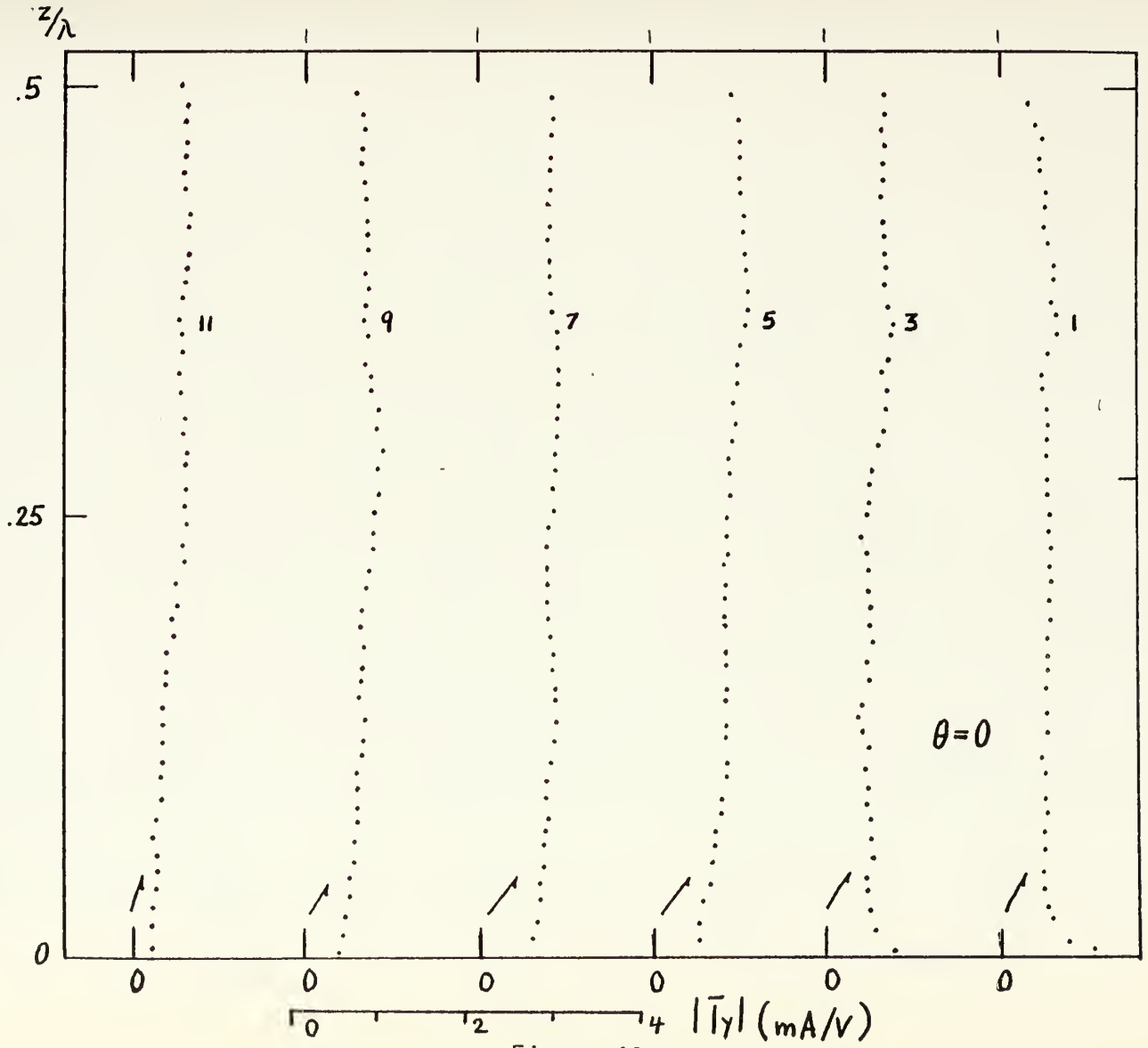

Figure 40.

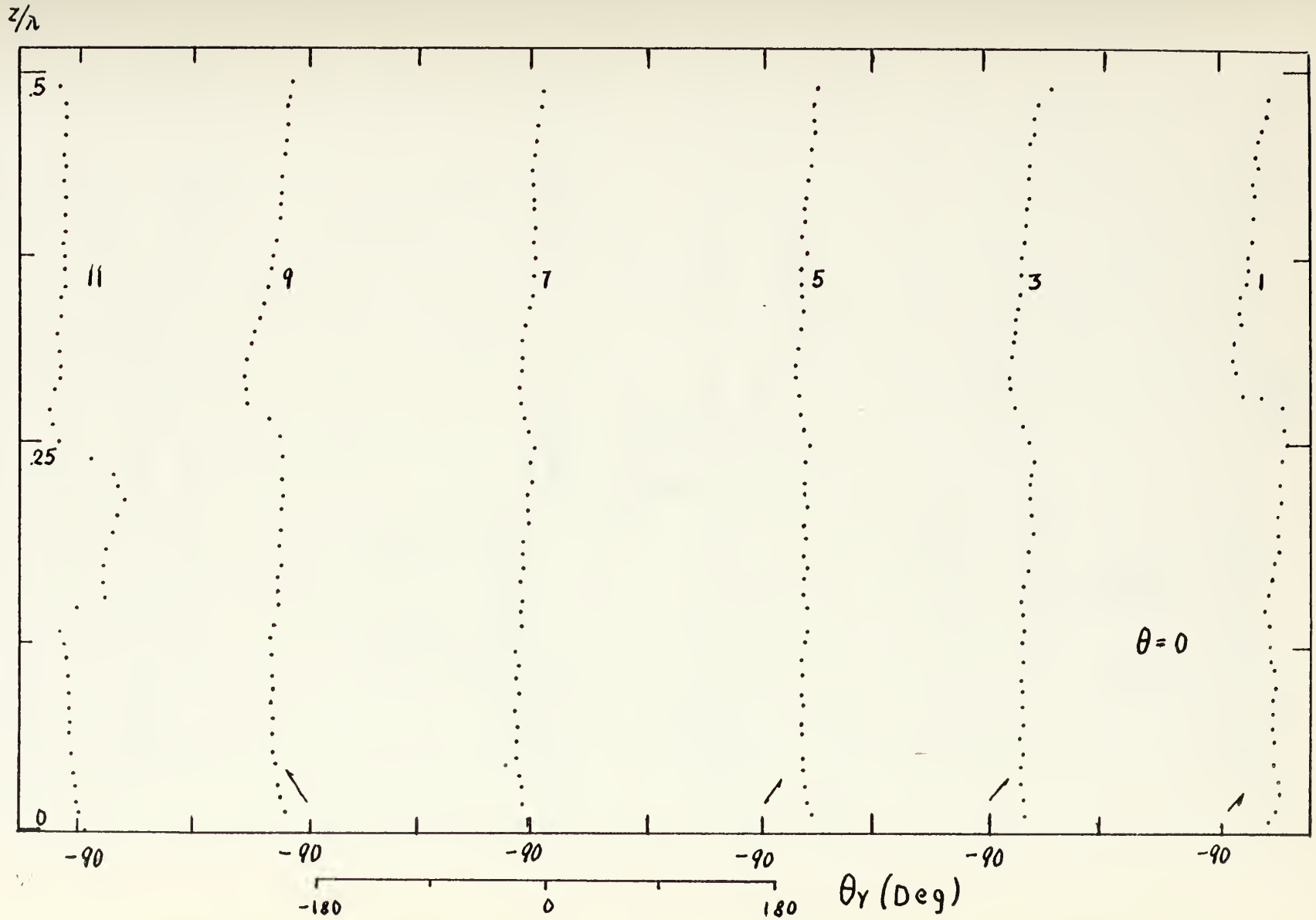

Figure 41.

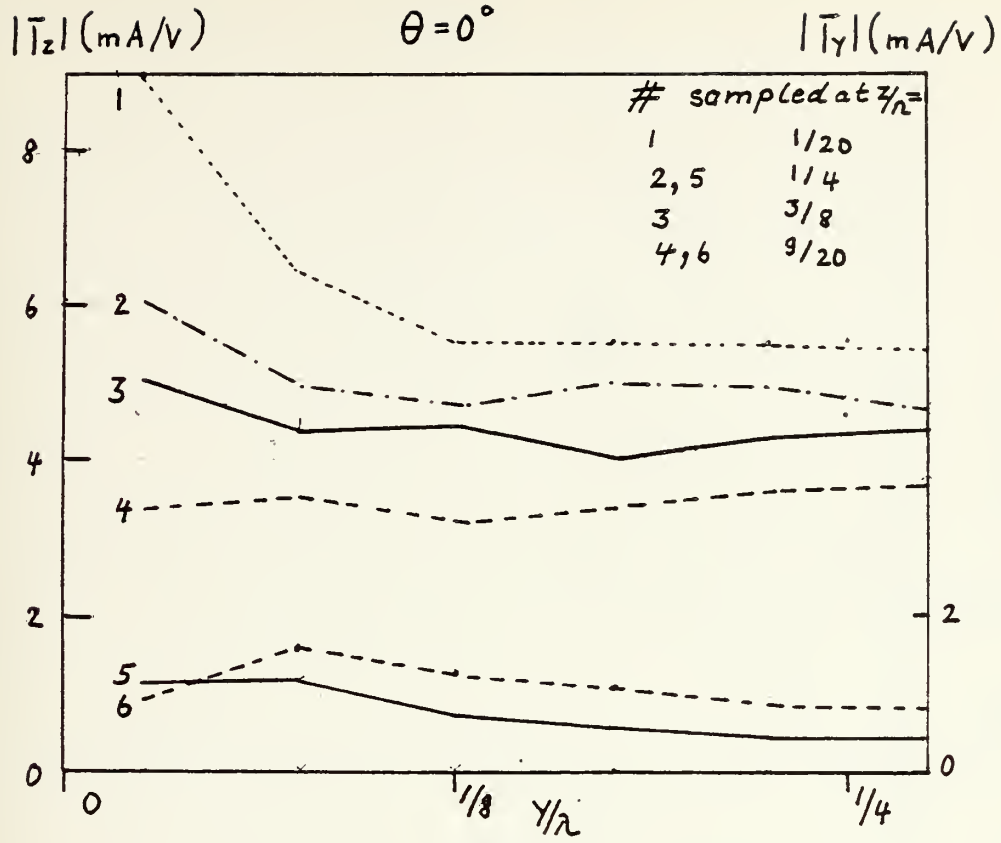

Figure 42.

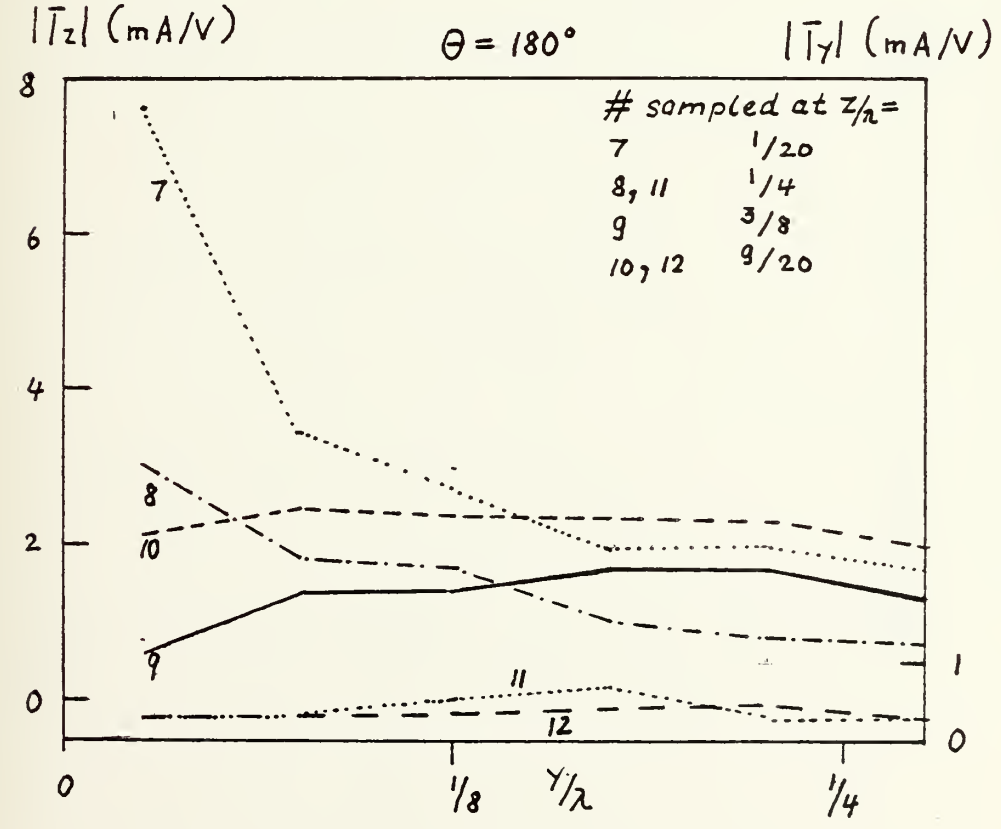

Figure 43.

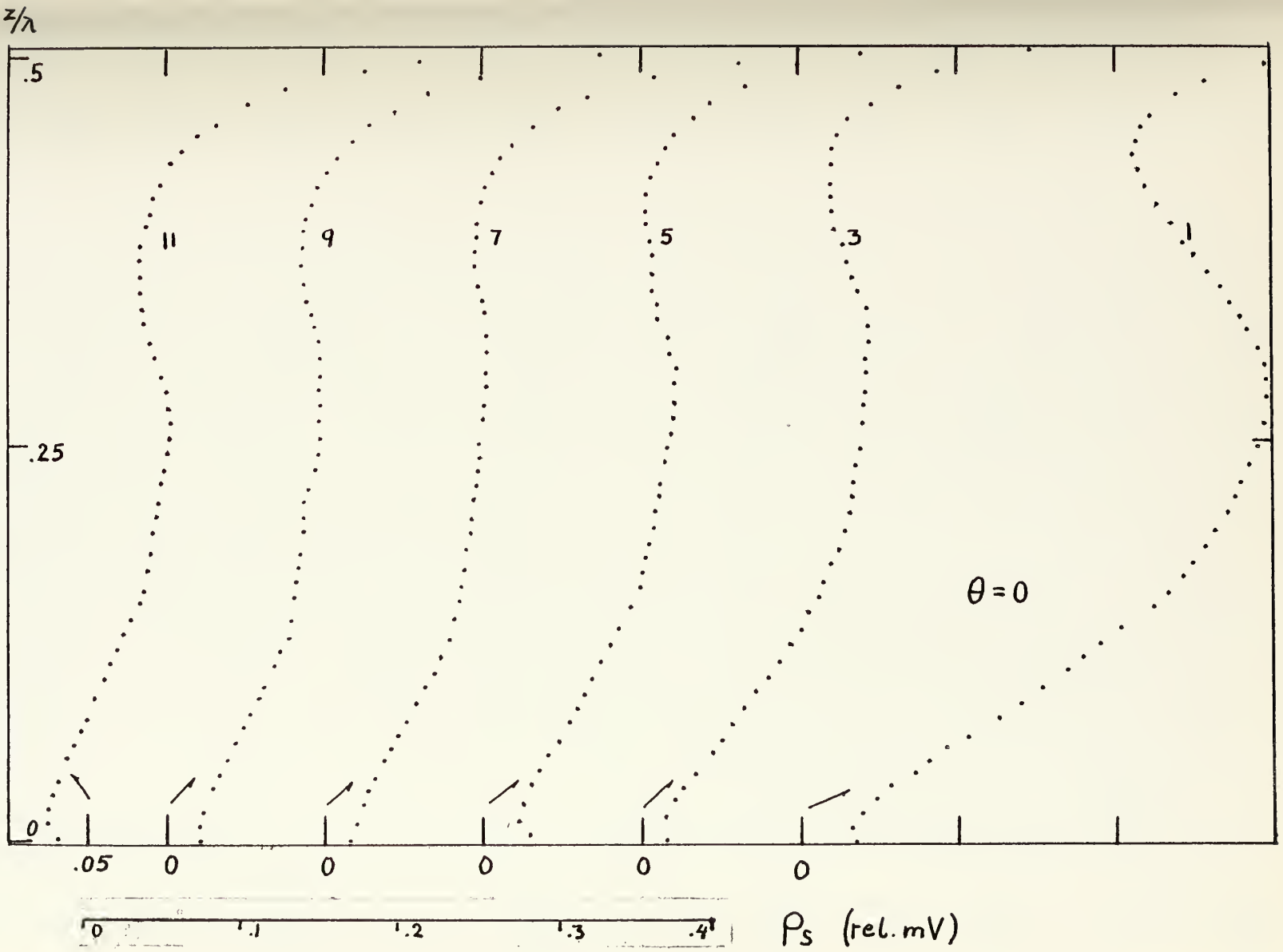

Figure 44.

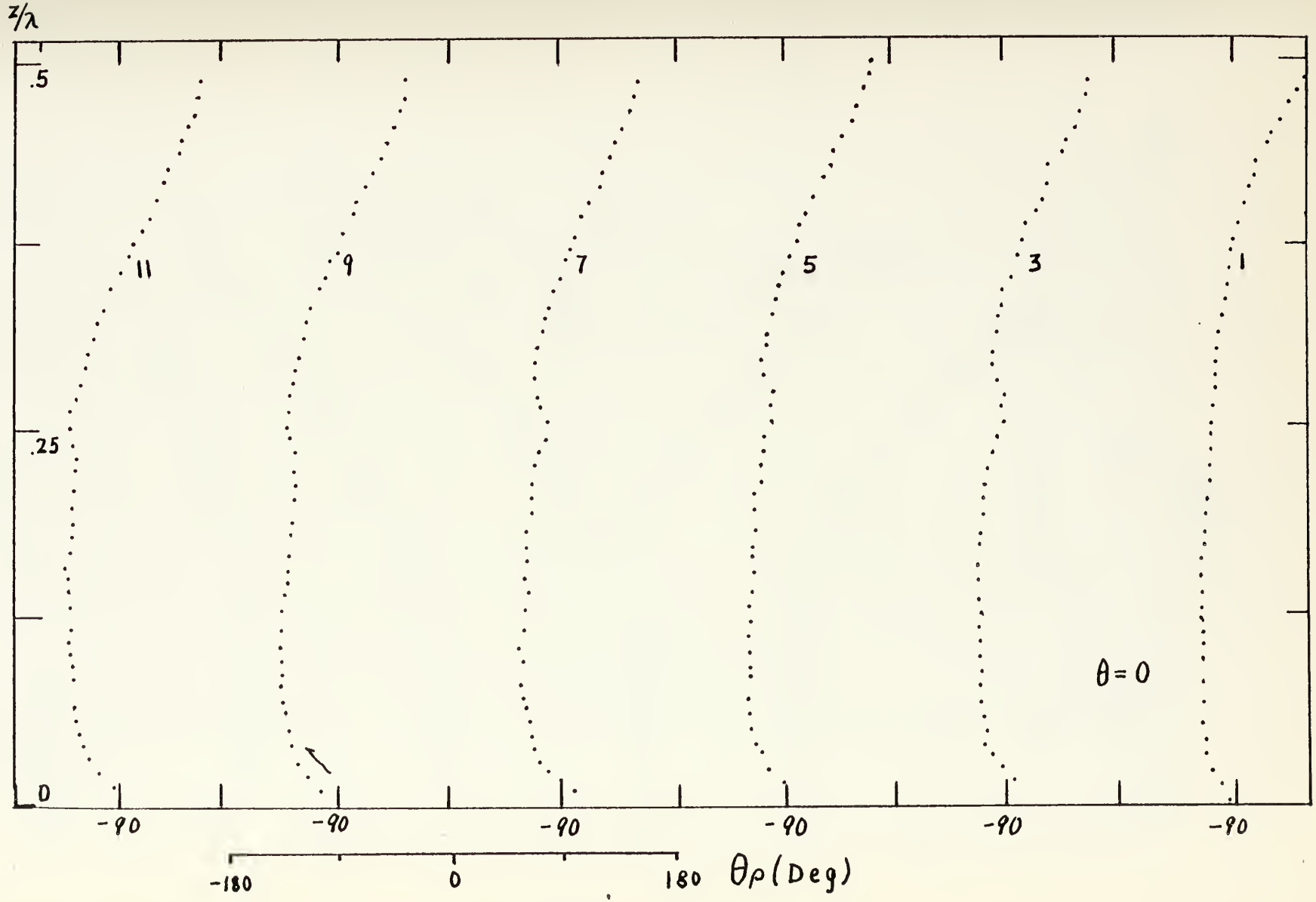

Figure 45.

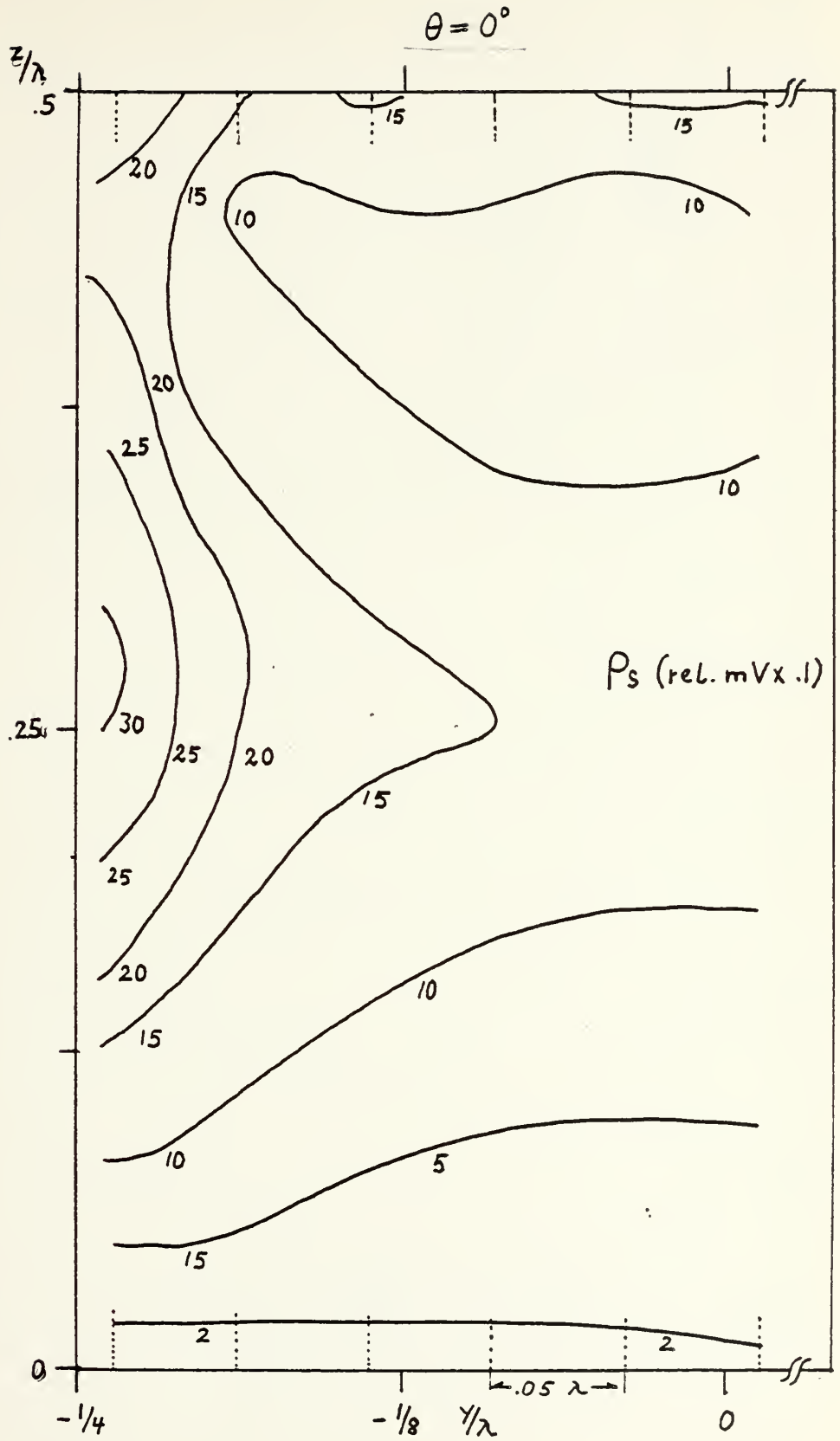
θ = 0°
z/λ
.5
.25
0
-1/4
-1/8
y/λ
0
.05 λ
Ps (rel. mVx .1)
15
15
20
15
10
10
10
20
25
30
25
20
15
25
20
15
10
10
5
15
2
2

Figure 46.

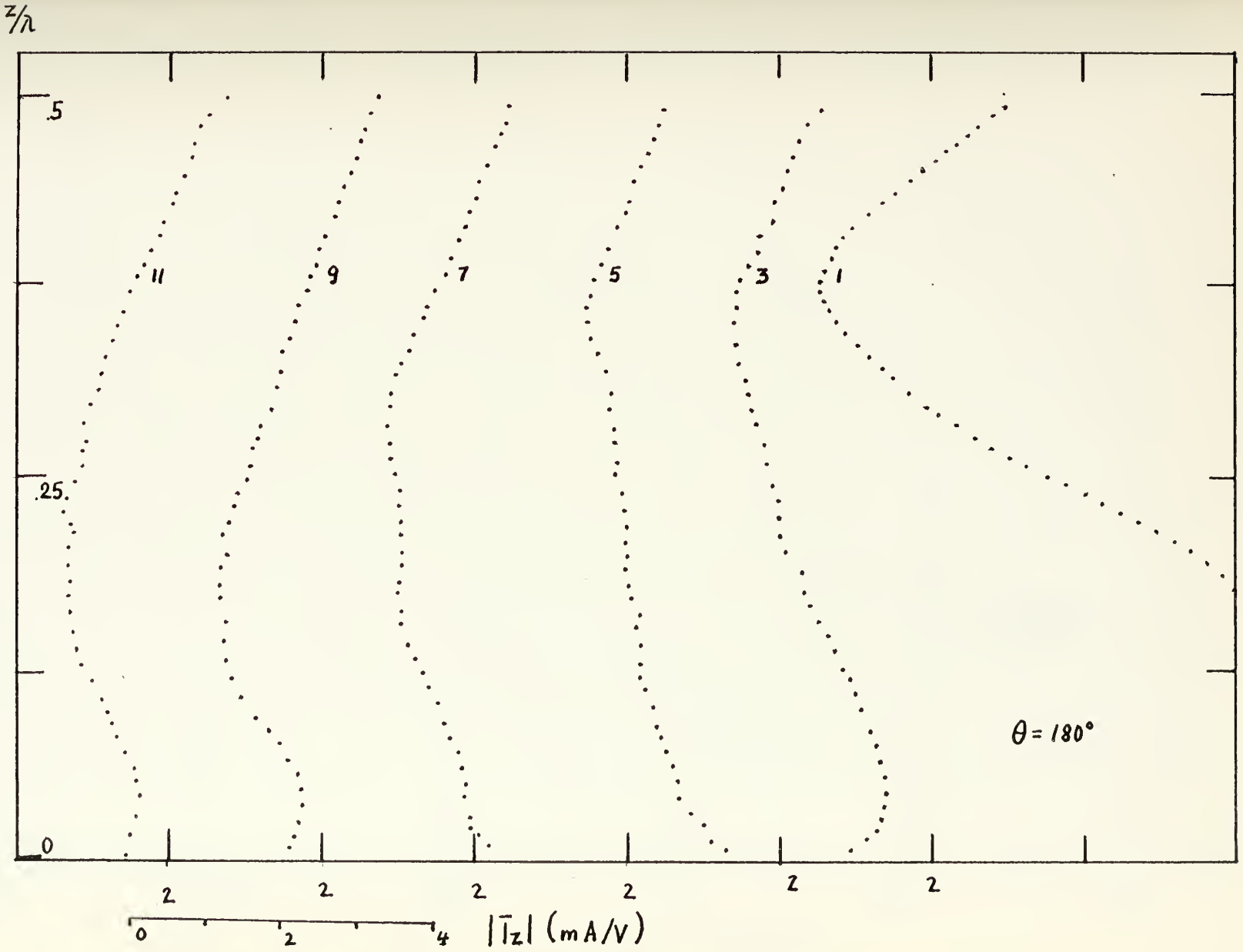

Figure 47.

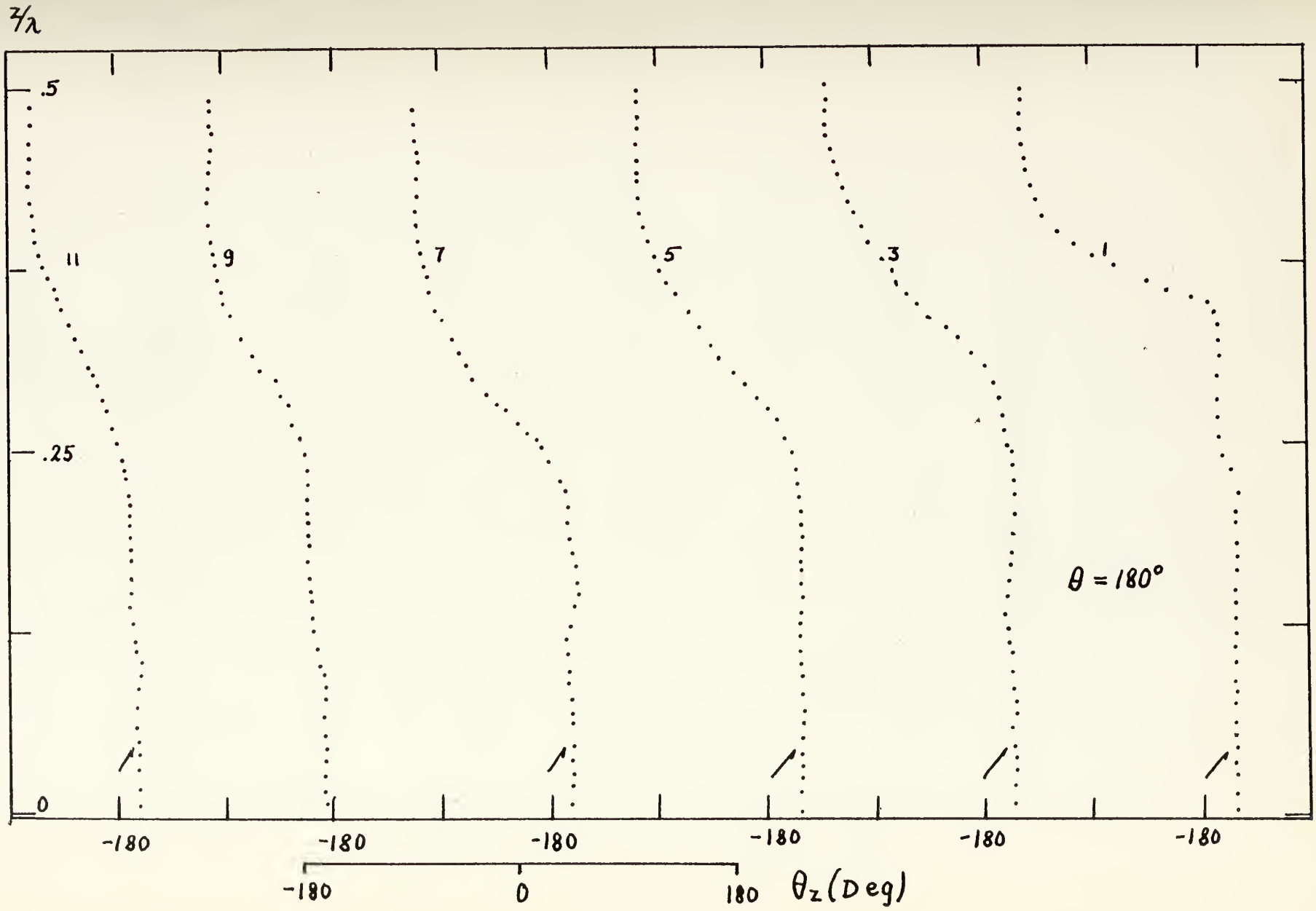

Figure 48.

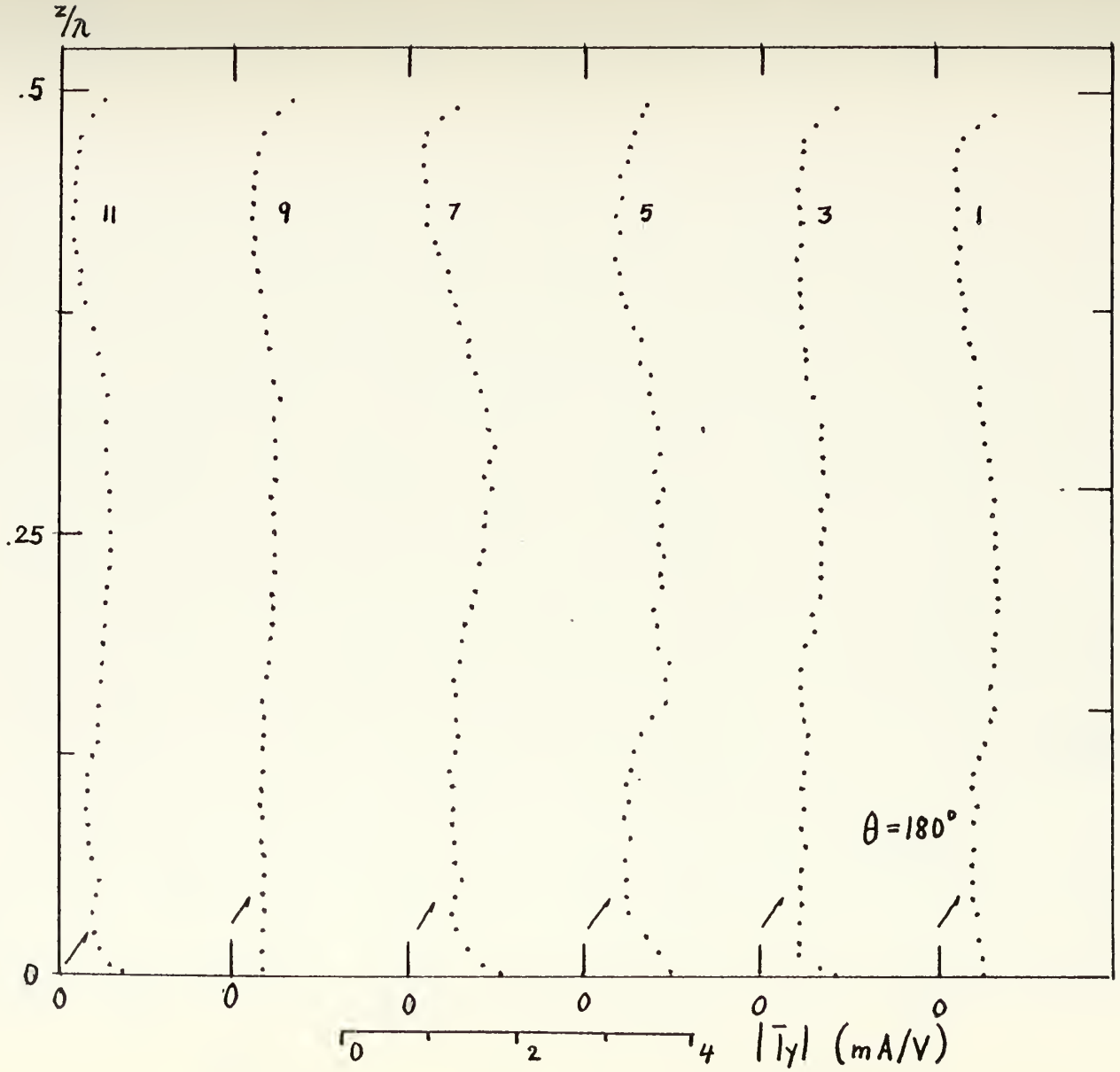

Figure 49.

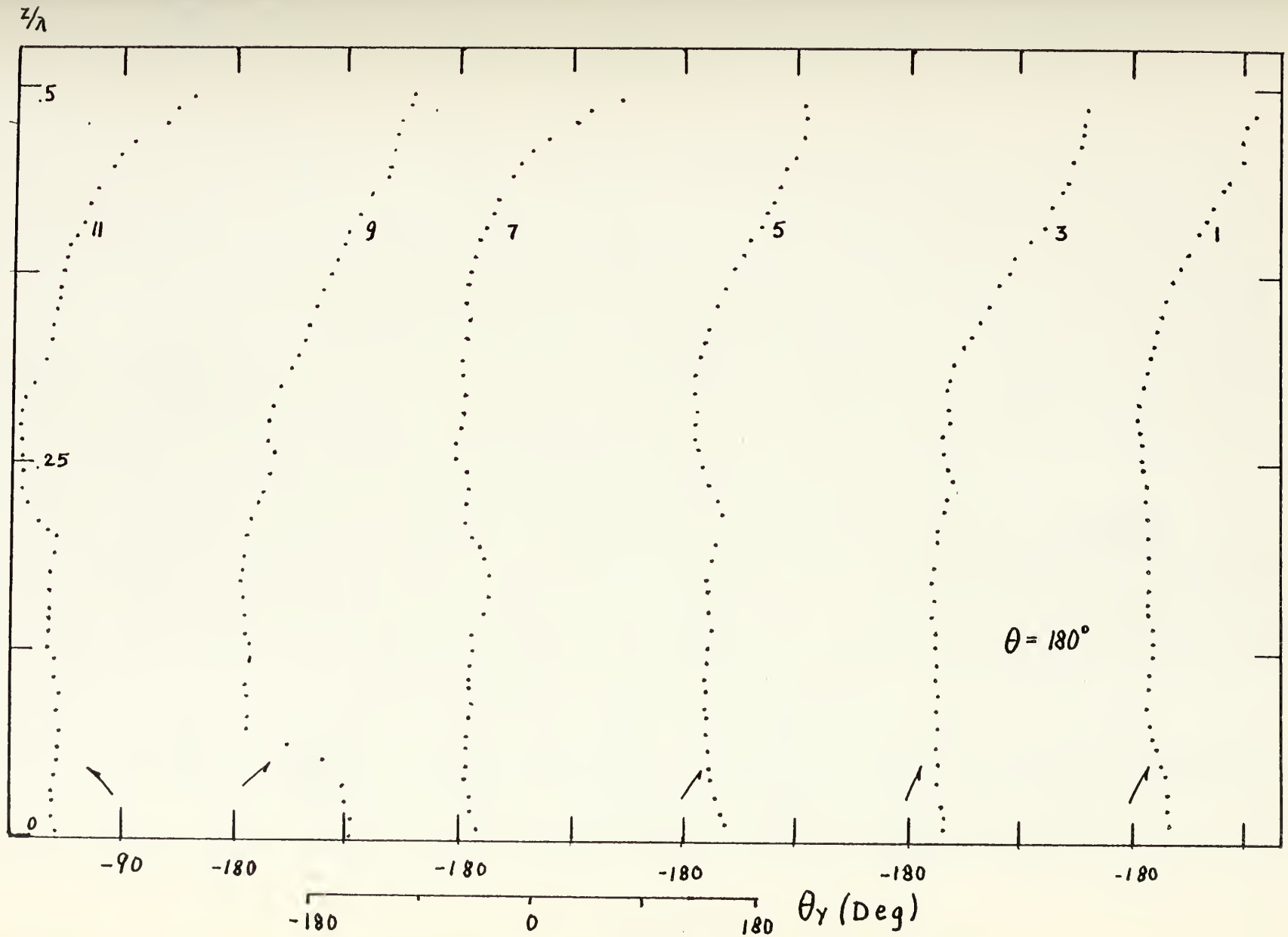

Figure 50.

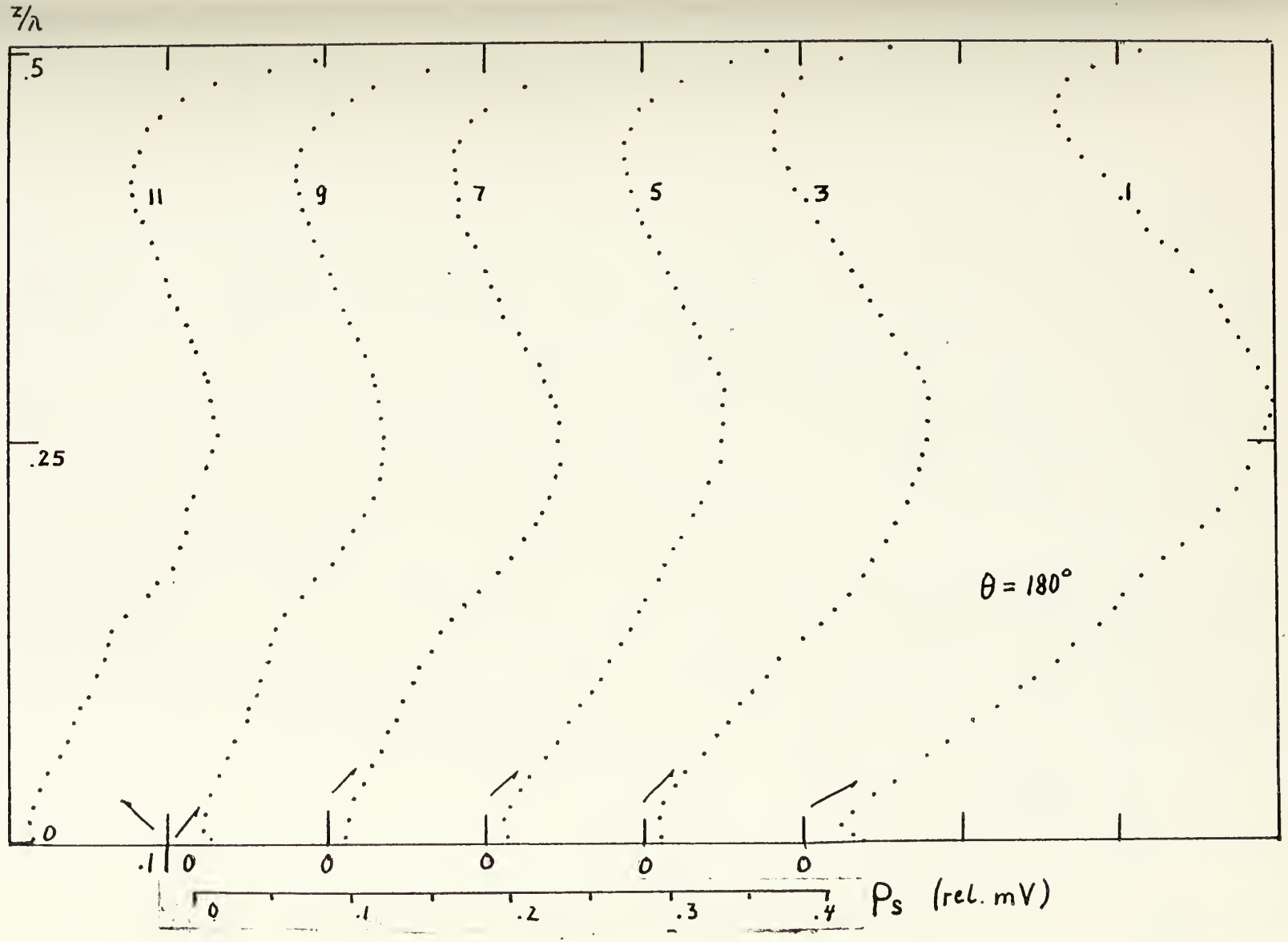

Figure 51.

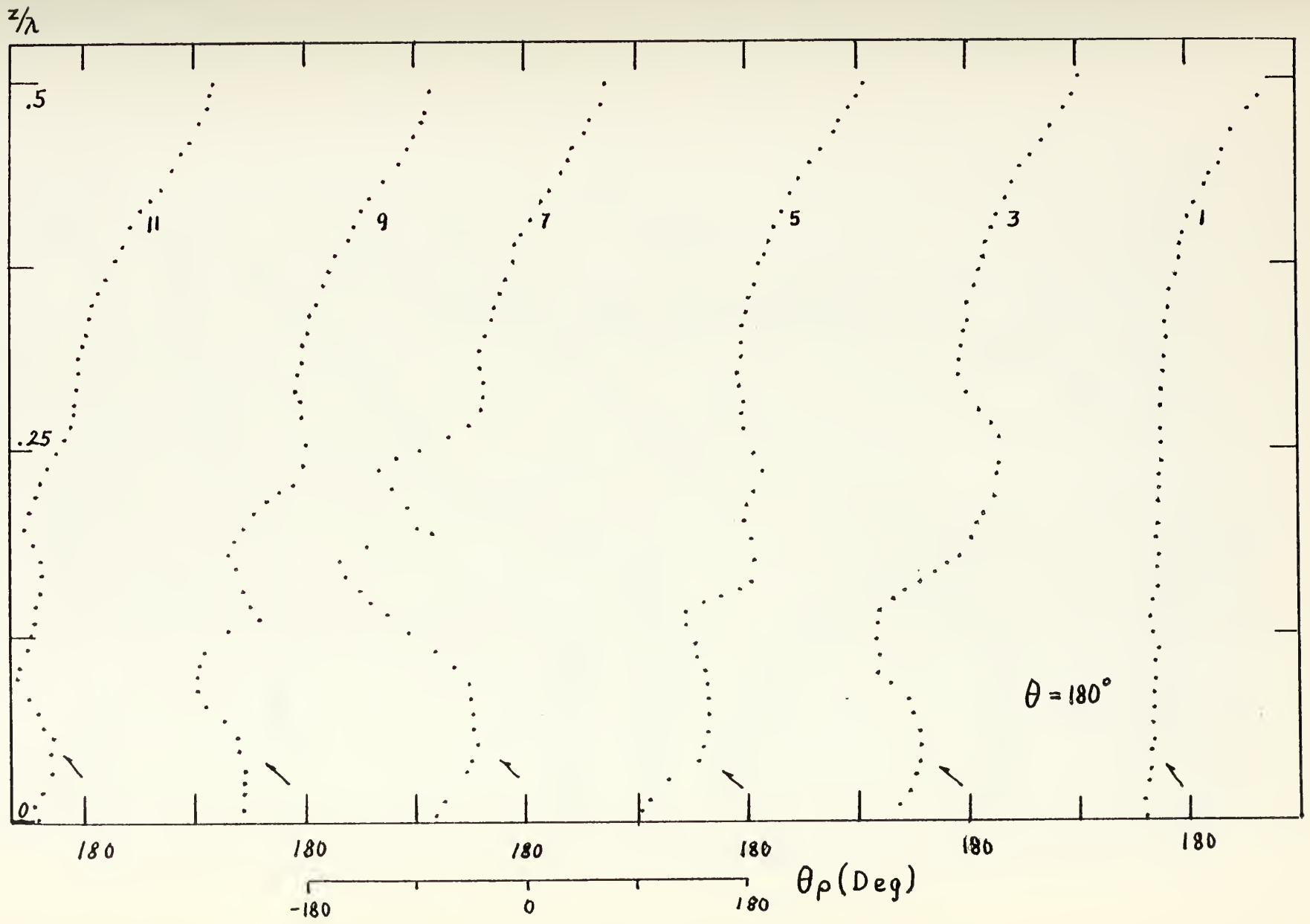

Figure 52.

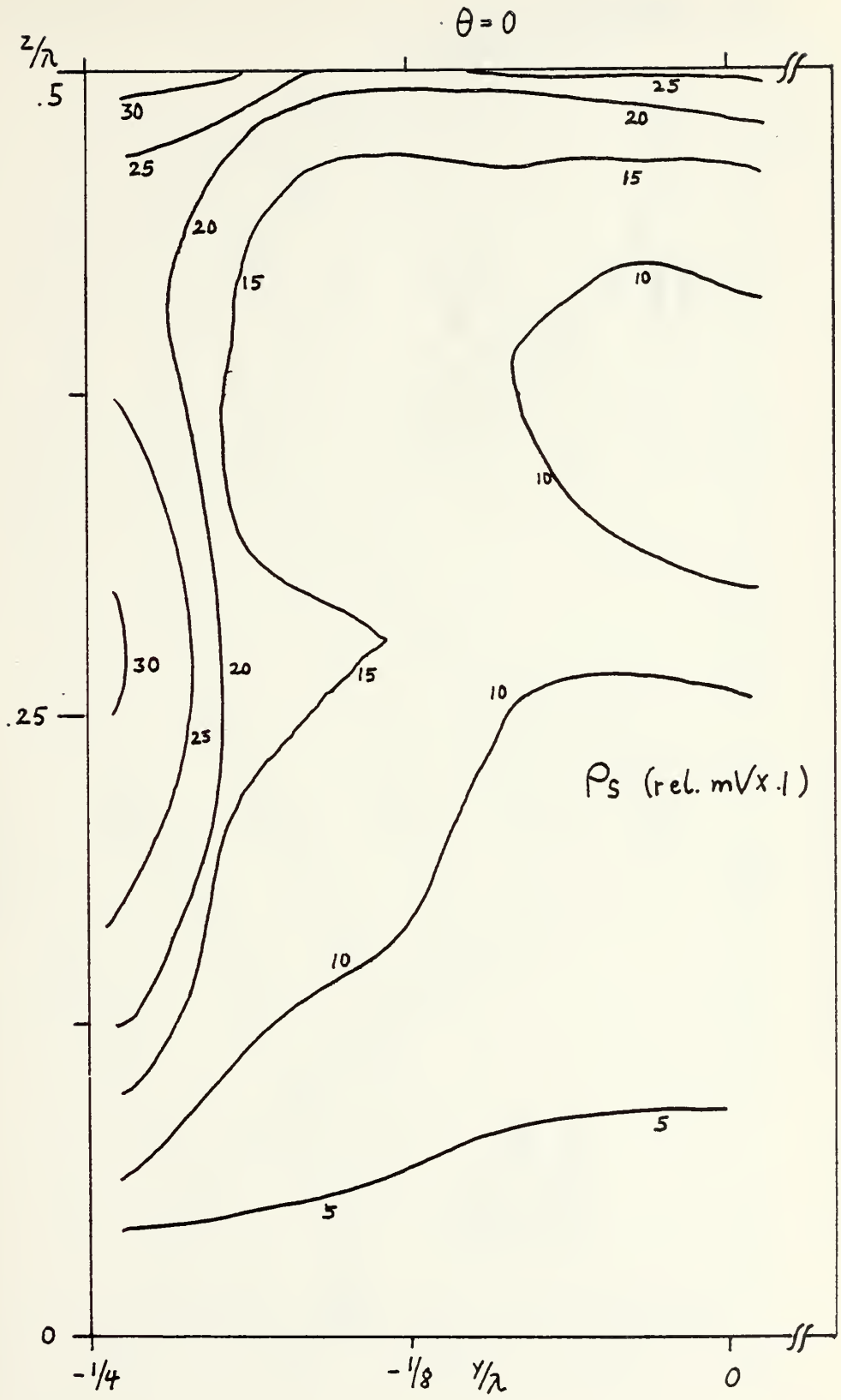

Figure 53.

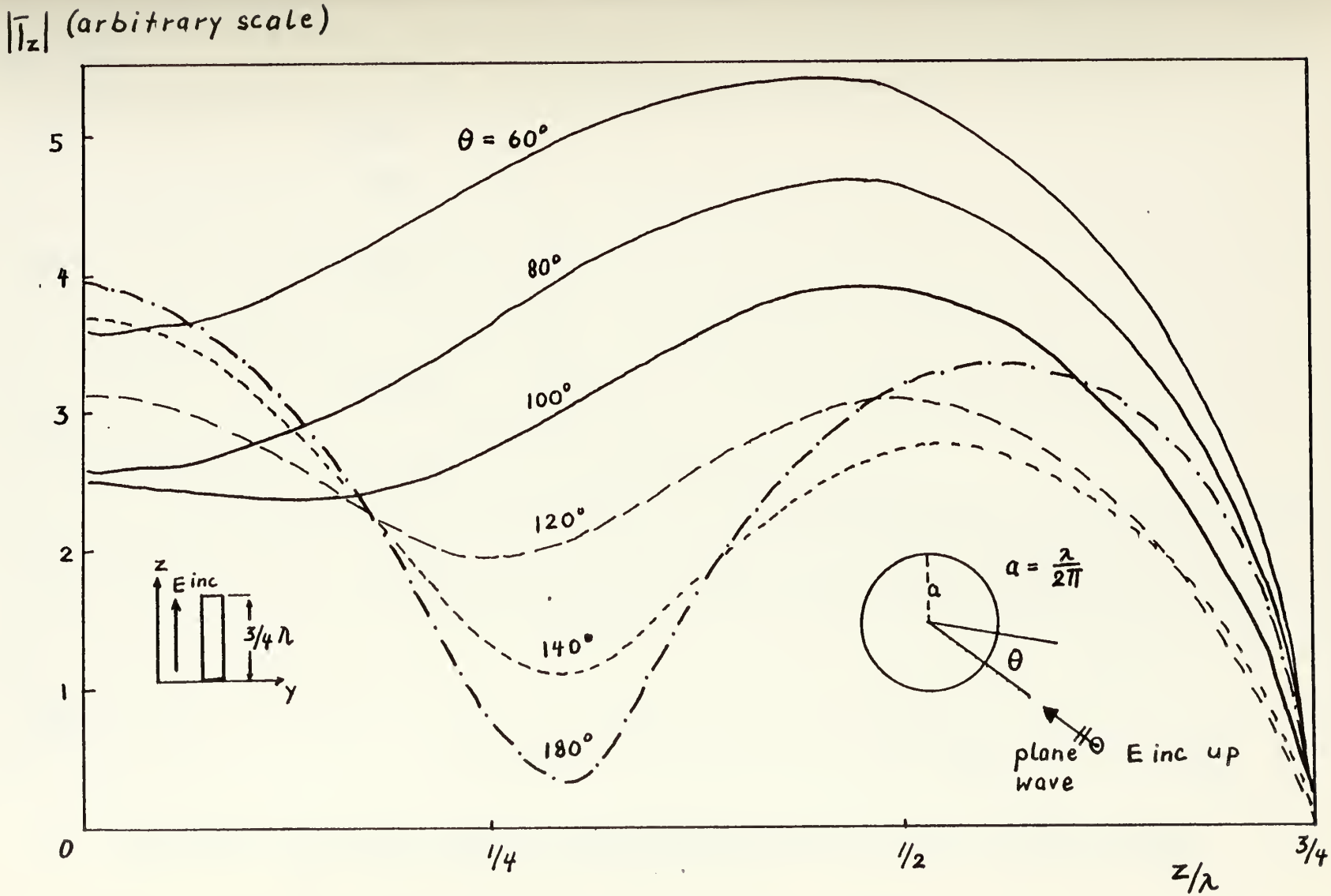

Figure 54a. Theoretical Magnitude of Axial Surface Current on a Fat Circular Cylinder [King, Burton, et al]

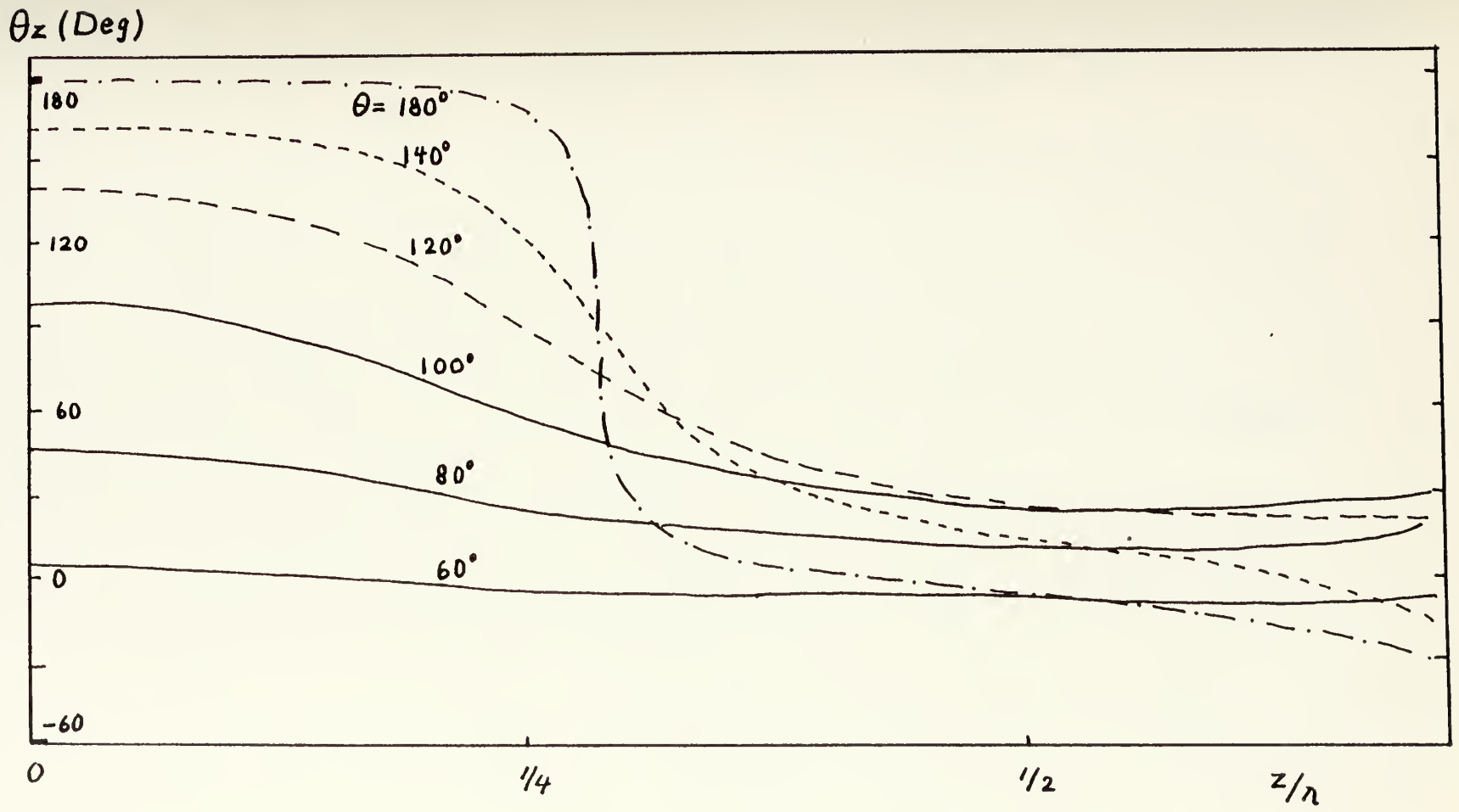

Figure 54b. Theoretical Phase of Axial Surface Current on a Fat Circular Cylinder (cf. Fig. 54a), [King, Burton et al]

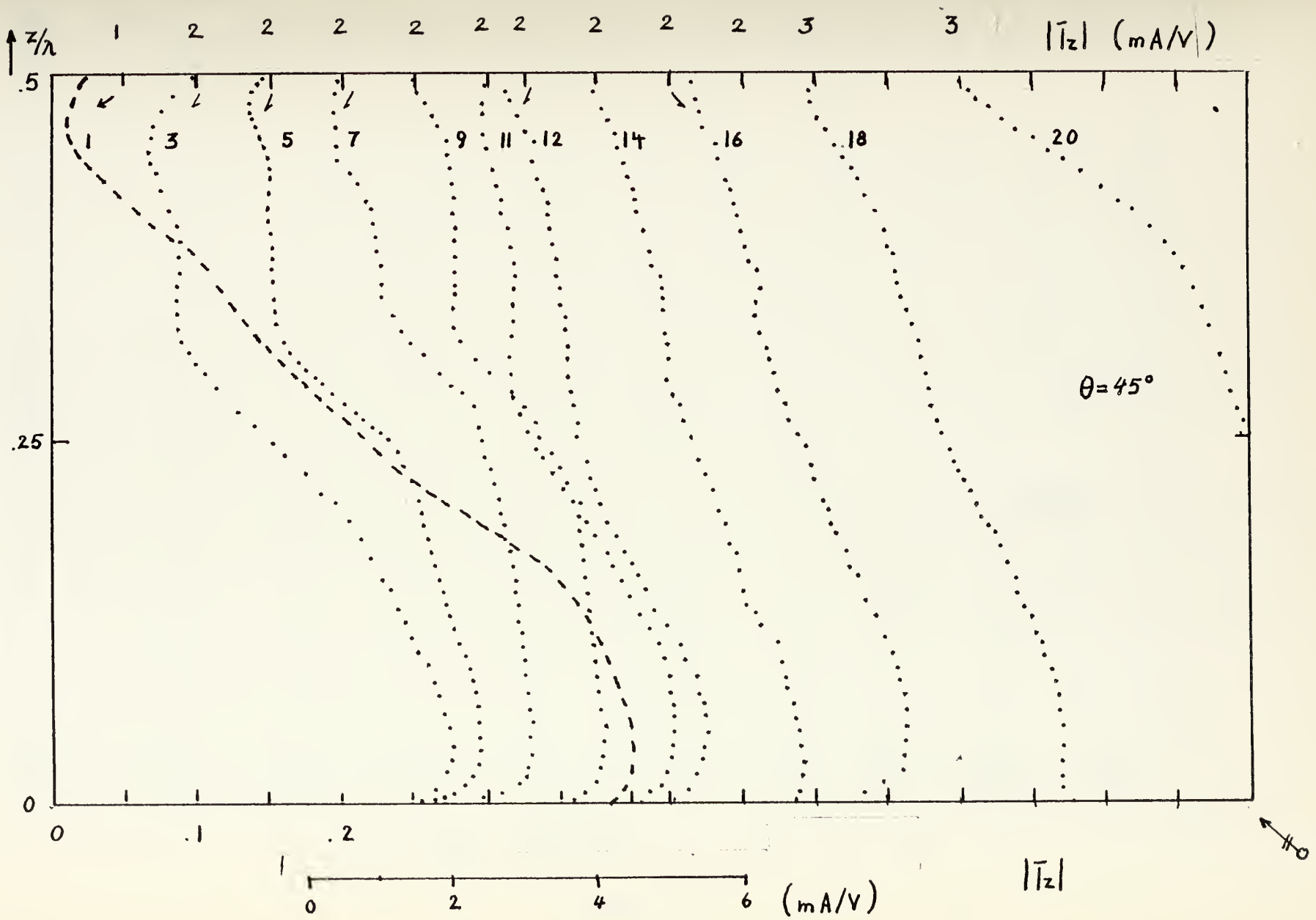
z/λ
1 2 2 2 2 2 2 2 2 2 2 3 3
|Īz| (mA/V)
.5
.25
0
1 3 5 7 9 11 12 14 16 18 20
θ=45°
0 .1 .2
|Īz|
0 2 4 6 (mA/V)

Figure 55.

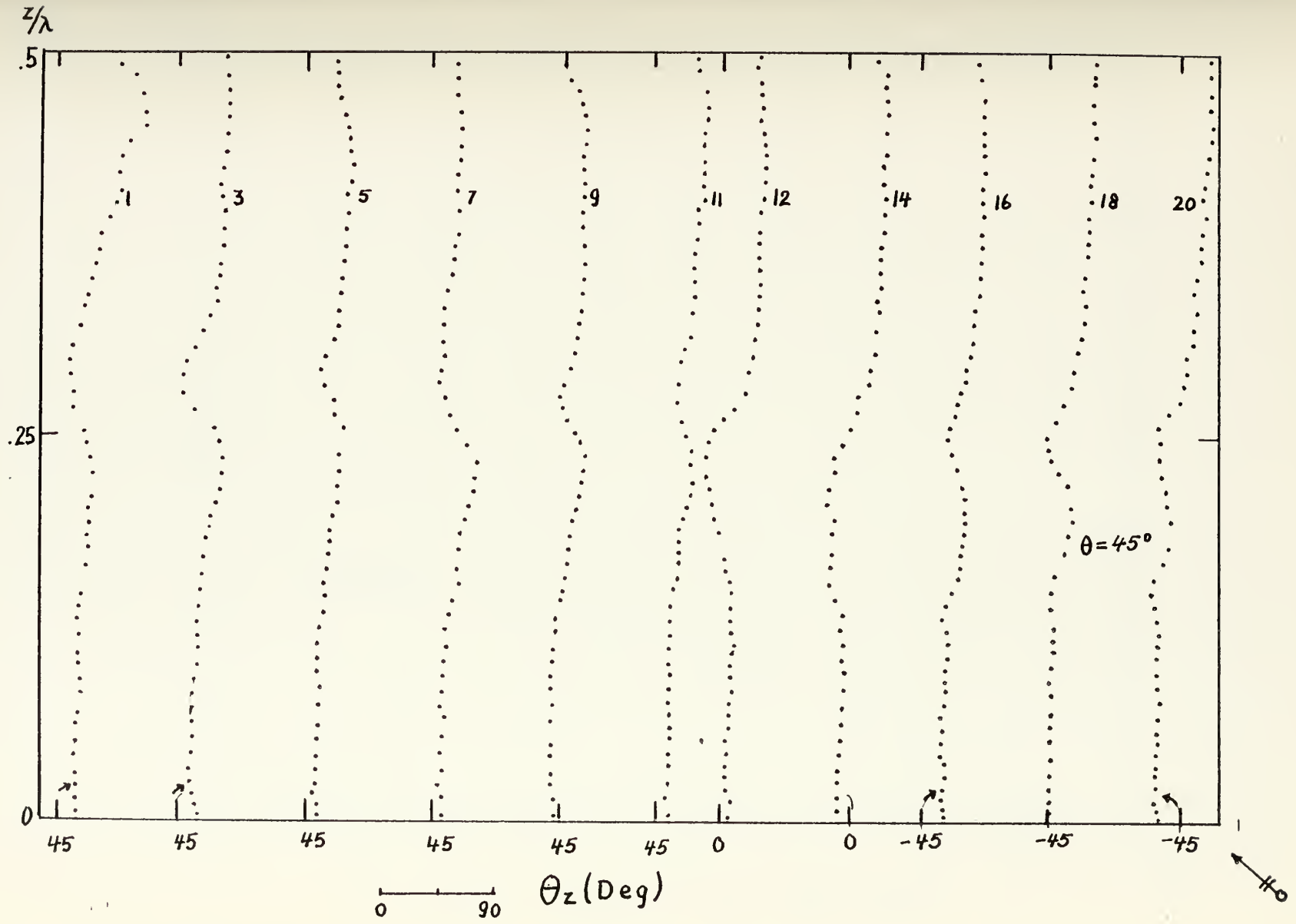
z/λ
.5
.25
0
1
3
5
7
9
11
12
14
16
18
20
θ=45°
45
45
45
45
45
45
0
0
-45
-45
-45
0
90
θz (Deg)

Figure 56.

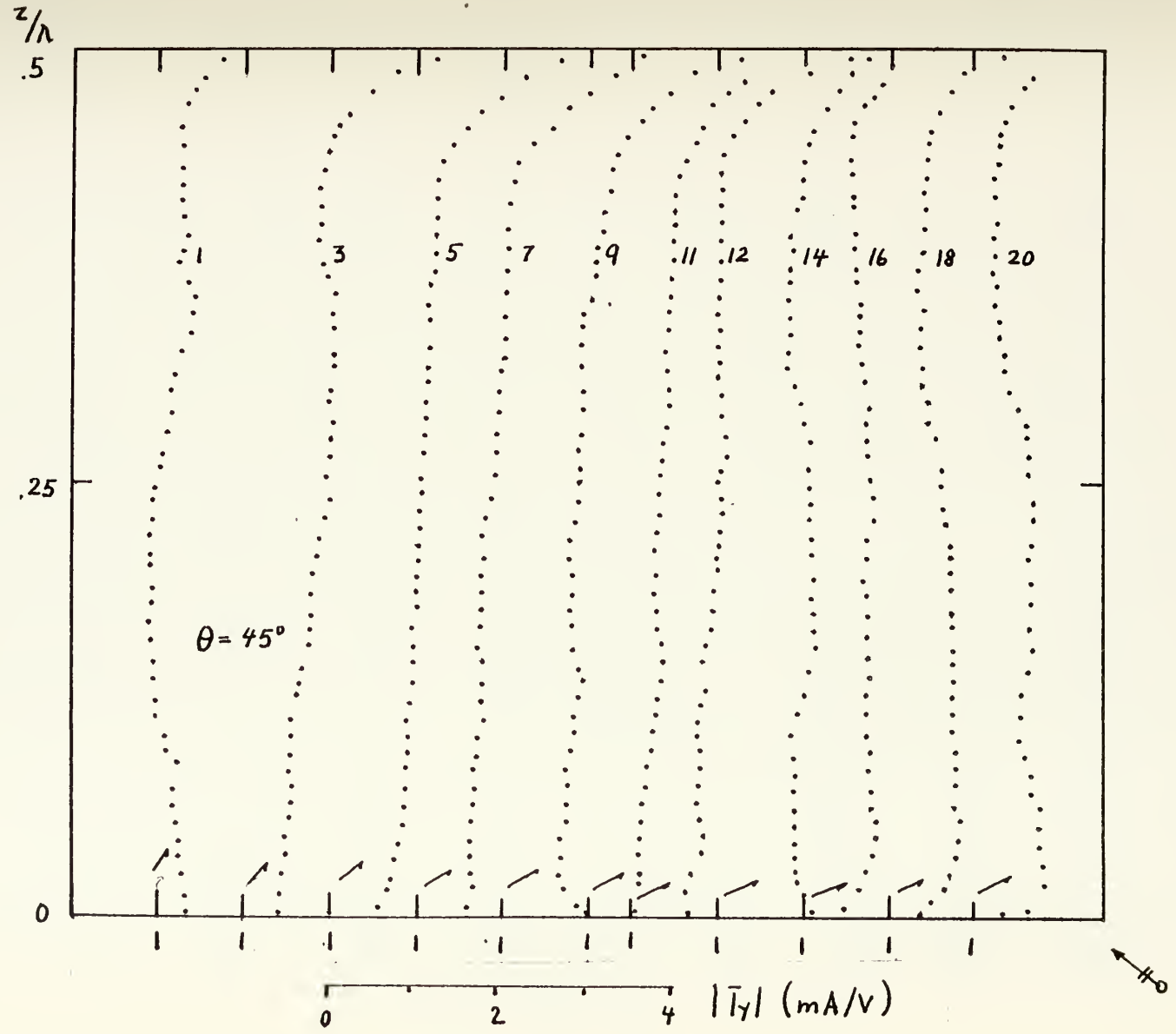

Figure 57.

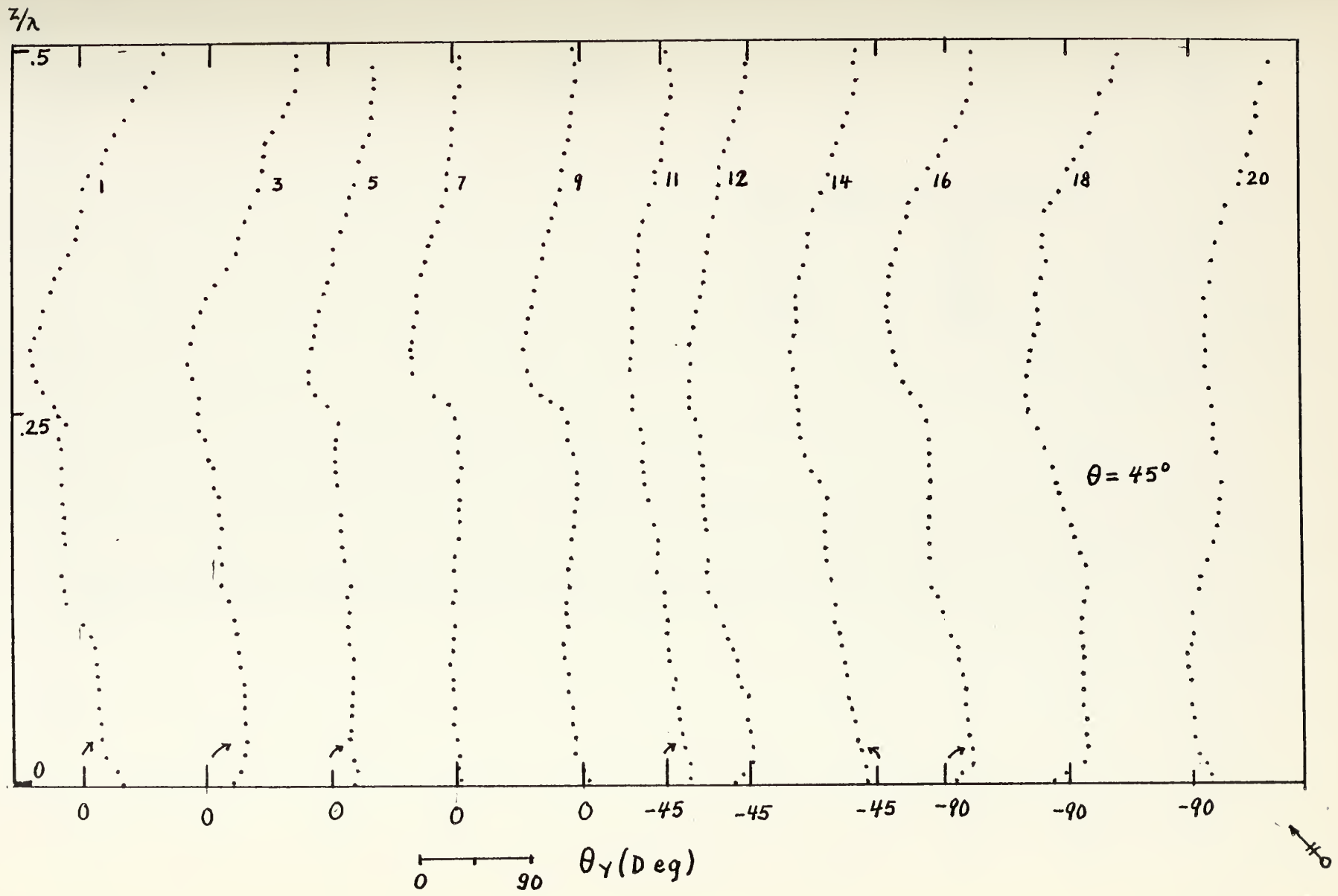
z/λ
.5
.25
0
1
3
5
7
9
11
12
14
16
18
20
θ = 45°
0
0
0
0
0
-45
-45
-45
-90
-90
-90
0
90
θY (Deg)

Figure 58.

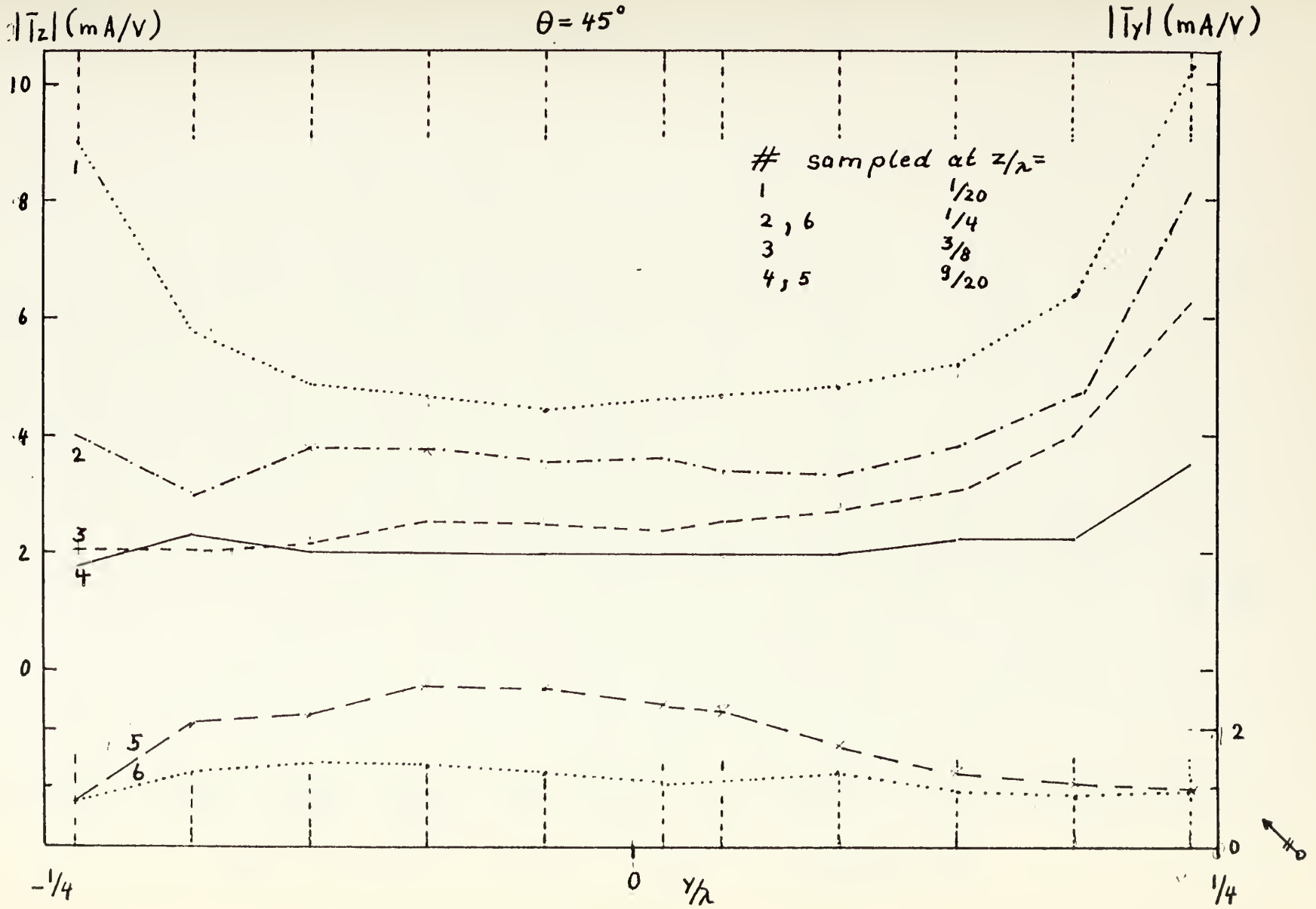
$|\bar{I}_z|$ (mA/V)
$\theta = 45°$
$|\bar{I}_y|$ (mA/V)
10
8
6
4
2
0
sampled at z/λ=
1 1/20
2, 6 1/4
3 3/8
4, 5 9/20
1
2
3
4
5
6
2
0
-1/4
0
Y/λ
1/4

Figure 59.

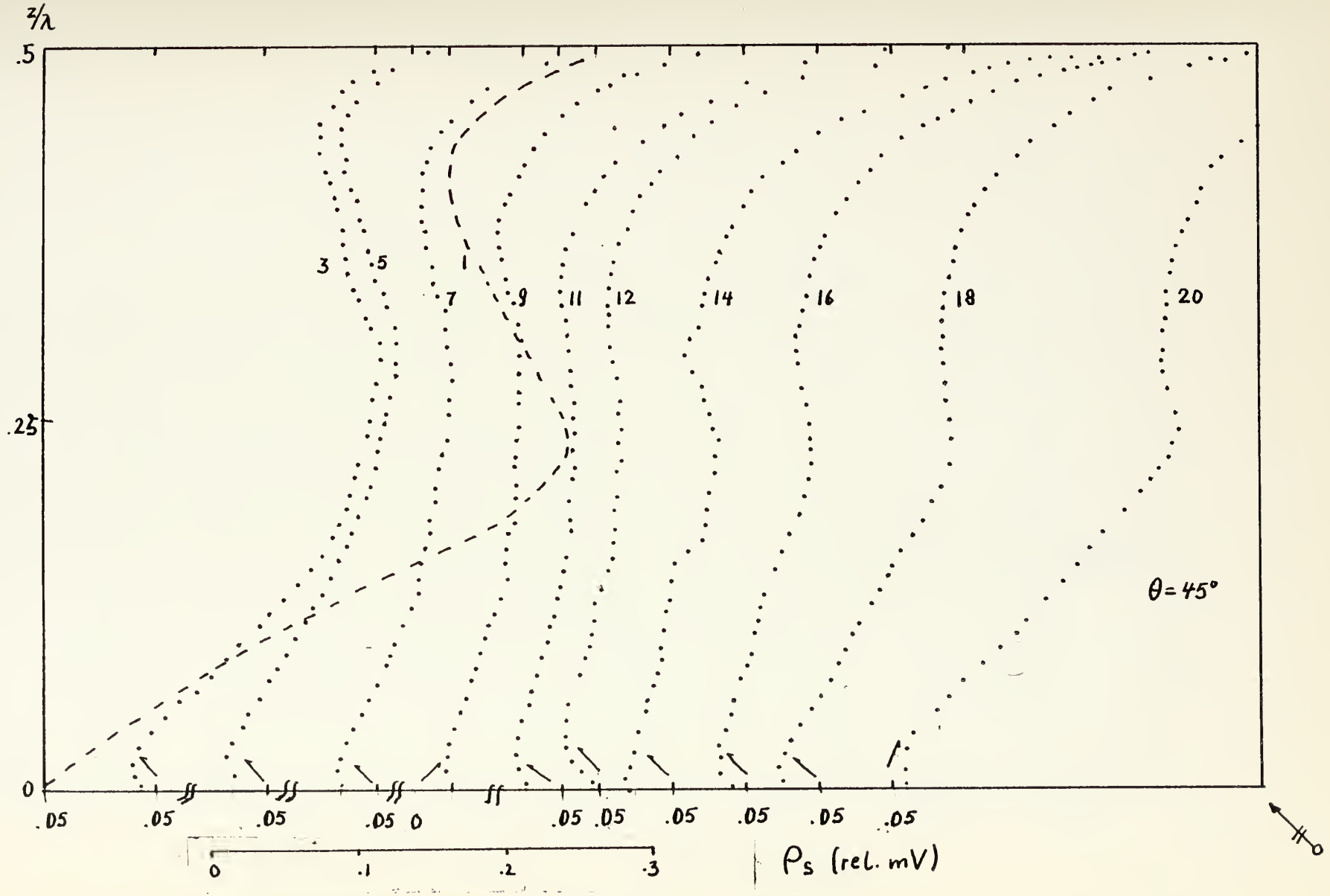
z/λ
.5
.25
0
3
5
1
7
9
11
12
14
16
18
20
θ = 45°
.05
.05
.05
.05
0
.05
.05
.05
.05
.05
.05
0
.1
.2
.3
Ps (rel. mV)

Figure 60.

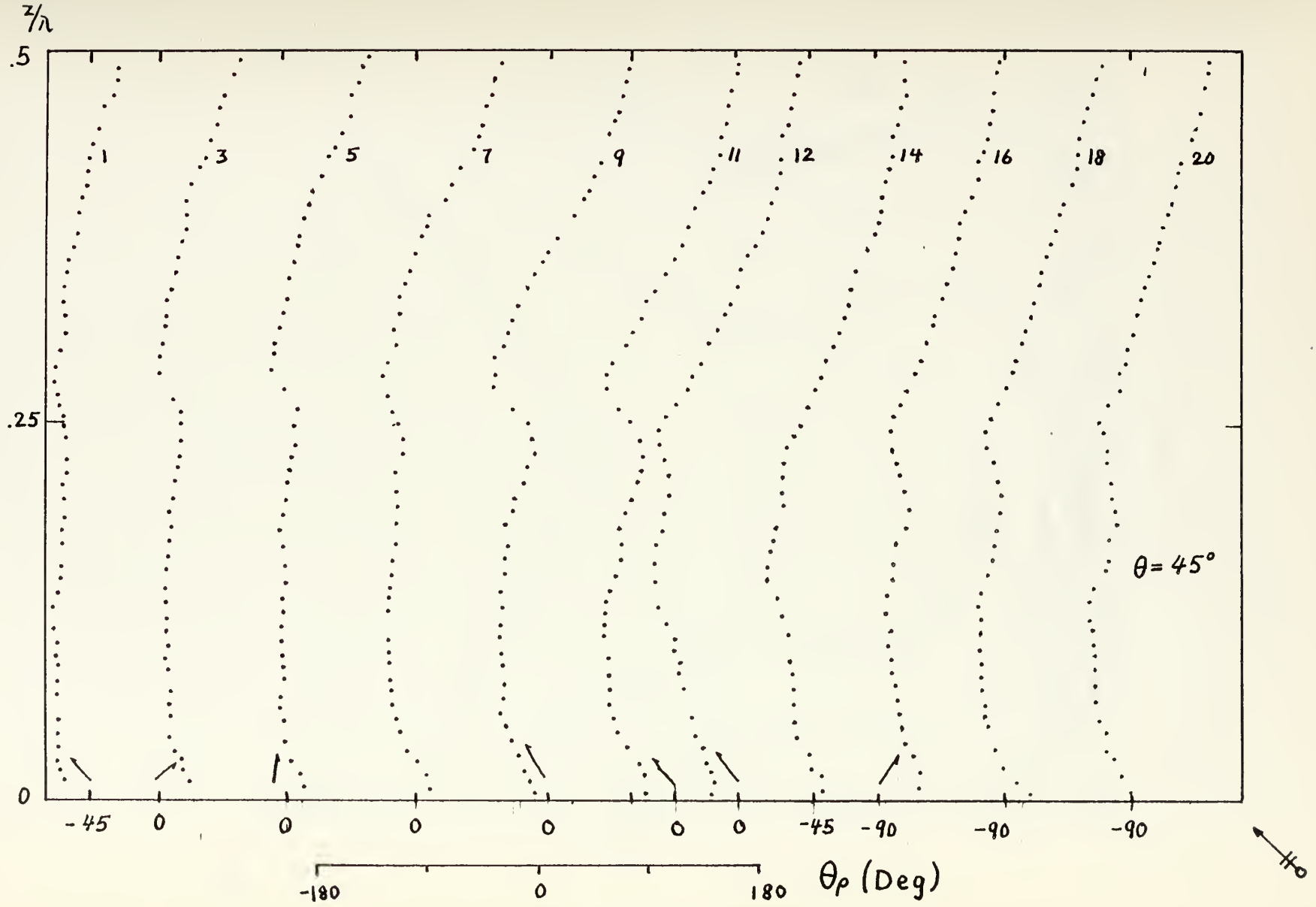
z/λ
.5
.25
0
1
3
5
7
9
11
12
14
16
18
20
θ= 45°
-45
0
0
0
0
0
0
-45
-90
-90
-90
-180
0
180
θp (Deg)

Figure 61.

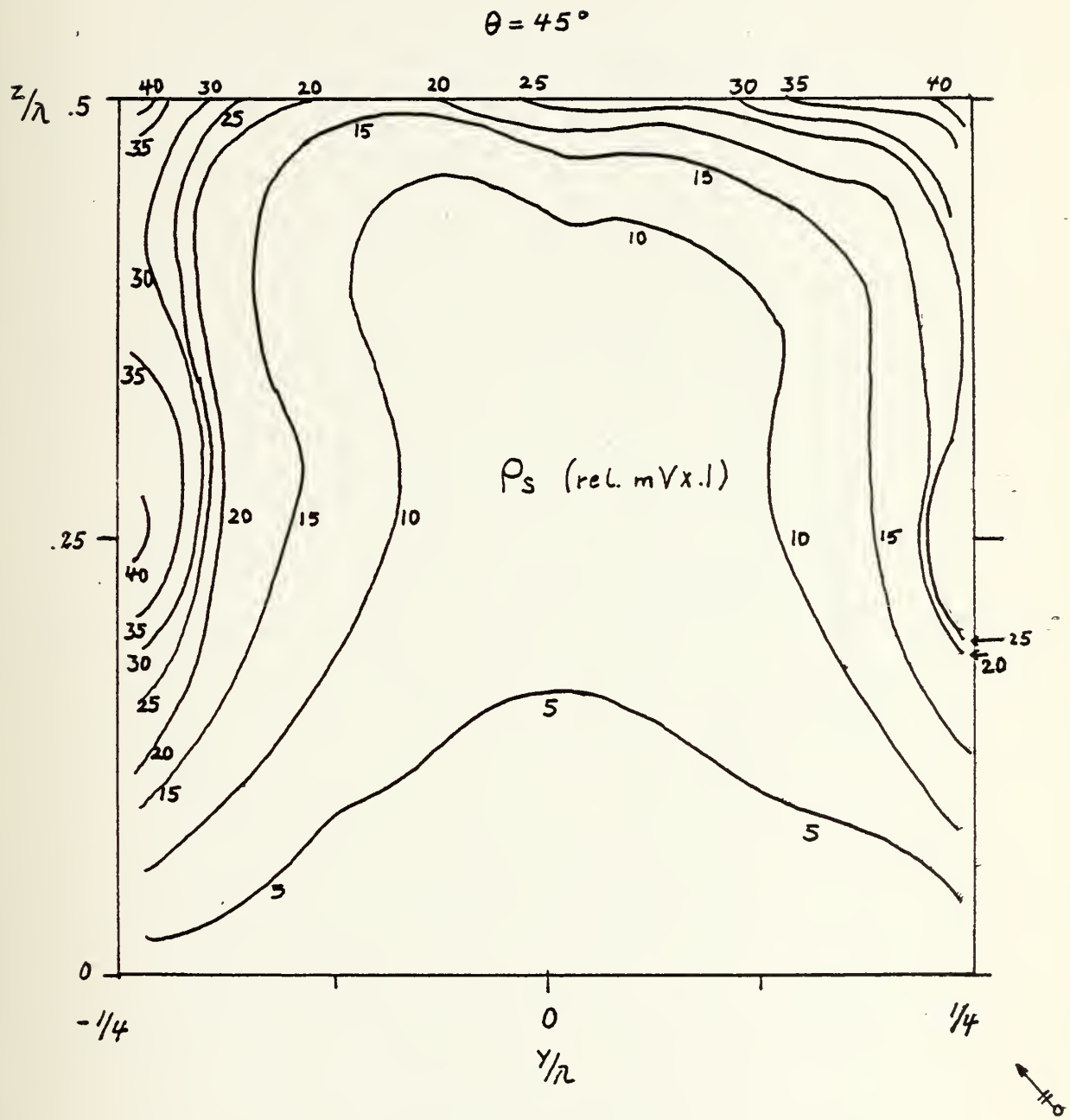
θ = 45°
z/λ .5
.25
0
-1/4
0
1/4
Y/λ
ρs (rel. mV x .1)
40
30
20
20
25
30
35
40
35
25
15
15
10
30
35
20
15
10
10
15
40
35
30
25
20
15
25
20
5
5
5

Figure 62.

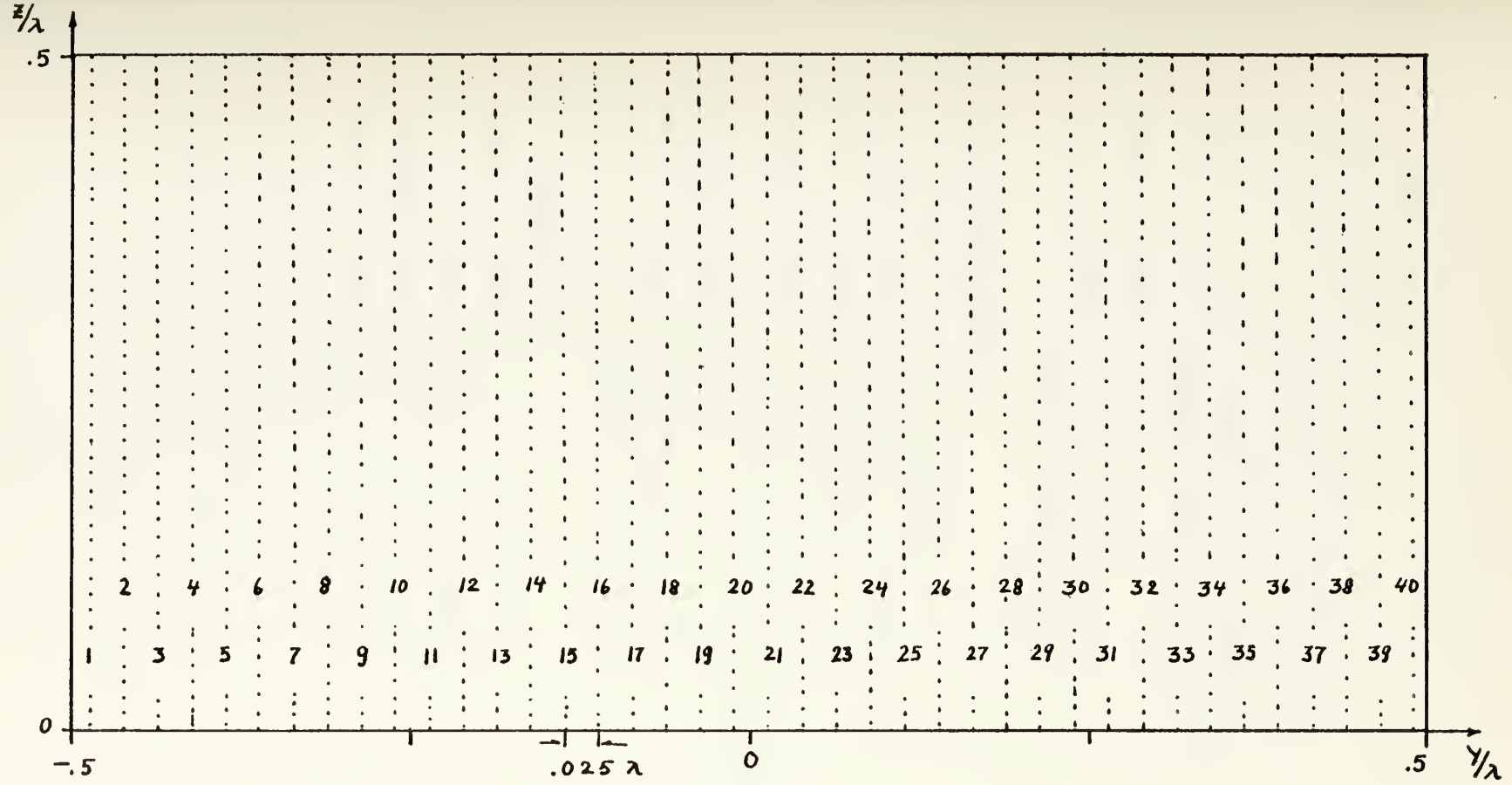

Figure 63a. Plate D

TITLE (PLATE D)	FIGURE
0° Aspect Angle	
Measured current in Z-direction	64
Measured phase of current in Z-direction	65
Measured current in Y-direction	66
Measured phase of current in Y-direction	67
Profile plot of measured currents in Y- and Z-direction	68
Measured charge density	69
Measured phase of charge density	70
Contour plot of measured charge density	71
180° Aspect Angle	
Measured current in Z-direction	74
Measured phase of current in Z-direction	75
Measured current in Y-direction	76
Measured phase of current in Y-direction	77
Profile plot of measured currents in Y- and Z-direction	78
Measured charge density	79
Measured phase of charge density	80
Contour plot of measured charge density	81
45° Aspect Angle	
Measured current in Z-direction	82
Measured phase of current in Z-direction	83
Measured current in Y-direction	84
Measured phase of current in Y-direction	85
Profile plot of measured currents in Y- and Z-direction	86
Measured charge density	87
Measured phase of charge density	88
Contour plot of measured charge density	89

Figure 63b. Titles of Graphs of Plate D

Current	Charge Density	Component			Sampling Direction		Magn.	Phase	Figure and Aspect		
		Y	Z	Total	Y	Z			0°	180°	45°
X			X			X	X		64	74	82
X			X			X		X	65	75	83
X		X				X	X		66	76	84
X		X				X		X	67	77	85
X		X	X		X		X		68	78	86
	X			X		X	X		69	79	87
	X			X		X		X	70	80	88
	X			X	X	X	X		71	81	89

Figure 63c. Labels of Graphs (Plate D)

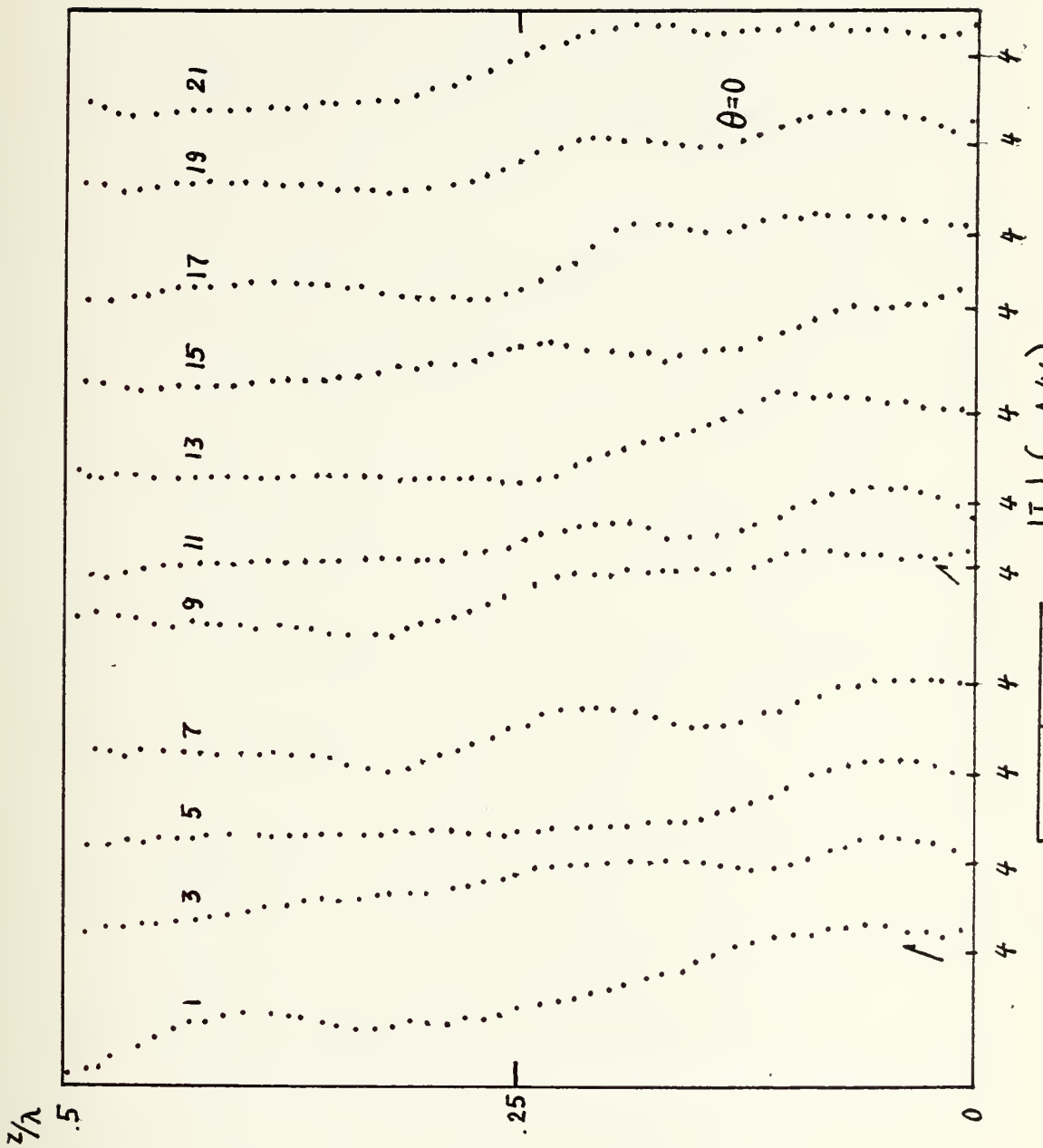

Figure 64.

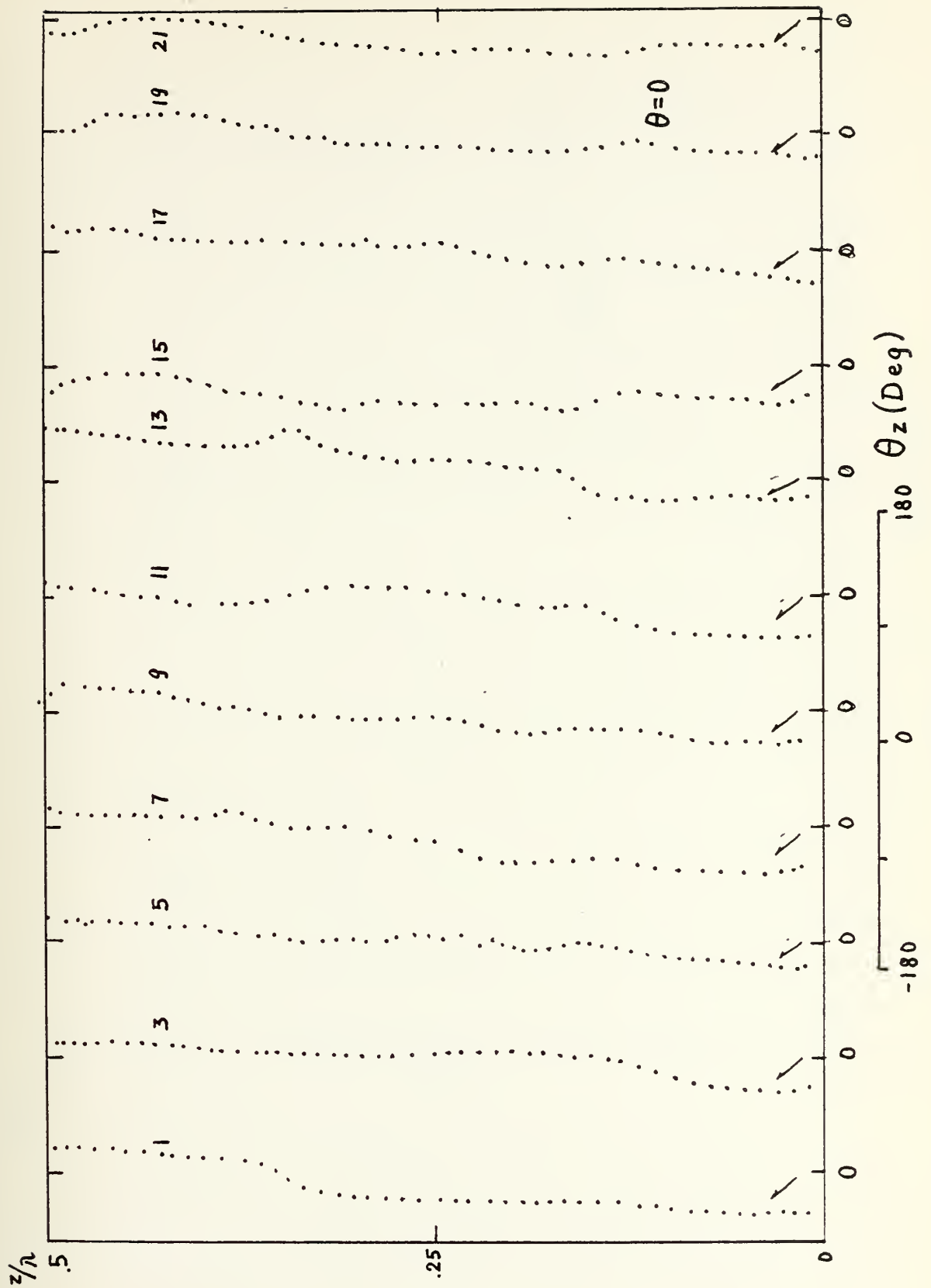

Figure 65.

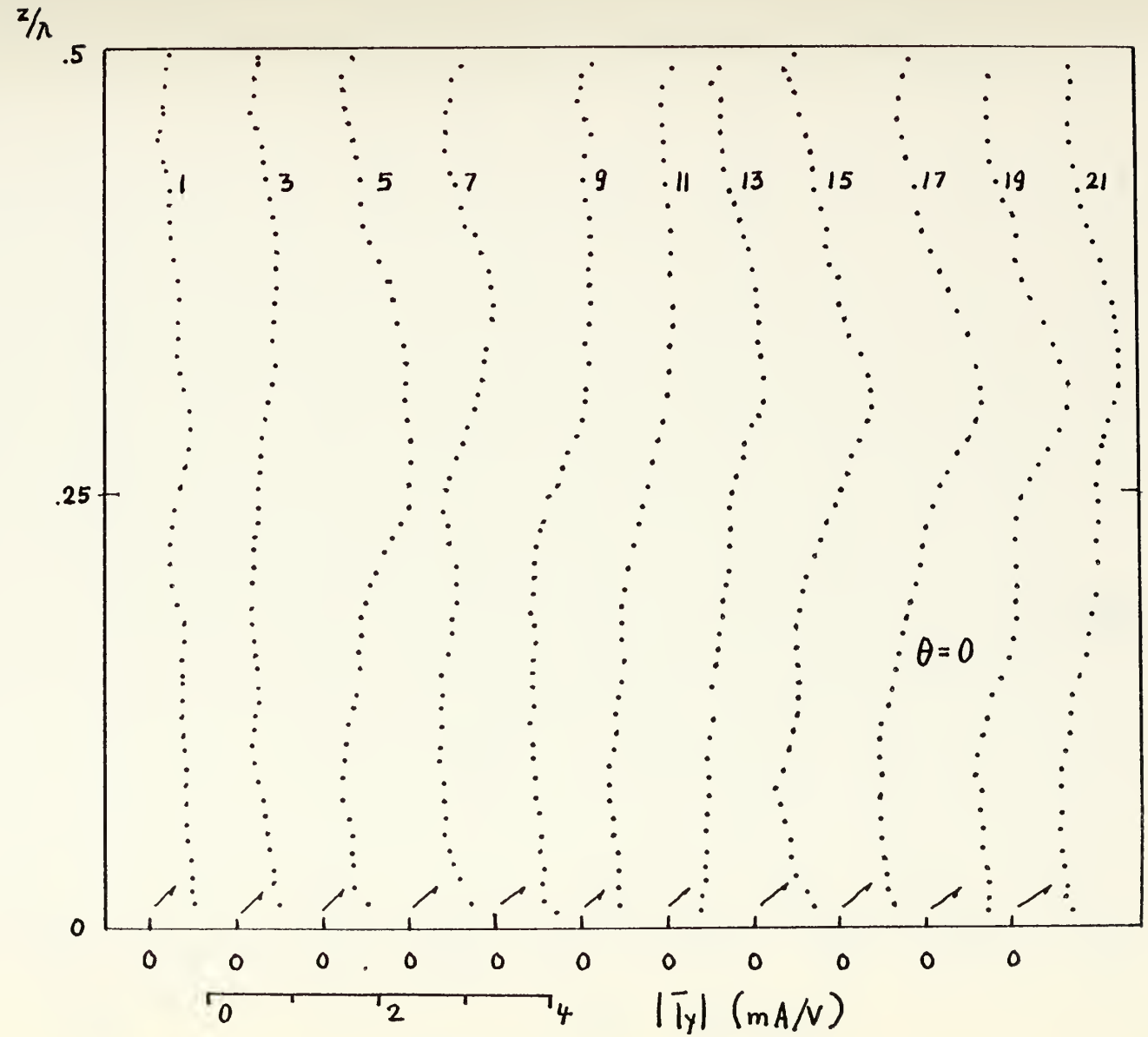

Figure 66.

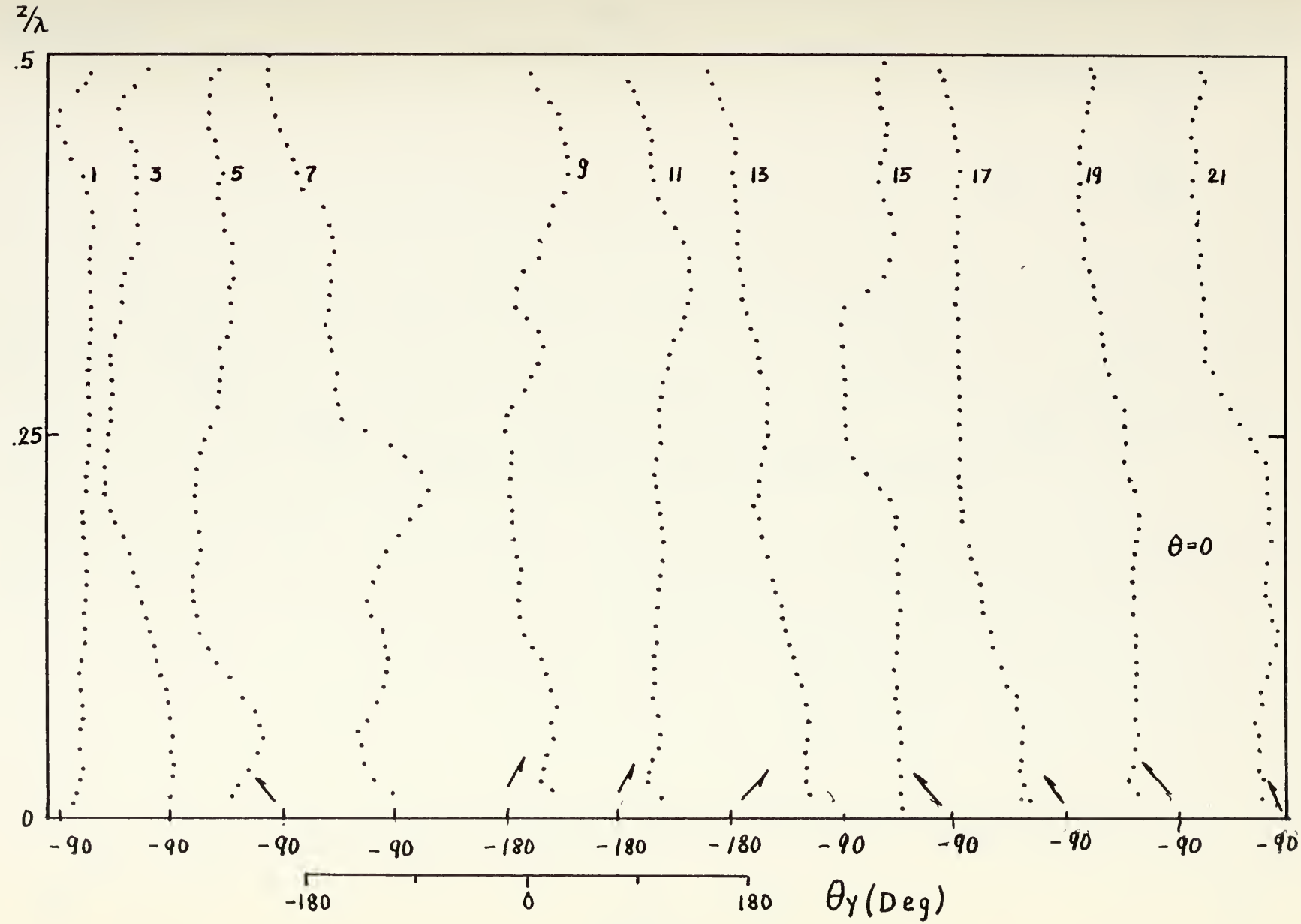
z/λ
.5
.25
0
1
3
5
7
9
11
13
15
17
19
21
θ=0
-90
-90
-90
-90
-180
-180
-180
-90
-90
-90
-90
-90
-180
0
180
θy (Deg)

Figure 67.

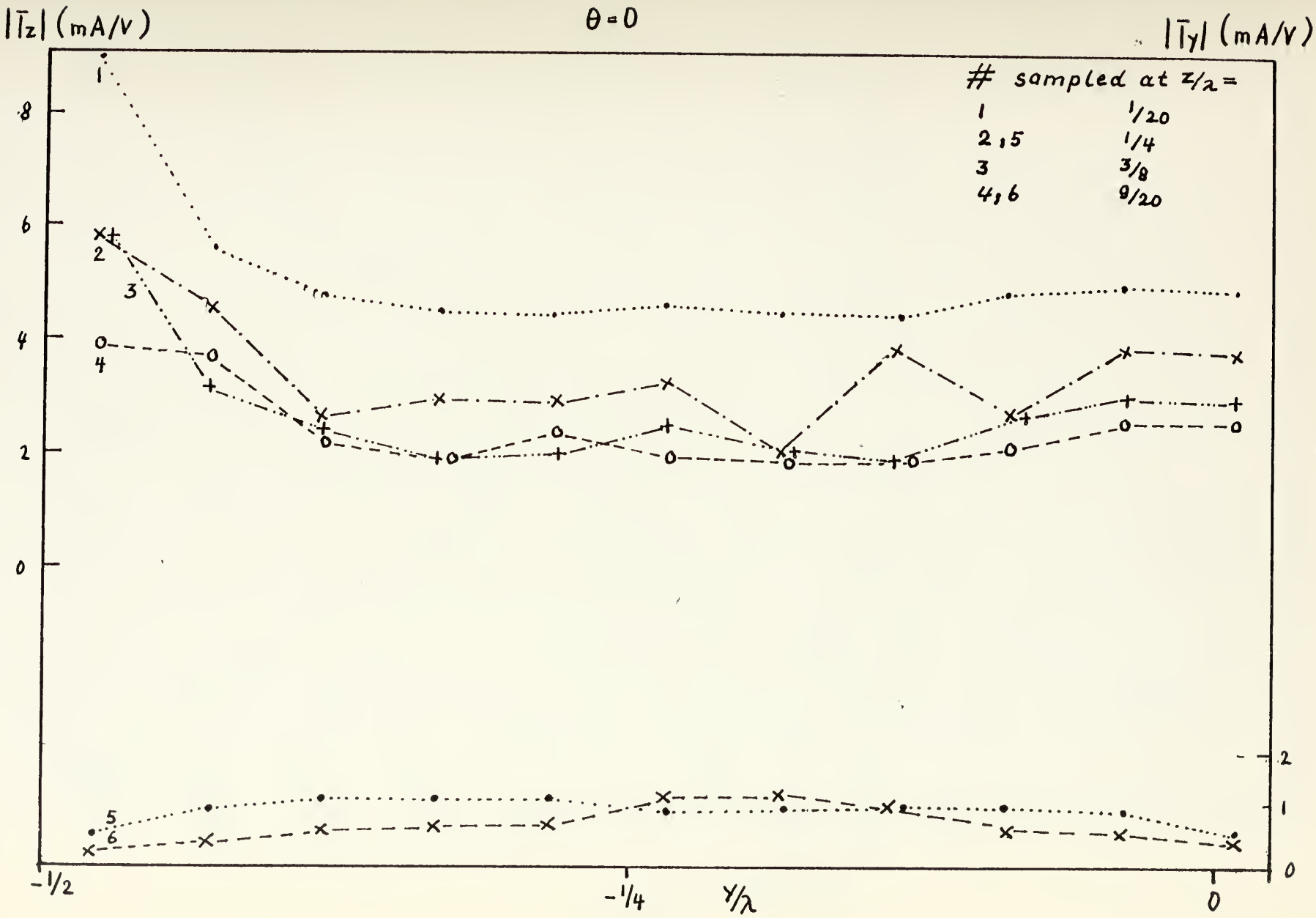
|Īz| (mA/V)
θ = 0
|Īy| (mA/V)
sampled at z/λ =
1 1/20
2,5 1/4
3 3/8
4,6 9/20
8
6
4
2
0
2
1
0
-1/2
-1/4
y/λ
0

Figure 68.

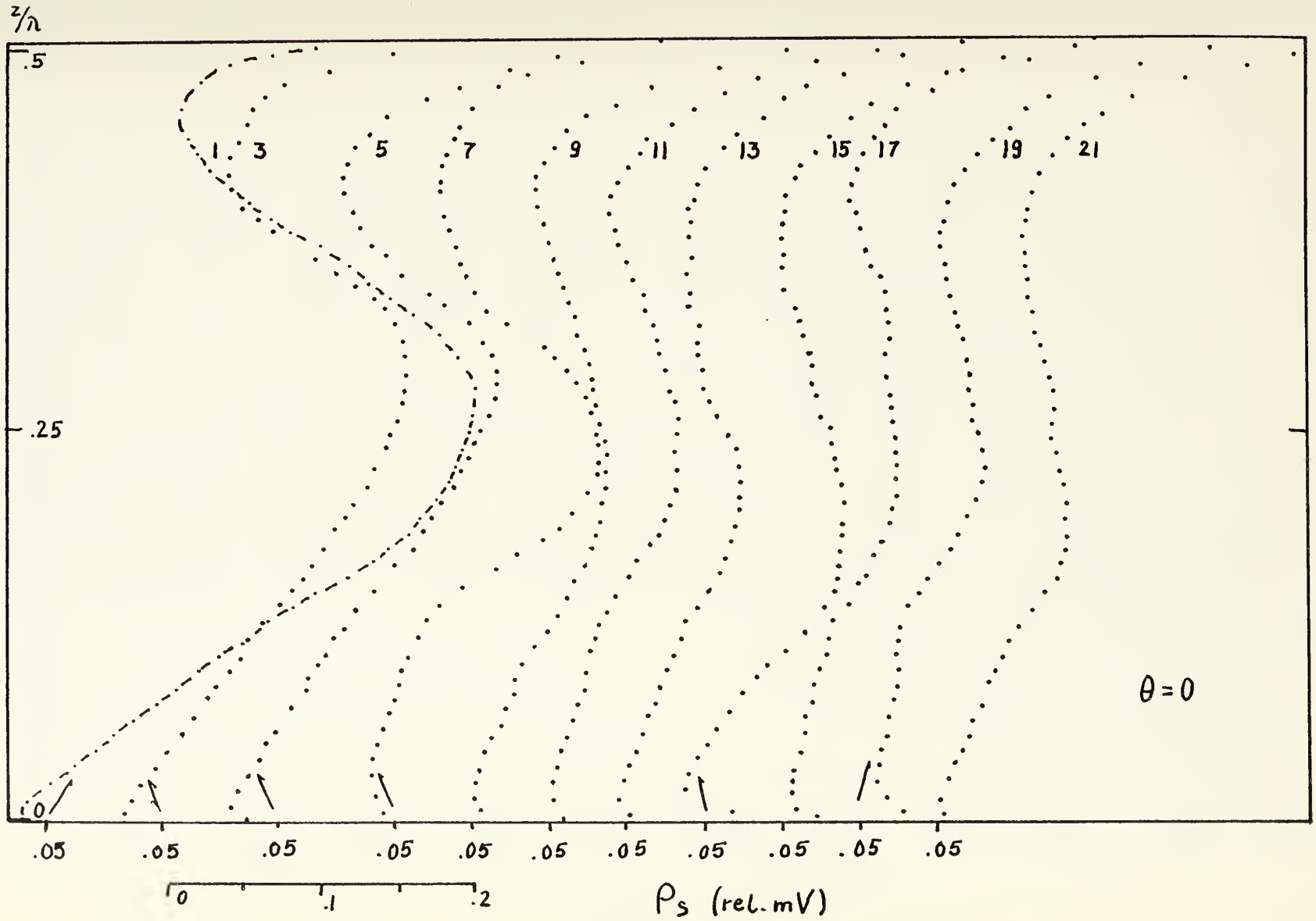
z/λ
.5
.25
0
1
3
5
7
9
11
13
15
17
19
21
θ = 0
.05
.05
.05
.05
.05
.05
.05
.05
.05
.05
.05
0
.1
.2
ρs (rel. mV)

Figure 69.

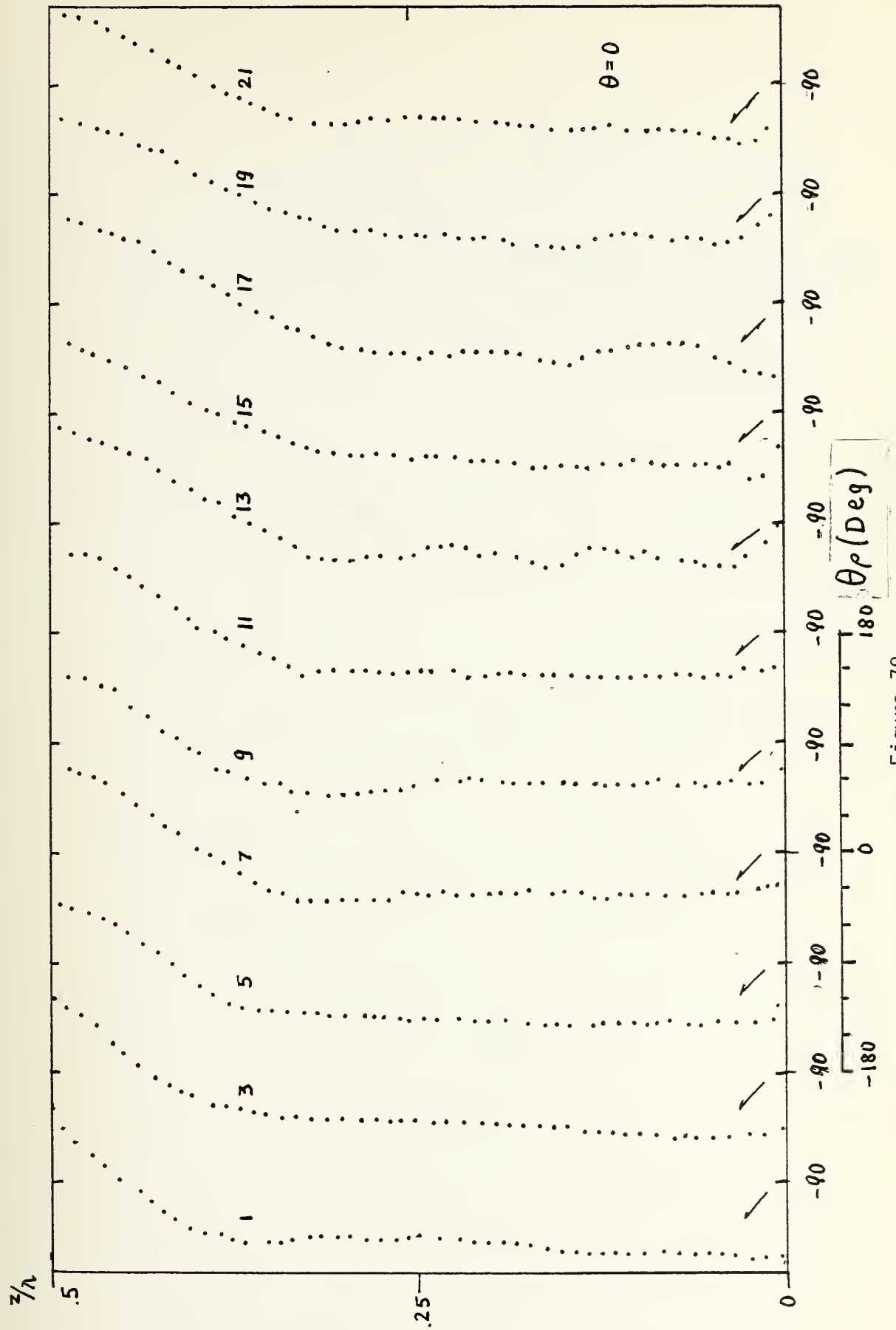

Figure 70.

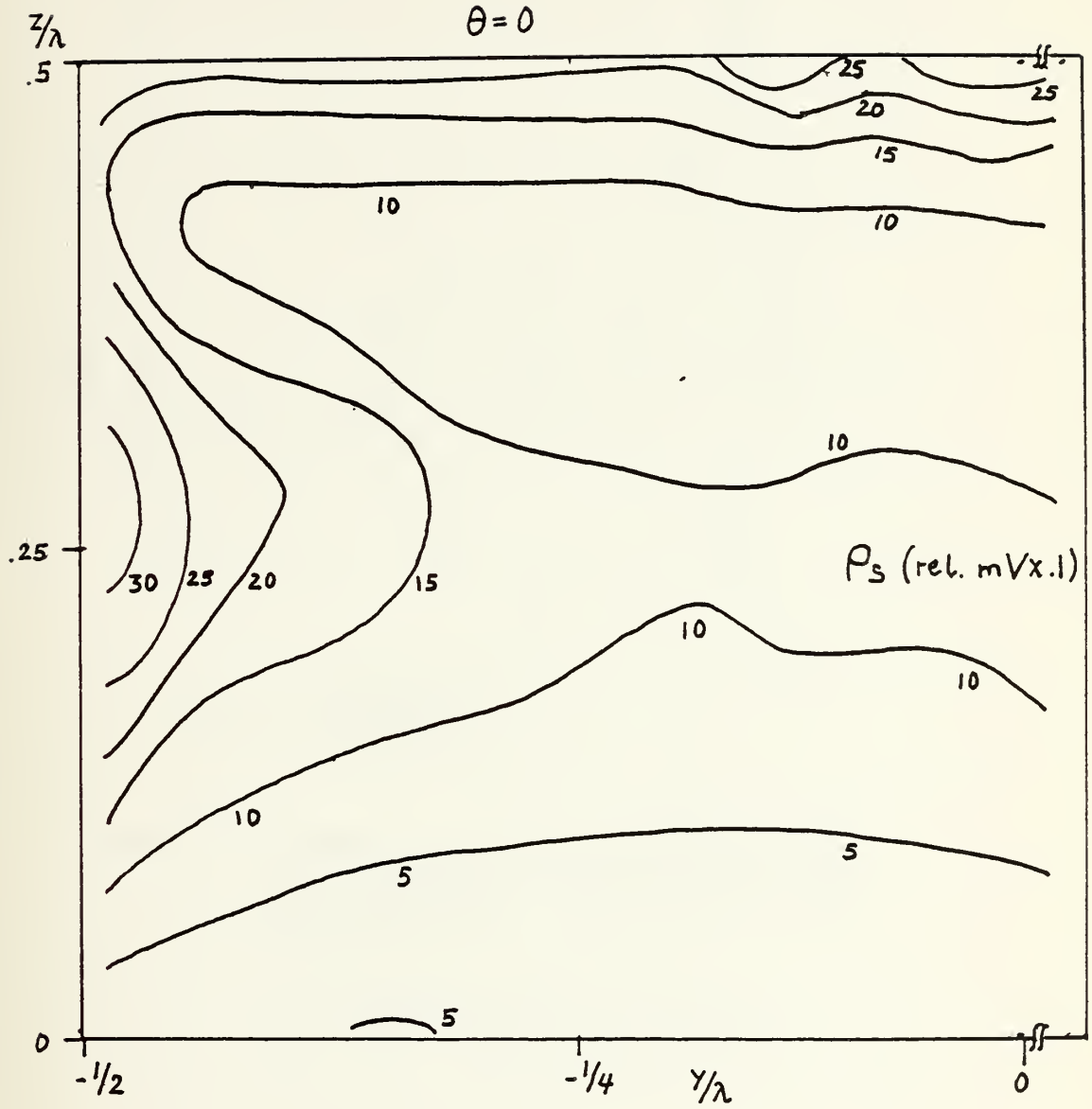
θ = 0
z/λ
.5
.25
0
-1/2
-1/4
y/λ
0
25
20
15
10
10
10
30
25
20
15
10
10
10
5
5
5
ρs (rel. mVx.1)

Figure 71.

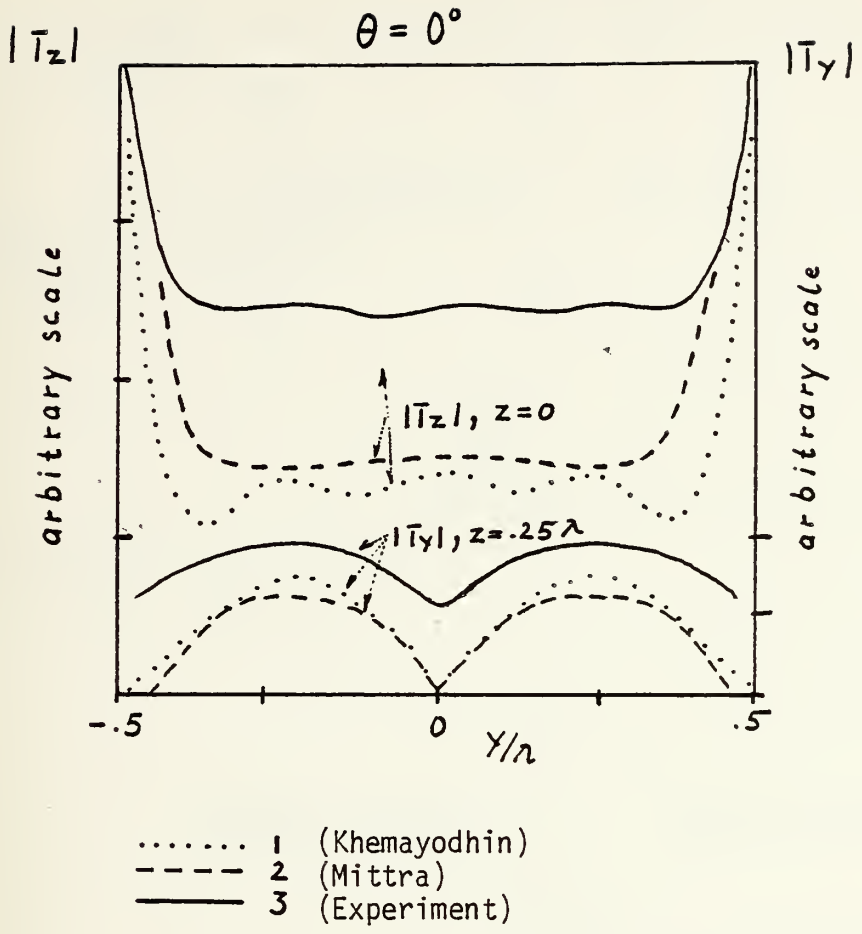

Figure 72. Comparison between a) theoretical and b) experimentally obtained surface current magnitudes. (Curves do not have same origin.)

a) Khemayodhin (1), Mittra (2),

b) result from discussed experiment (3)

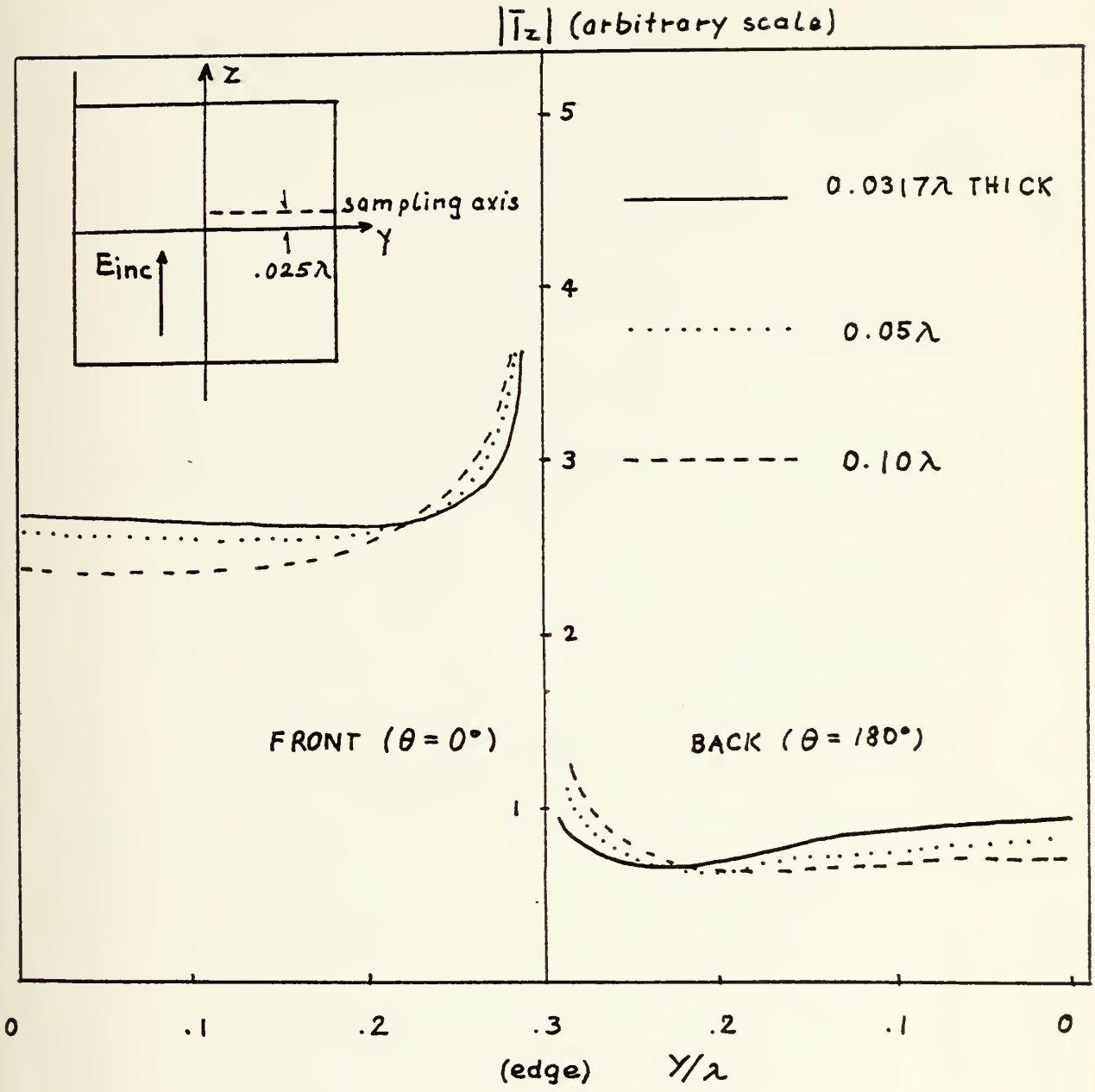

Figure 73. Surface current in Z-direction on .6λ x .6λ square plate (Tsai, et al)

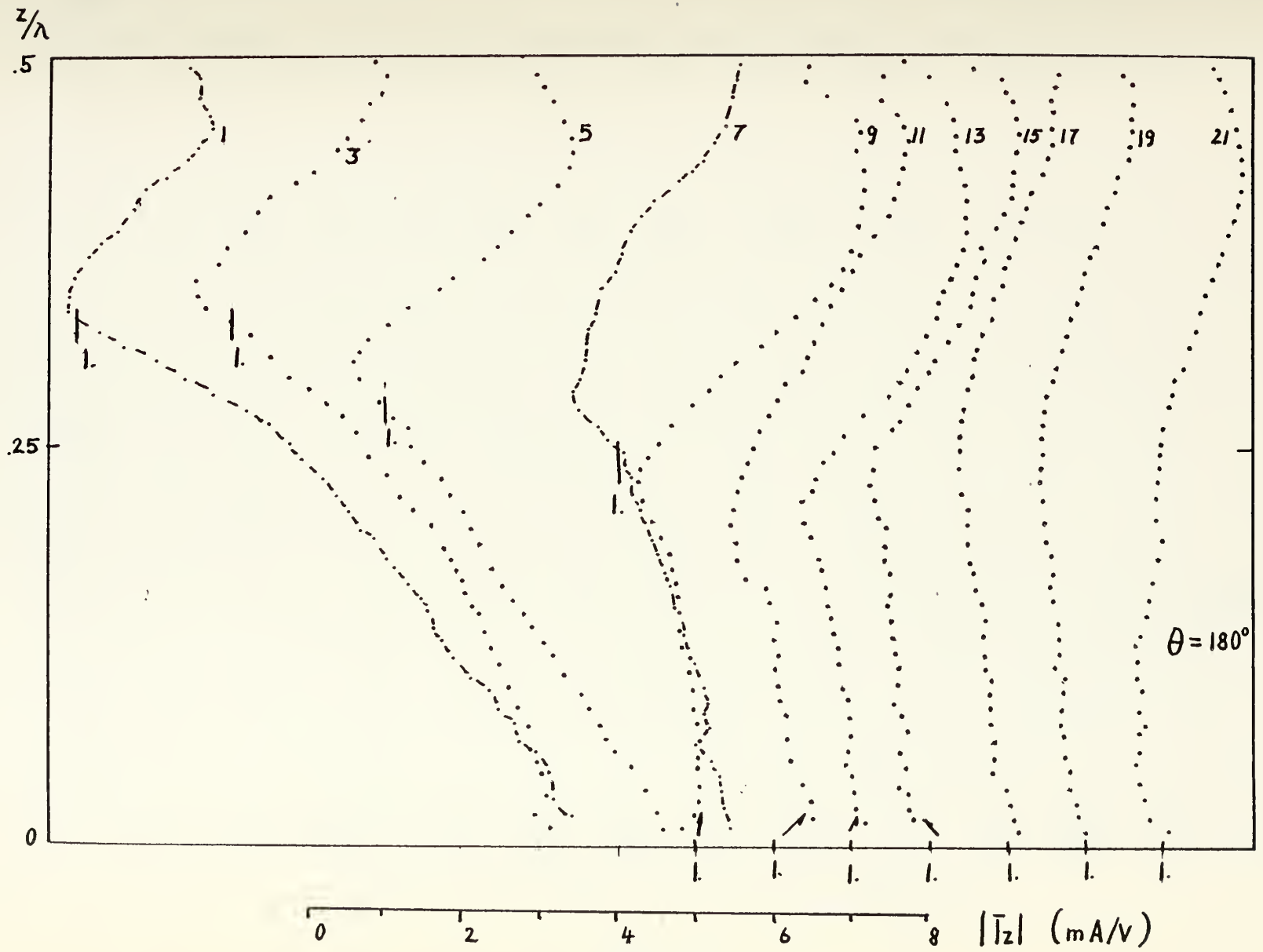

Figure 74.

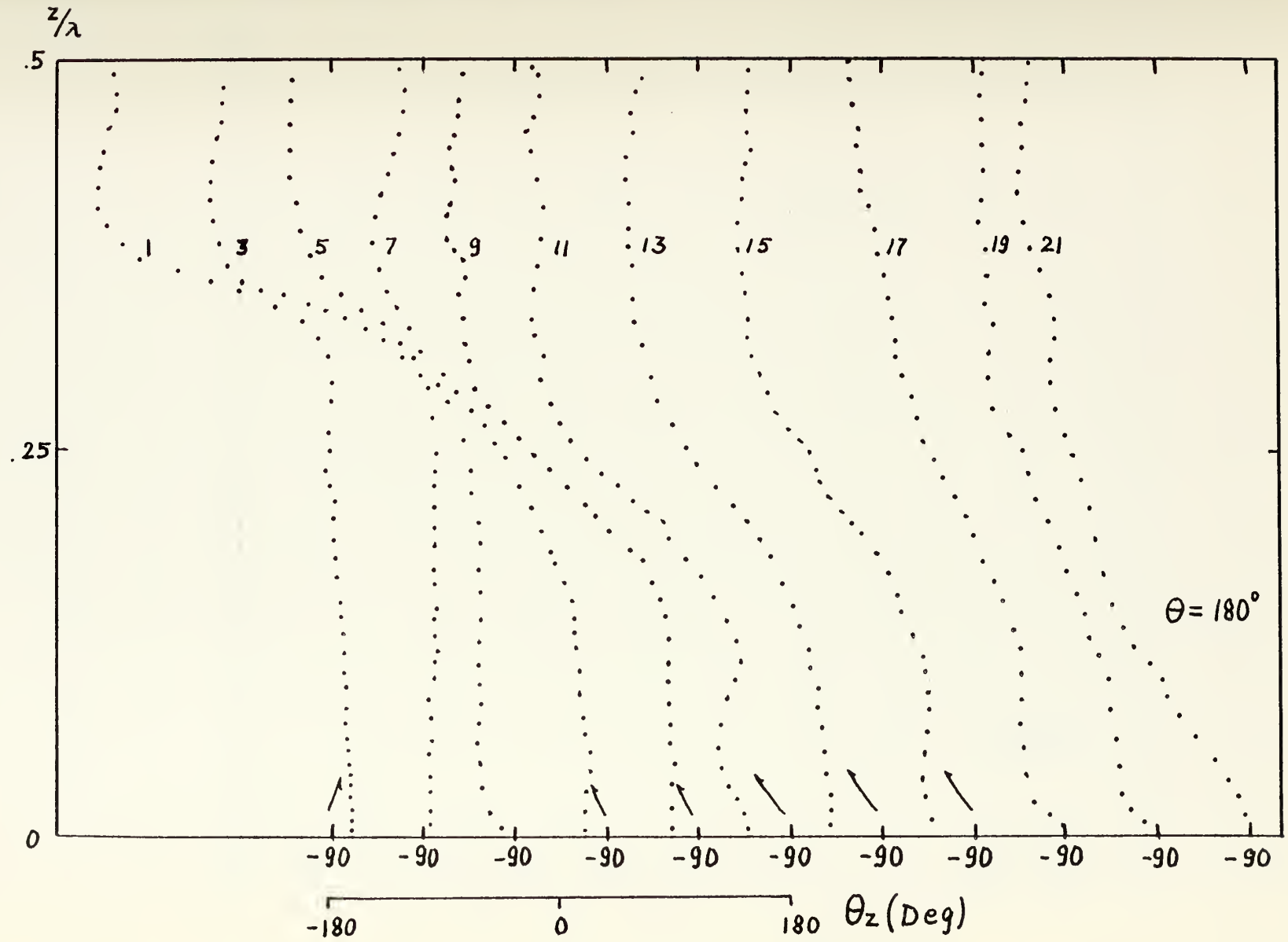

Figure 75.

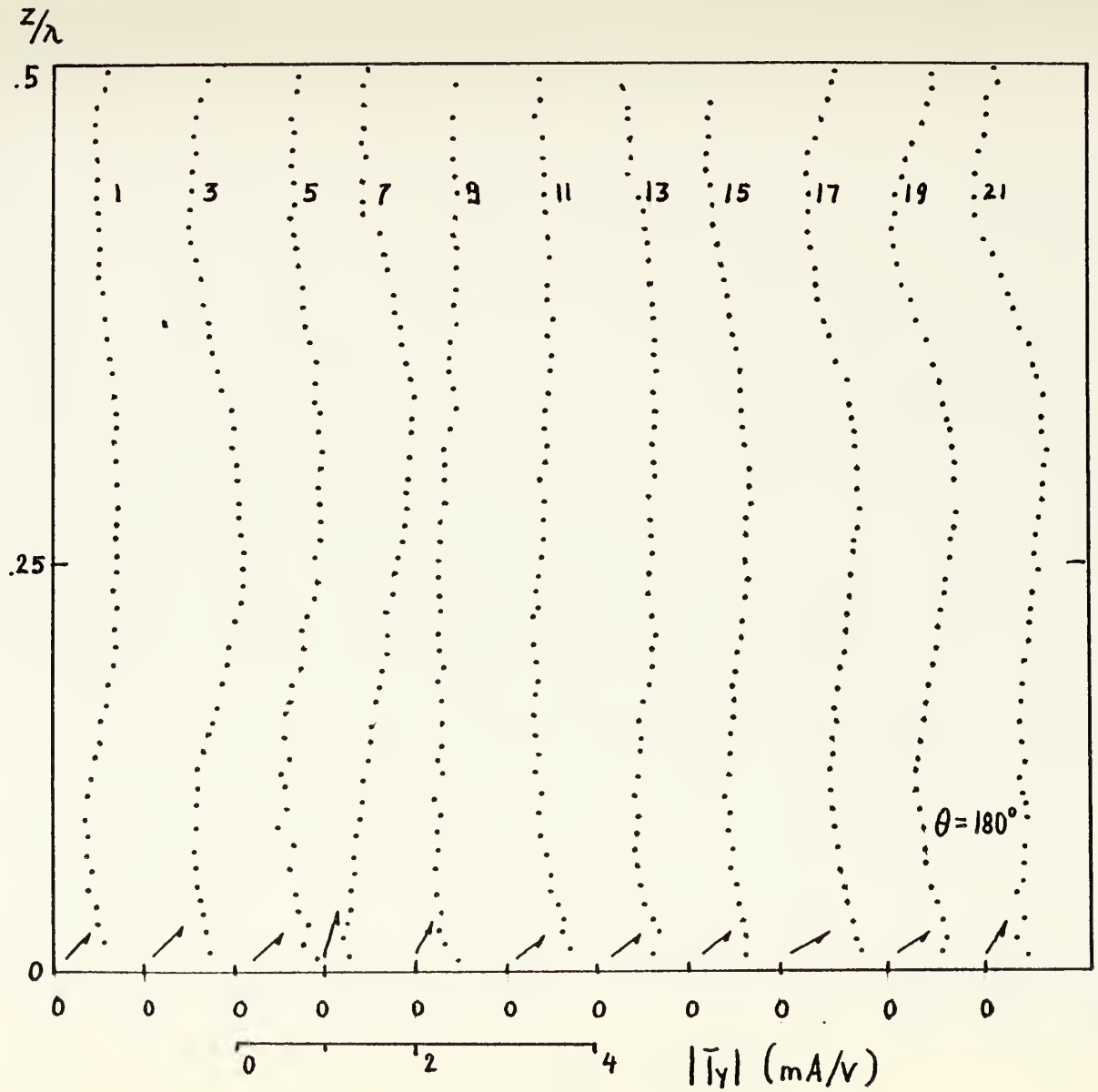

Figure 76.

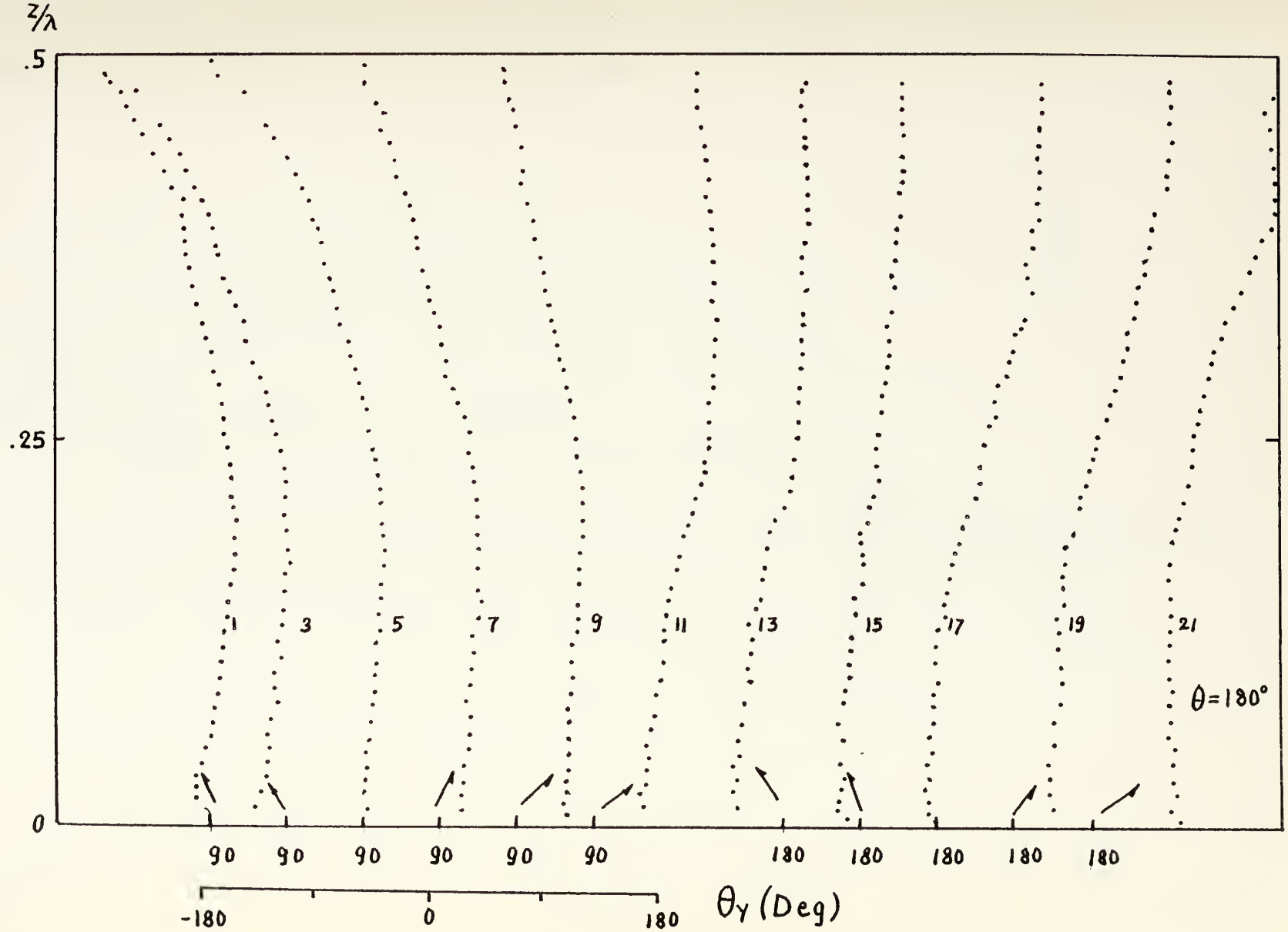
z/λ
.5
.25
0
1
3
5
7
9
11
13
15
17
19
21
θ=180°
90
90
90
90
90
90
180
180
180
180
180
-180
0
180
θY (Deg)

Figure 77.

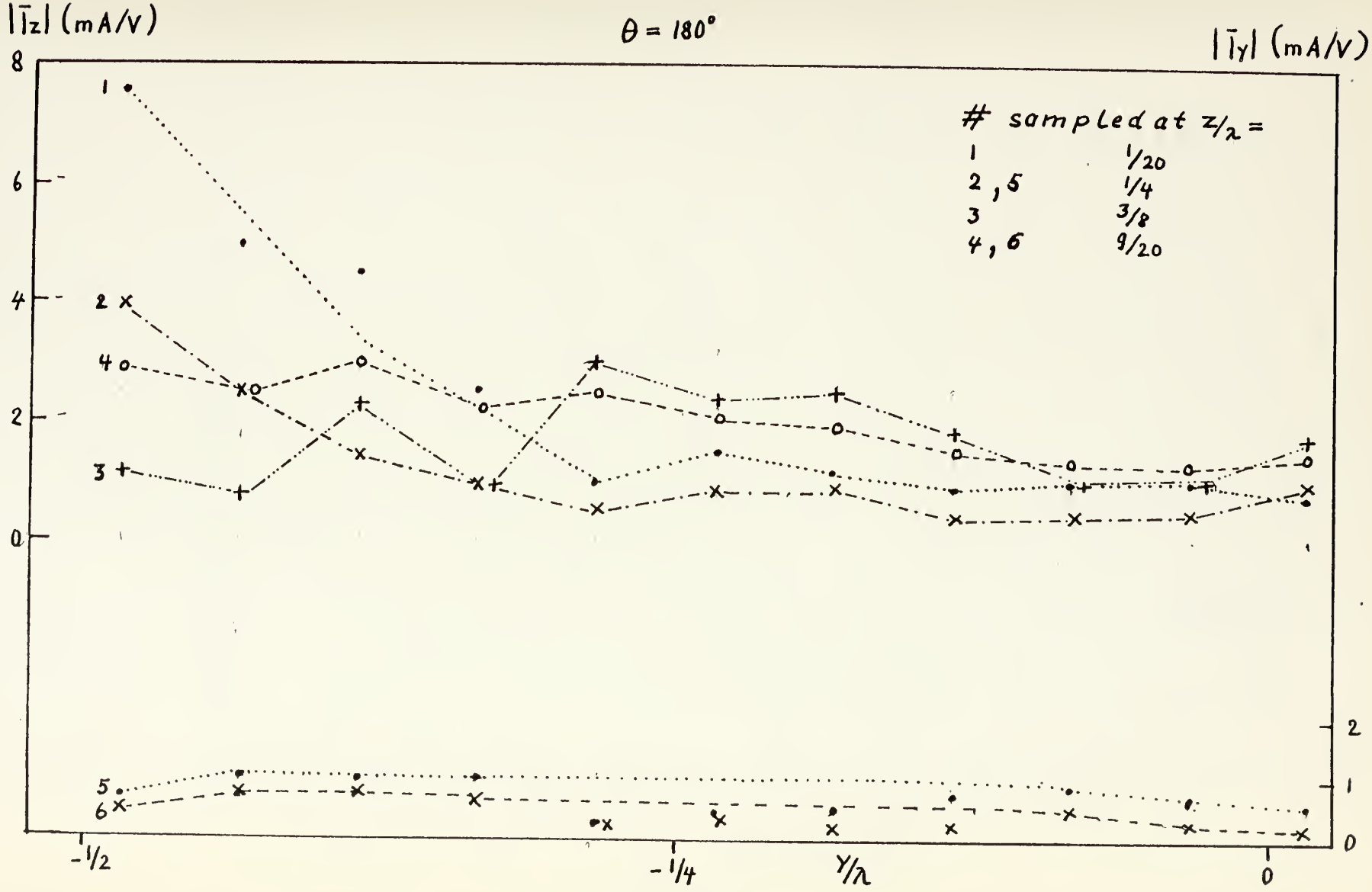
$|\bar{I}_z|$ (mA/V)
$\theta = 180°$
$|\bar{I}_y|$ (mA/V)
sampled at z/λ =
1 1/20
2, 5 1/4
3 3/8
4, 6 9/20
8
6
4
2
0
2
1
0
-1/2
-1/4
Y/λ
0

Figure 78.

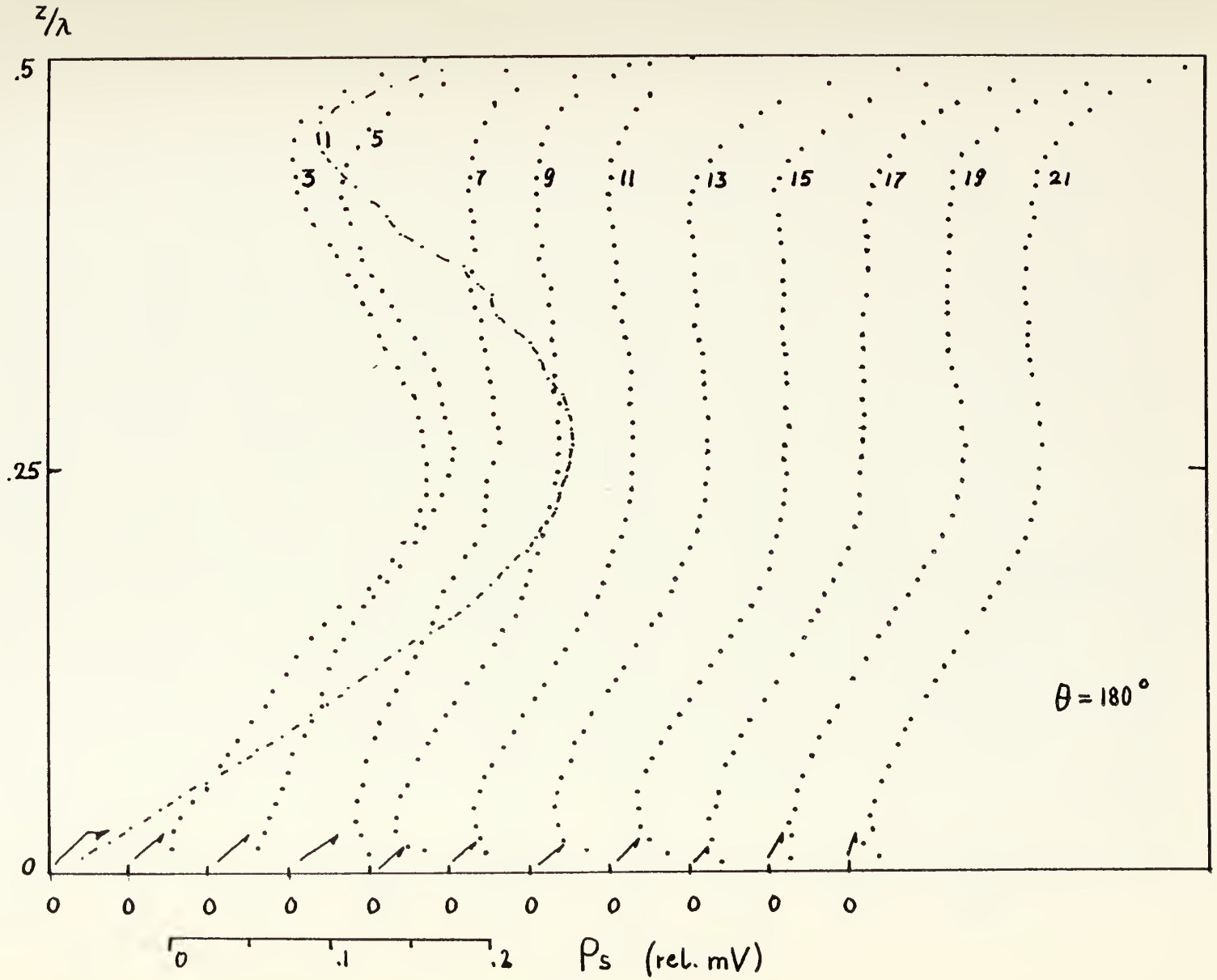

Figure 79.

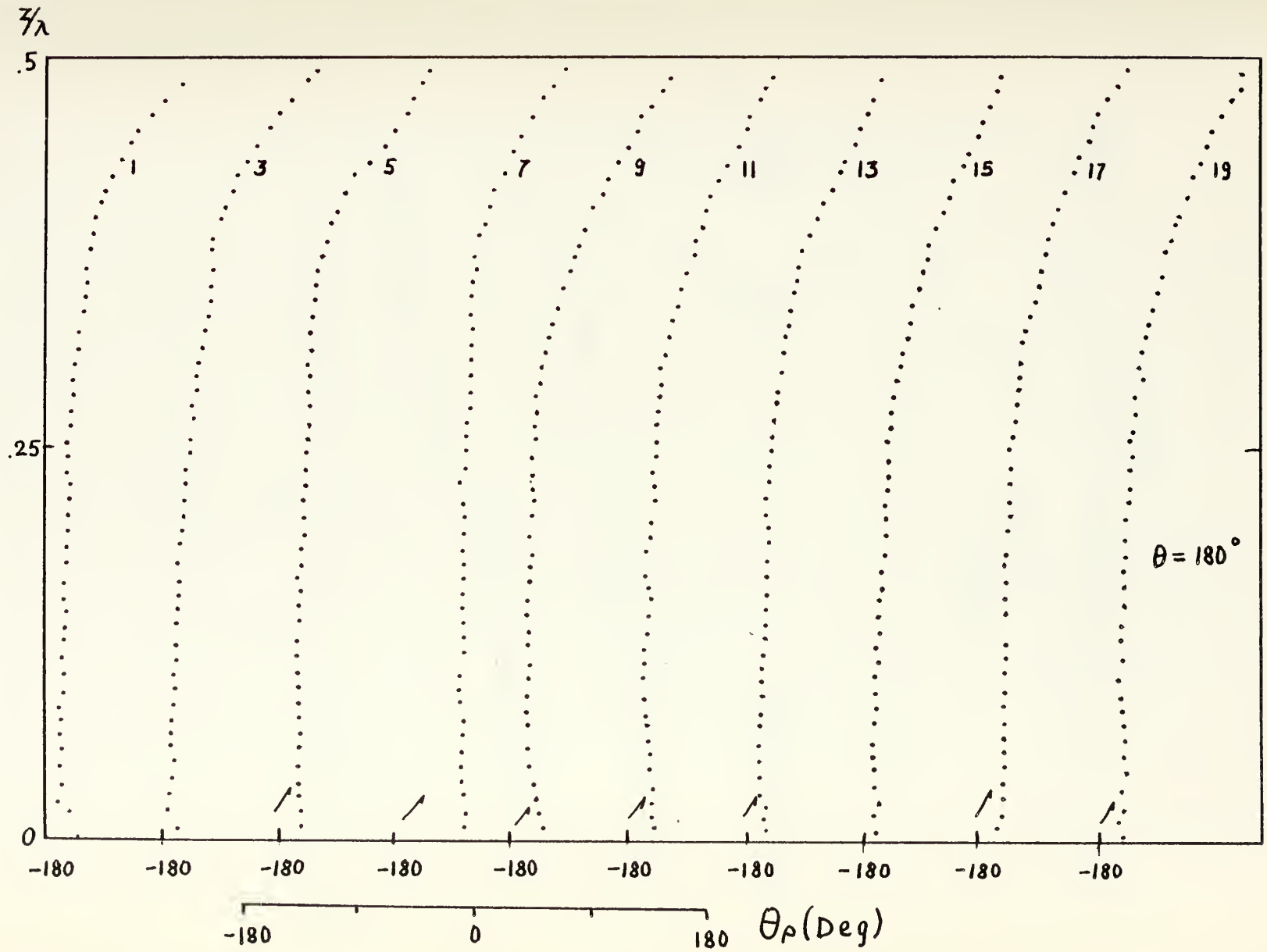
z/λ
.5
.25
0
1
3
5
7
9
11
13
15
17
19
θ = 180°
-180
-180
-180
-180
-180
-180
-180
-180
-180
-180
-180
0
180
θp(Deg)

Figure 80.

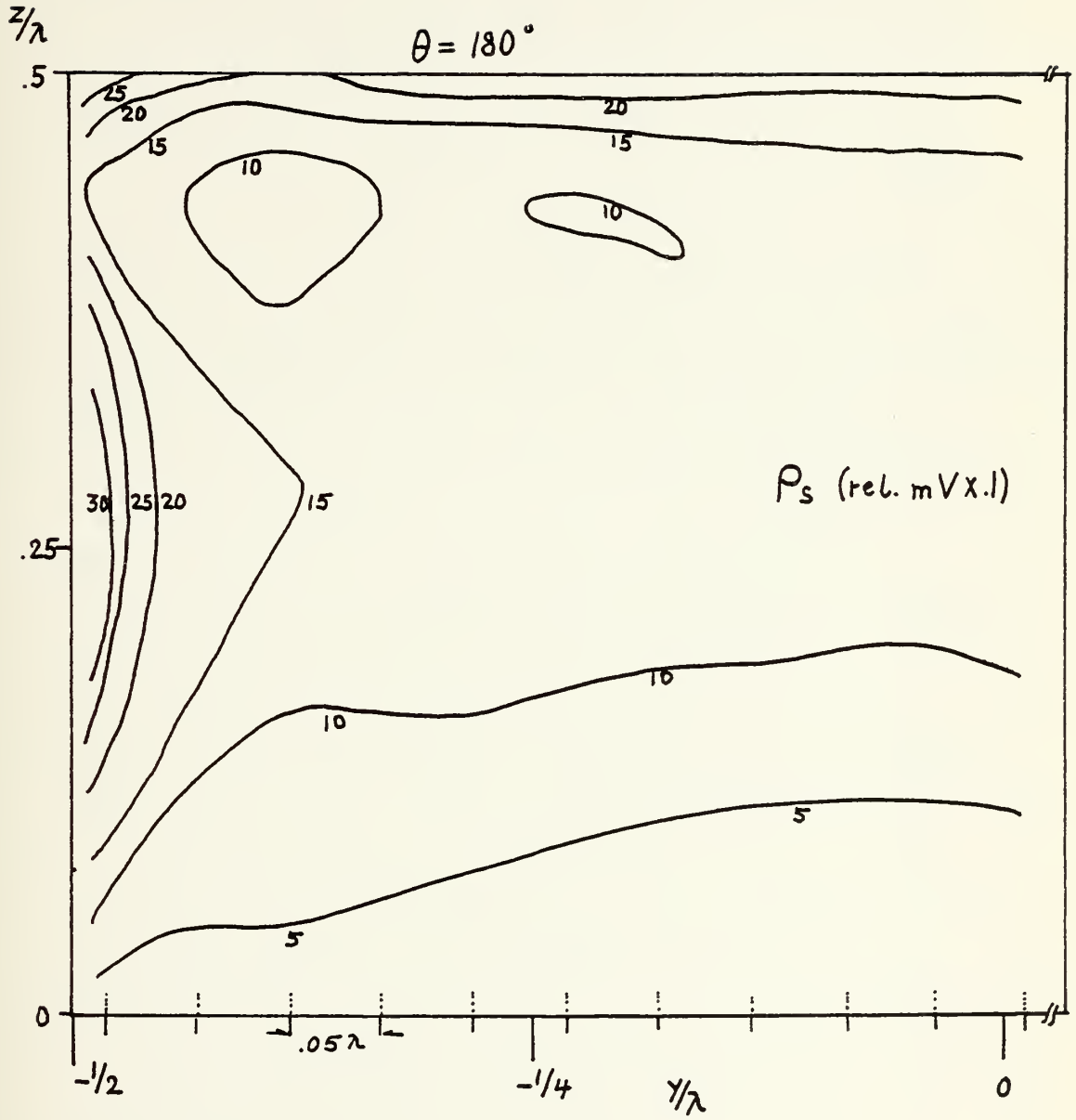
Z/λ
θ = 180°
.5
.25
0
25
20
15
10
20
15
10
30
25
20
15
10
10
5
5
Ps (rel. mV x.1)
.05λ
-1/2
-1/4
Y/λ
0

Figure 81.

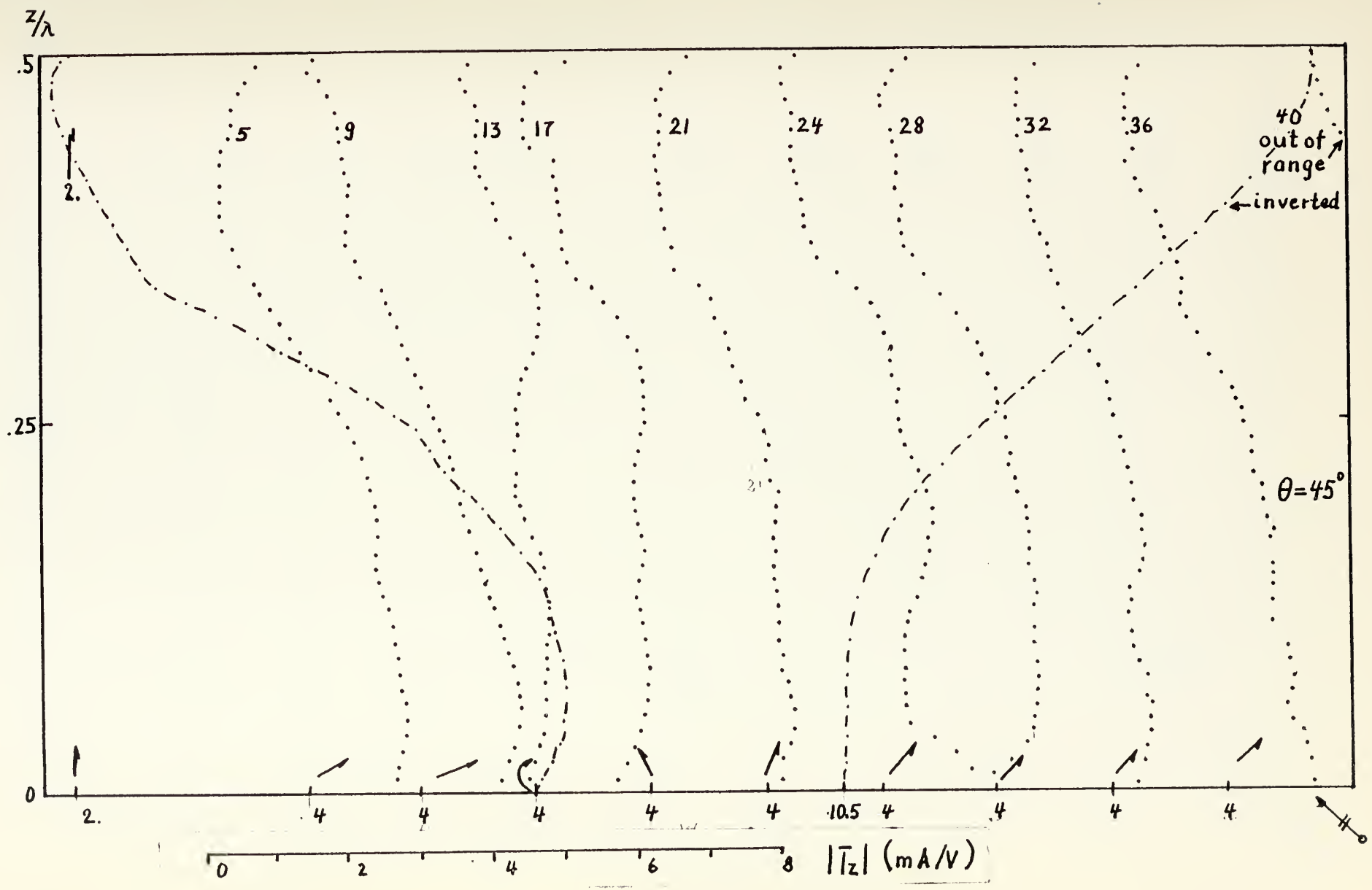
z/λ
.5
.25
0
2.
5
9
13
17
21
24
28
32
36
40
out of range
inverted
θ=45°
2.
4
4
4
4
4
10.5
4
4
4
4
0
2
4
6
8
|Iz| (mA/V)

Figure 82.

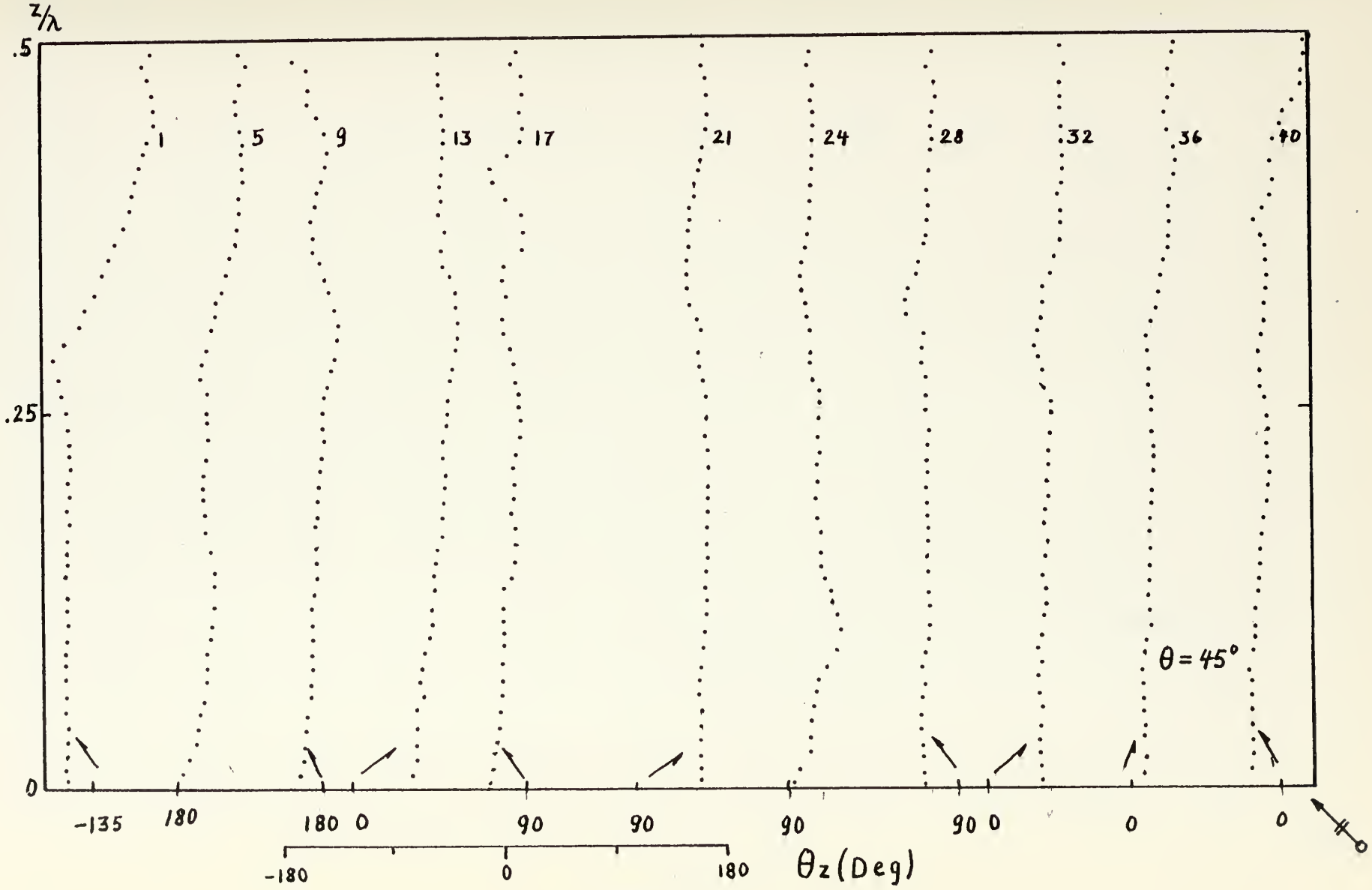
z/λ
.5
.25
0
1
5
9
13
17
21
24
28
32
36
40
θ = 45°
-135
180
180 0
90
90
90
90 0
0
0
-180
0
180
θz (Deg)

Figure 83.

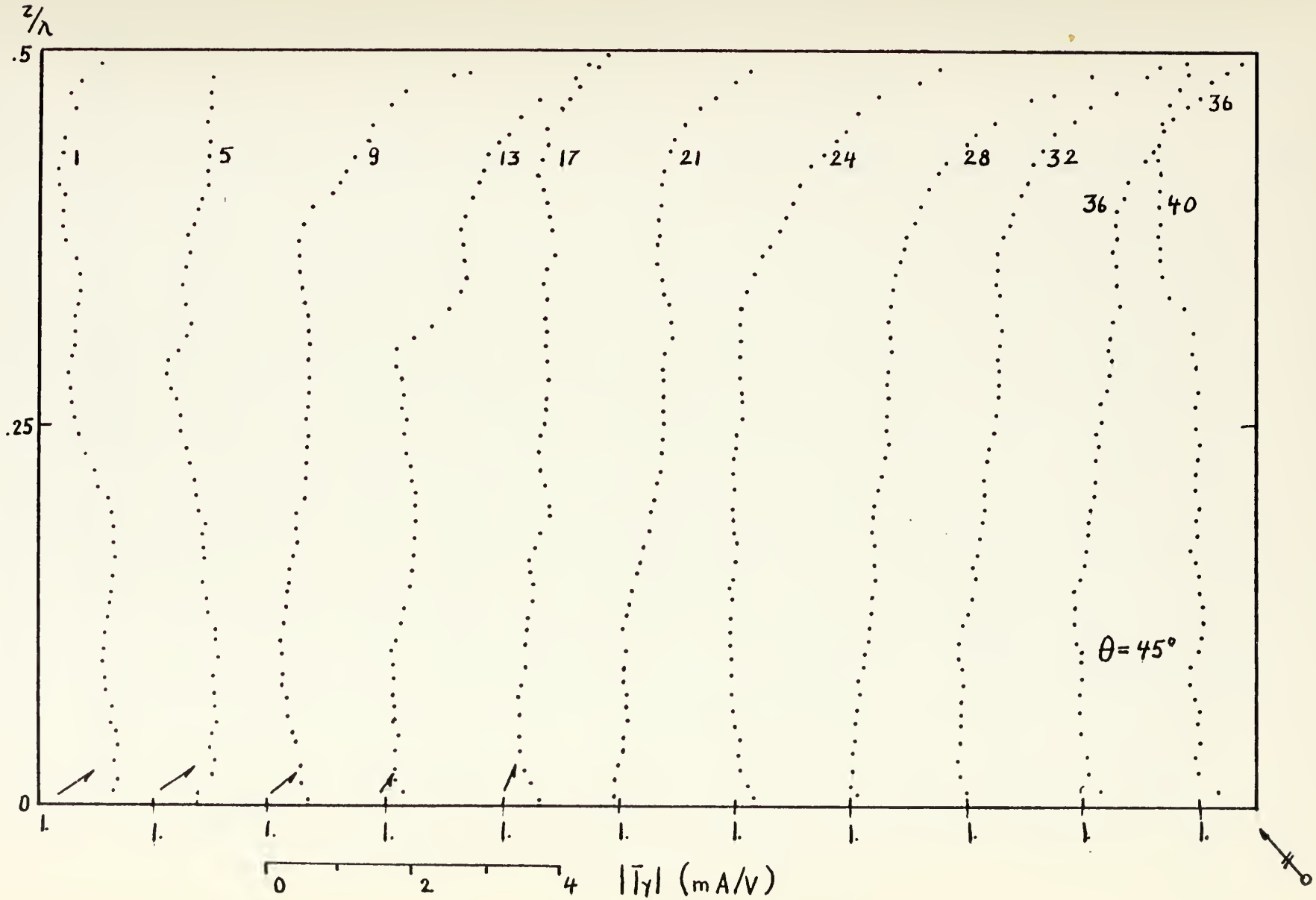

Figure 84.

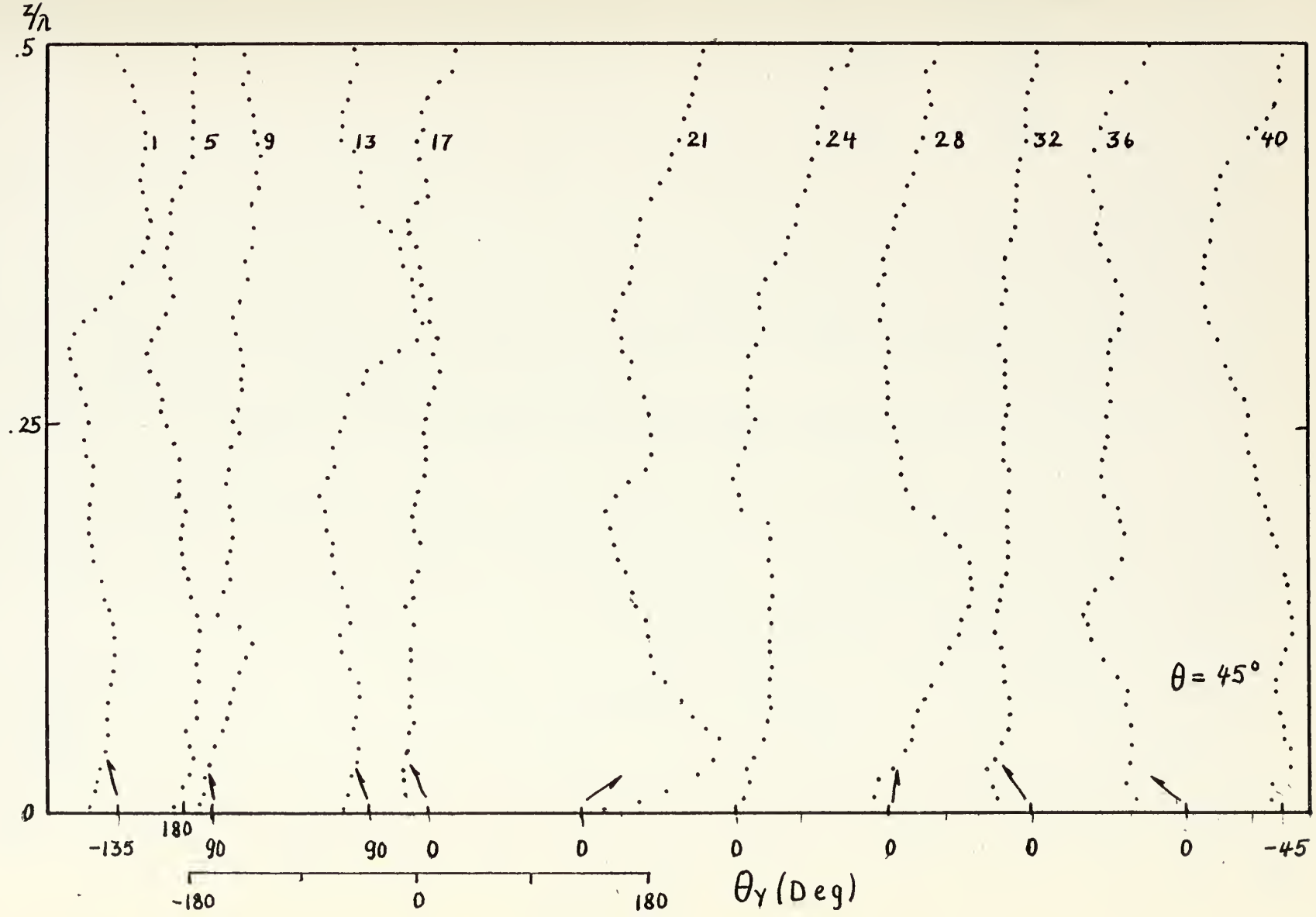
z/λ
.5
.25
0
1
5
9
13
17
21
24
28
32
36
40
θ = 45°
-135
180
90
90
0
0
0
0
0
0
-45
-180
0
180
θY (Deg)

Figure 85.

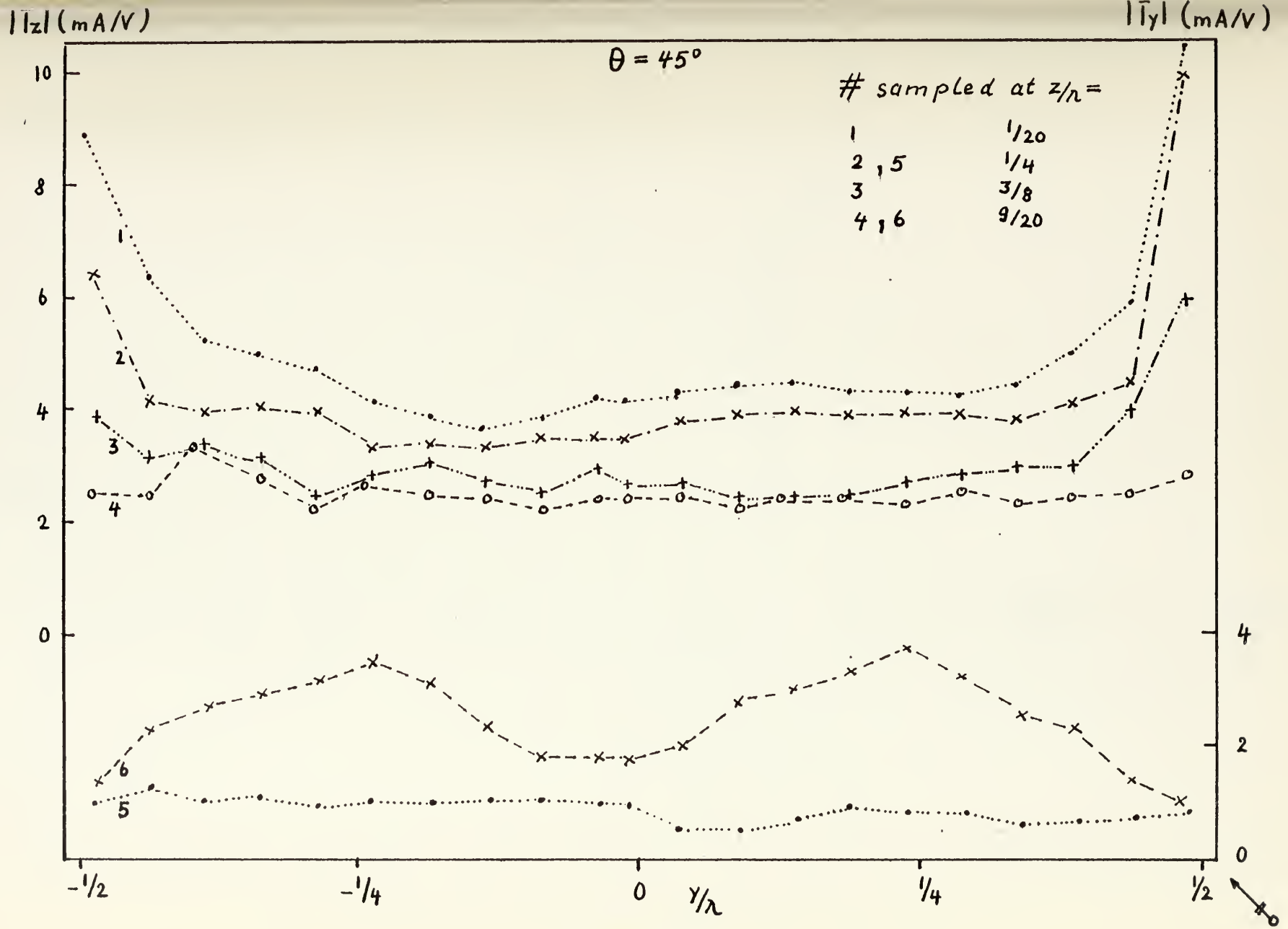
|Iz| (mA/V)
|Iy| (mA/V)
θ = 45°
sampled at z/λ=
1 1/20
2 , 5 1/4
3 3/8
4 , 6 9/20
10
8
6
4
2
0
4
2
0
1
2
3
4
5
6
-1/2
-1/4
0
Y/λ
1/4
1/2

Figure 86.

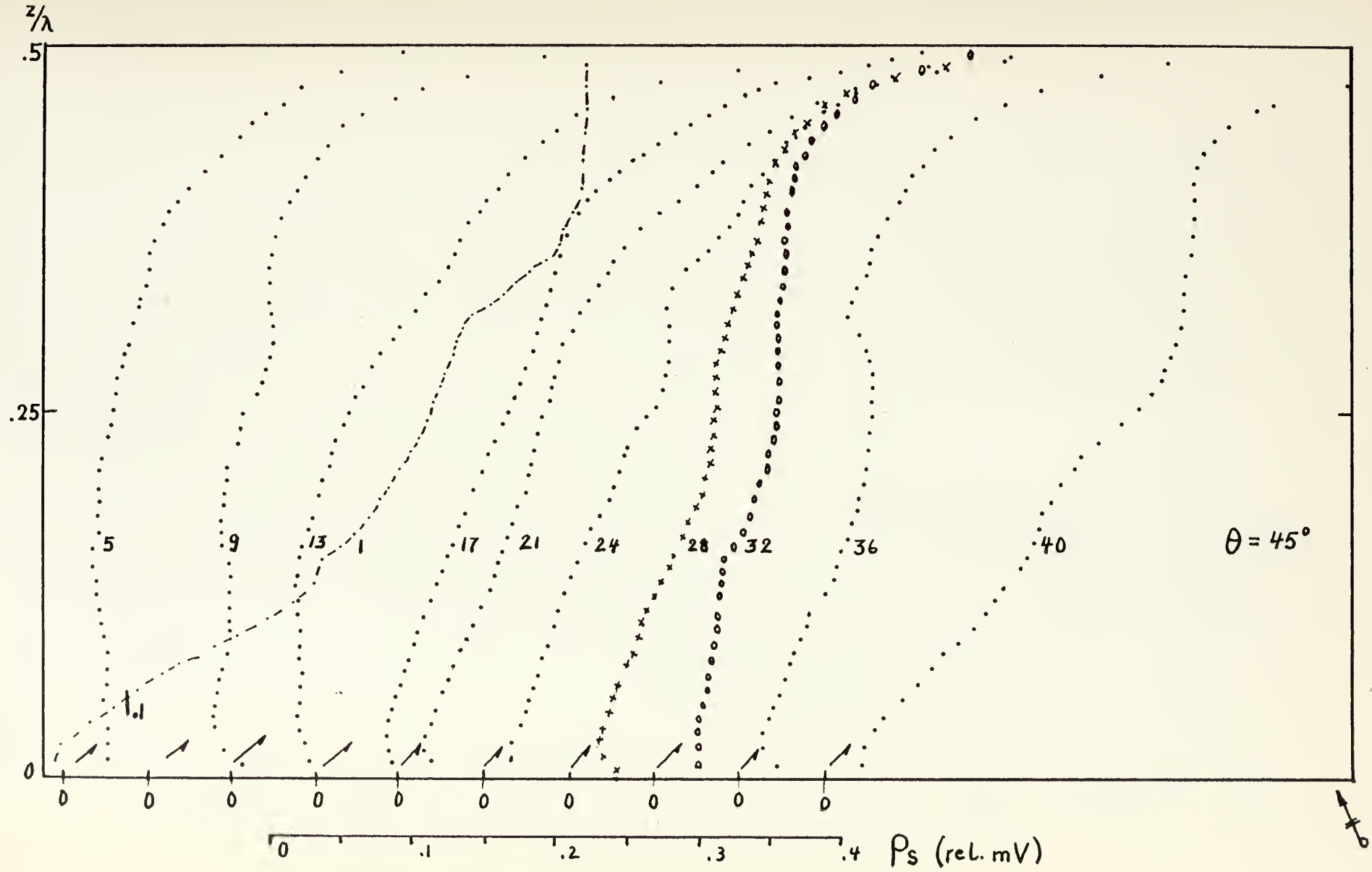

Figure 87.

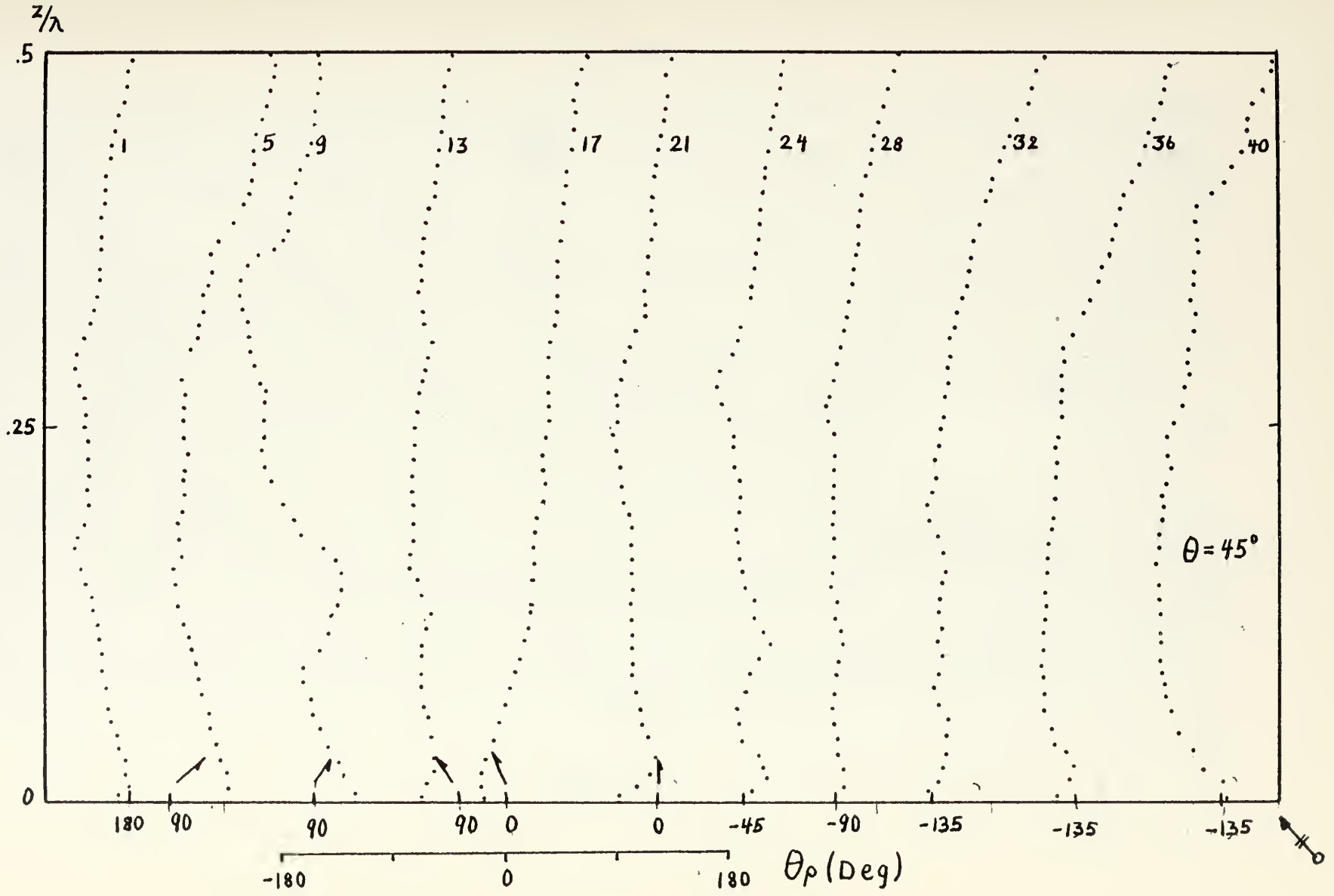
z/λ
.5
.25
0
1
5
9
13
17
21
24
28
32
36
40
θ = 45°
180
90
90
90
0
0
-45
-90
-135
-135
-135
-180
0
180
θp (Deg)

Figure 88.

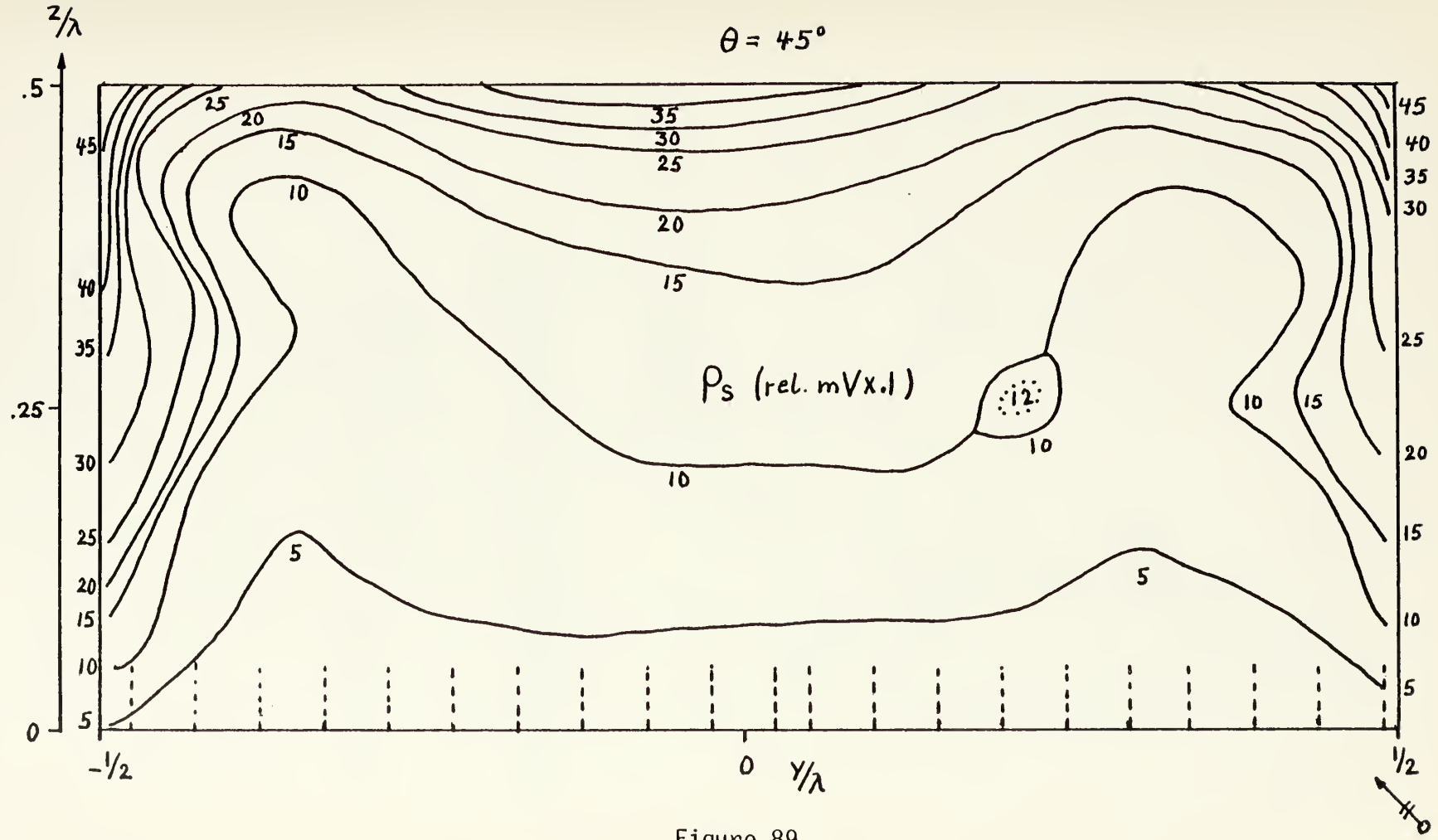

Figure 89.

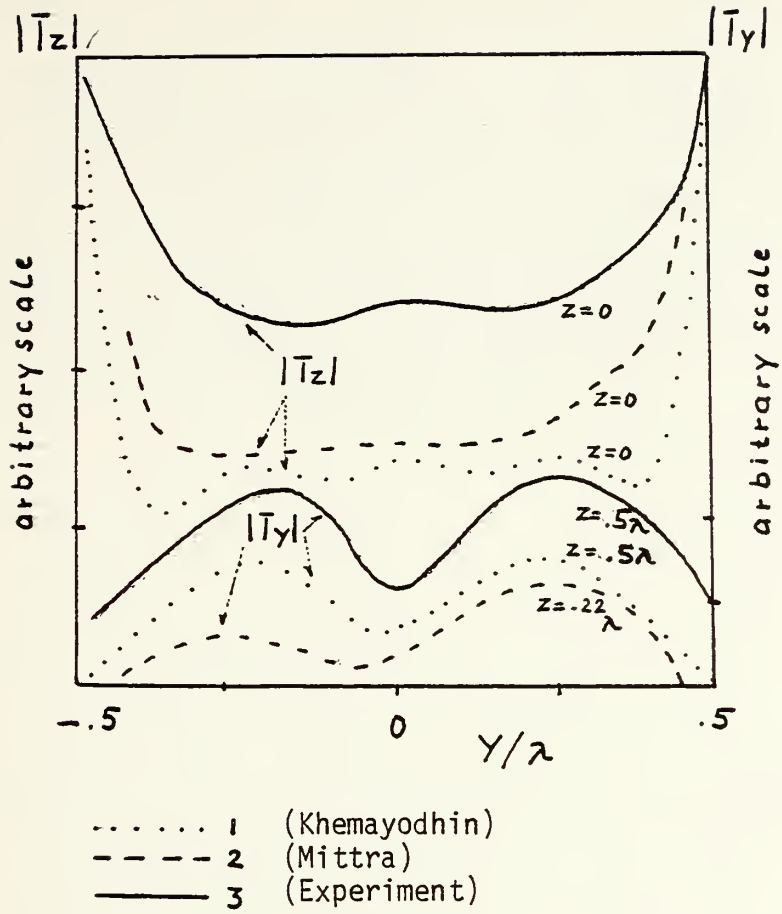

Figure 90. Comparison between a) theoretical and b) experimentally obtained surface current magnitudes. (Curves do not have same origin.)

a) Khemayodhin (1), $\theta = 45°$
Mittra (2), $\theta = 85°$

b) Result from discussed experiment (3)
$\theta = 45°$

F. SUMMARY

The analysis revealed a close relationship between all plates under study. In particular, it was shown, that the shape of the current component in the Z-direction and the charge density remained essentially unchanged for all plates that were discussed herein, so that a prediction for a broader set of plate-width seems possible. The current in the Y-direction developed gradually with plate width and cannot be predicted easily by means of this experiment alone.

IV. CONCLUSIONS AND RECOMMENDATIONS

A. RESUME

The experimental apparatus produced meaningful outputs. The data were found to be valid to allow a detailed comparison between experiment and theoretical models. The results gave profound insight into the transitional behavior of surface charge and current distributions when the dimensions of the plates were changed or a different aspect angle was chosen. The charge plots and current profiles (sampling in the Y-direction) were particularly interesting. A close agreement between experiment and theory - when available - was demonstrated.

B. REMARKS ON PRACTICAL APPLICATION

1. Locating Antennas on Ships or Aircraft

Generally, ships have metal structures with edges. A study of the current profiles and charge density contour plots of plates B, C and D make clear, that the vicinity of an edge often is not a good choice to install antennas. This is true, if some antenna illuminates the metal structure and is causing high current and charge peaks at the edge. This will contaminate the environment near the edge making it possibly unsuitable for antennas connected to sensitive systems. (This argument is given with the assumption, that the distributions presented herein will be similar even for far greater thickness of the plates. This is supported by the results of the computational investigation conducted by Tsai et al (Fig. 91).) Similar conditions can be met on aircraft where wings and tail unit constitute relatively well isolated metal near flat surfaces.

2. Penetrating Radiation

Some ships and airplanes have doors that are fairly well isolated against the hull becuase of the use of weather-strips. The experiment with the plates showed that a reradiation takes place on the shadowed side also. Thus, doors might radiate considerable energy into the interior of ships and aircraft and cause performance degradation of high sensitive instruments. This is particularly probable, if the field, that is incident on the outside surface, is strong, as can be expected in case of the electromagnetic pulse related to a nuclear blast.

3. Focussing Effect

The metal plates, when illuminated as described before, reradiated a "distorted" field, which did not have the properties of a uniform plane wave. The major contributors of the reradiation were the edges parallel to the incident E-field. Due to this effect, the plates had reradiation patterns with distinct maxima and minima of the reradiated field, which were dependent on the edge-spacing.

4. Recommendation for Further Research

a. Resonance

It is believed that the reradiated field can be made much stronger if the frequency of illumination is changed to resonate the Z-component of the current on the edges. This can be determined experimentally using the same apparatus as in this experiment.

b. The Plate as Antenna

Since the plates reradiated on both sides, it seems possible to illuminate or drive the plate from one side and utilize the other side as radiating antenna. This principle might be favorable where a closed

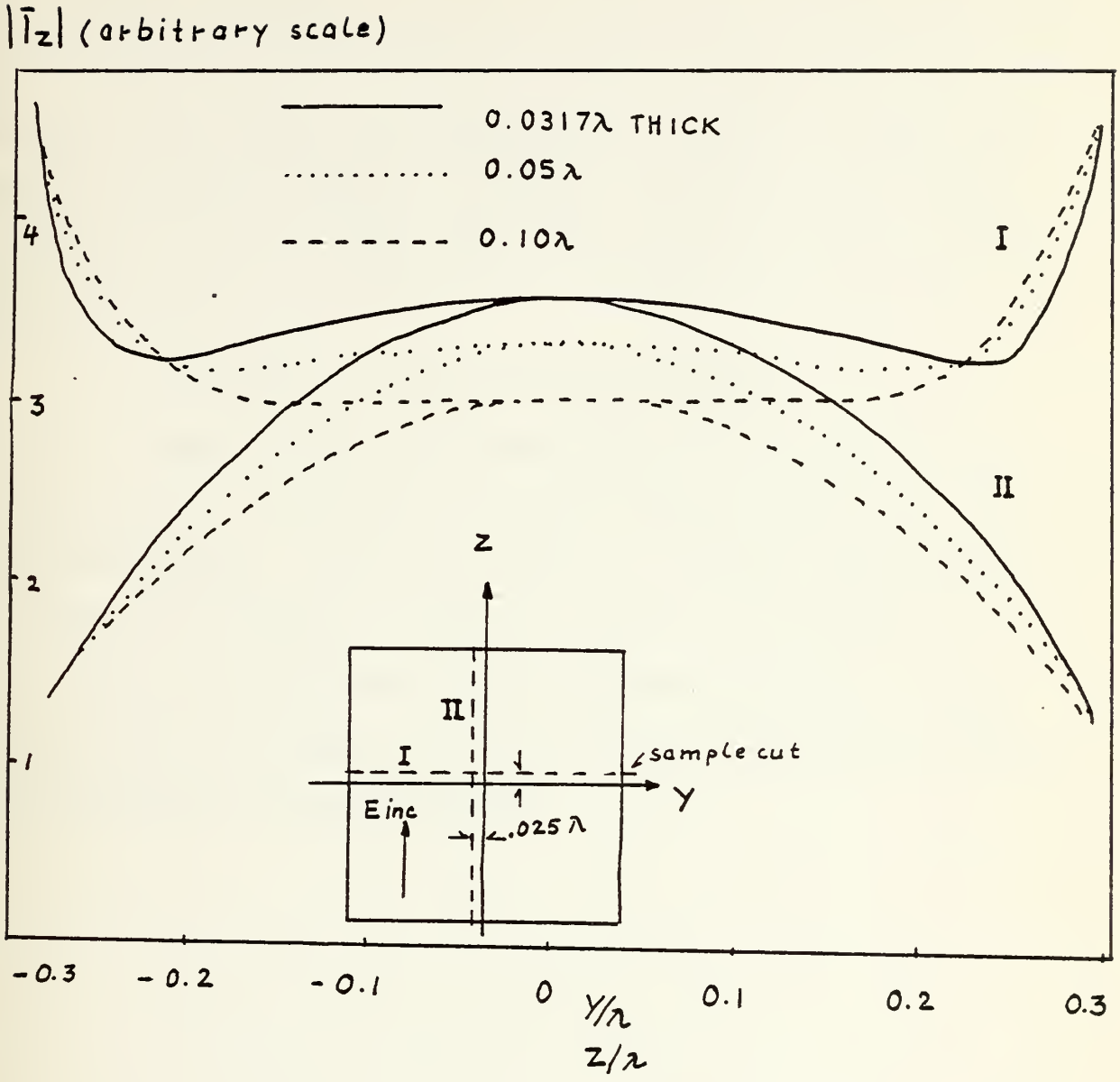

Figure 91. Theoretical magnitude of current in the Z-direction on a .6λ x .6λ square plate, computed for different values of thickness (Tsai, et al).

surface is necessary, and could be subject of further research. Also, it is proposed to illuminate a plate by a single antenna (monopole or a horn) and determine, how much the plate can be moved into the near-field of the source and still obtain high edge currents on the plate. Another proposal is to determine whether it is possible to drive the plate directly utilizing the reprocity theorem and the magnitude and phaserelationships presented in this thesis.

c. The Imbedded Plate and the Role of the Gap

When the plate is integrated into a ship's (or aircraft's) surface, it will be surrounded by a metal sheet separated from it by a small isolating gap. The role of this gap is believed to be important and might be experimentally examined. (A gap of $1/4\lambda$ width could be a good choice, but a different width might be more favorable.) Matched plate and gap are believed to be the solution to a large surface-integrated receiving and transmitting antenna.

LIST OF SYMBOLS

A	Letter designator for used plates
B	Letter designator for used plates
C	Letter designator for used plates
D	Letter designator for used plates
$\vec{E}_{inc}$	Electric field vector incident on structure
h	Half-length
$\vec{I}$	Current vector
$\lvert\bar{I}_y\rvert$	Current component in Y-direction, abs. value
$\lvert\bar{I}_z\rvert$	Current component in Z-direction, abs. value
$\vec{J}$	Current density
$\vec{Q}$	Charge vector
$\vec{Q}_z$	Charge vector on a thin, linear antenna parallel to Z-direction
Q_i	Charge, enclosed in a volume
S	Surface
t	Time
v	Volume
Δv	Incremental volume
X	Designate axes of coordinate system used
Y	Designate axes of coordinate system used
Z	Designate axes of coordinate system used
$\beta = \frac{2\pi}{\lambda}$	
θ	Aspect Angle
θ_y	Phase of current component in Y-direction
θ_z	Phase of current component in Z-direction
λ	Wavelength

ρ Charge per unit volume

ρ_s Charge density on a surface

d Denotes partial derivative

$\oint$ Integration over a closed surface

$\int_v$ Integration of a volume

$$\vec{\Delta} \cdot \vec{J} = \frac{\partial Jx}{\partial x} + \frac{\partial Jy}{\partial y} + \frac{\partial Jz}{\partial z}$$ Divergence

LIST OF REFERENCES

[1] Mittra, R., Rahmat-Samii, Y., Jamnejad, D. V., and Davis, W. A., A New Look at the Thin-Plate Scattering Problem, Radio Science, Vol. 8, No. 10, p. 869-875, October 1973.

[2] Tsai, L. L., Dudley, D. G., and Wilton, D. R., Electromagnetic Scattering by a Three-Dimensional Conducting Rectangular Box, Journal of Applied Physics, Vol. 45, No. 10, p. 4393-4400, October 1974.

[3] Khemayodhin, K., Calculation of Surface Current on Perfectly Conducting Bodies of Arbitrary Shape, Electrical Engineer Thesis, Naval Postgraduate School, Monterey, 1974.

[4] Kraus, J. D., Antennas, p. 328-336, McGraw-Hill, 1950.

[5] Weeks, W. L., Antenna Engineering, p. 324, McGraw-Hill, 1968.

[6] King, R. W., Linear Antennas, p. 127-141, 475-477, Harvard University Press, 1956.

[7] Gordon McKay Laboratory, Harvard University, Cambridge, Bi-monthly R & D Status Report No. 3 for Contract F29601-75-C-0119, Advanced Aircraft EMP Model Development, for the period October - December 1975, January 1976.

[8] Mentzer, J. R., Scattering and Diffraction of Radio Waves, Pergamon, 1955.

[9] Ross, R. A., Radar Cross-Section of Rectangular Flat Plates as a Function of Aspect Angle, IEEE Trans. Antennas and Propagation, AP-14(3), 329-335, May 1966.

[10] Richmond, J. H., A Wire-Grid Model for Scattering by Conducing Bodies, IEEE Trans. Antennas Propagation, Vol. AP-14, p. 782-786, November 1966.

[11] Richmond, J. H. and Wang, N., Sinusoidal Reaction Formulation for Radiation and Scattering from Conducting Surfaces, NASA CR-2398, June 1974.

[12] Hayt, W. H., Engineering Electromagnetics, p. 130-131, McGraw-Hill, 1974.

[13] King, R. W. and Burton, R. W. et al., Surface Currents and Charges on a Thick Conducting Tube in an E-Polarized Plane-Wave Field, I. Theory, to be published in Radio Science.

[14] King, R. W., Notes on Antennas, p. 73-83, Harvard University, Engineering 270, 1943

[15] Burton, R. W., Induced Currents and Charges on Thin Cylinders in a Time-Varying Electromagnetic Field, IEEE Trans. EMC, Vol. 17, No. 3, August 1975.

[16] Burton, R. W., The Crossed-Dipole Structure of Aircraft in an Electromagnetic Pulse Environment, Paper reprinted from conference preprint No. 159 on Electromagnetic Noise Interference and Compatibility, Advisory Group for Aerospace Research and Development, 1974.

[17] Rahmat-Samii, Y. and Mittra, R., Integral Equation Solution and RCS Computation of a Thin Rectangular Plate, IEEE Trans. Antenna and Propagation, July 1974.

INITIAL DISTRIBUTION LIST

		No. Copies
1.	Defense Documentation Center Cameron Station Alexandria, Virginia 22314	2
2.	Library, Code 0212 Naval Postgraduate School Monterey, California 93940	2
3.	Department Chairman, Code 52 Department of Electrical Engineering Naval Postgraduate School Monterey, California 93940	2
4.	Assoc. Prof. Robert W. Burton, LT COL, USAF Code 52Zn, Department of Electrical Engineering Naval Postgraduate School Monterey, California 93940	10
5.	Assoc. Prof. Richard W. Adler, Code 52Ab Department of Electrical Engineering Naval Postgraduate School Monterey, California 93940	1
6.	Post-Doctoral Program, RADC-RBC Rome Air Development Center Griffiss AFB New York 13441	1
7.	Mr. Philip Blacksmith, Code LZR Air Force Research Lab Laurence G. Hanscom Field Bedford, Massachusetts 01730	1
8.	Air Force Weapons Laboratory/PRP Attn: CAPT Harrison Kirtland AFB New Mexico 87117	2
9.	Prof. R. W. P. King Gordon McKay Laboratory Harvard University 9 Oxford Street Cambridge, Massachusetts 02138	1
10.	Dr. Marlan Kvigne, Code 2110 Naval Electronic Laboratory Center San Diego, California 92152	1

11. Marineamt -A1-
294 Wilhelmshaven
Federal Republic of Germany — 1

12. Dokumentationszentrale der Bundeswehr (See)
53 Bonn
Friedrich-Ebert-Allee 34
Federal Republic of Germany — 1

13. Kommandeur
Marineortungsschule
285 Bremerhaven
West Germany — 1

14. Kptlt. Hans-J. Wiedemann
Marineortungsschule
285 Bremerhaven
West Germany — 4